Development of self-assembling protein only nanoparticles for targeted therapies.

Naroa Serna Romero

PhD Thesis 2018

CONCLUSIONS

1) The engineering principle based on controlling the cationic load of the homing peptide at the amino terminal region allows fusion proteins to self-assemble in nanoparticles with predictable size.

2) Protein´s self-assembling process is determined by a minimum number of positive charges as well as charge distribution in the amino terminus peptide.

3) The stability of nanoparticles obtained by the enginnering tool should be further studied due to a probable instability and disassembling of nanoentities in the blood stream.

4) The high cellular penetrability of protein nanoparticles in cultured cells *in vitro* does not guarantee efficient BBB crossing and brain targeting. Thus, the principles that rule the biodistribution of protein nanoparticles displaying BBB-homing peptides when comparing with those that display tumor homing peptides may be different, questioning the convenience of using protein nanoparticulated materials for the treatment of CNS diseases.

5) Cytotoxic proteins of different origins such as proapoptotic factors, antimicrobial peptides and catalytic domains of microbial toxins have been successfully engineered to self-assemble as chemically homogeneous protein-only nanoparticles that act simultaneously as vehicle and drug, showing excellent biodistribution and local antitumoral effects in $CXCR4^{+}$ colorectal cancer mouse model upon systemic administration. Generic applicability of this protein oligomerization platform to generate protein only NPs with intrinsic cytotoxic activity has been demonstrated.

6) Toxin based protein only NPs effectively target, kill and overcome the resistance presented by colon CSCs to traditional therapy, being valuable therapeutics against colon CSCs.

7) The proton sponge effect expected by His-rich peptide is inefficient promoting the release of the fusion protein into the cytosol and, may decrease the cytotoxic effect of therapeutic proteins. Thus, the exploration and suitable incorporation of endosomolytic domains into building blocks may favor the transfection of the fusion protein into the cytosol.

8) The use of human scaffold proteins and/or deimmunization-oriented engineering of non-human building blocks forming the NPs may allow their evaluation in clinical trials.

9) Cationic antimicrobial peptide GWH1 fused to GFP-H6 acts as an antimicrobial agent and as architectonic tag forming NPs with antimicrobial activity. This oligomerization platform shows promises for the generation of antimicrobial protein-only nanoparticles as alternatives to conventional antibiotics.

REFERENCES

(1) Wagner V, Dullaart A, Bock AK, Zweck A. The emerging nanomedicine landscape. *Nat Biotechnol* 2006;24:1211-1217.

(2) Satalkar P, Elger BS, Shaw DM. Defining Nano, Nanotechnology and Nanomedicine: Why Should It Matter? *Sci Eng Ethics* 2016;22:1255-1276.

(3) Freitas RA, Jr. What is nanomedicine? *Nanomedicine* 2005;1:2-9.

(4) European Science Foundation´s Forward Look Nanomedicine: An EMRC Consensus opinion. 2005. http://www.esf.org.

(5) Dos Santos Ramos MA, Da Silva PB, Sposito L et al. Nanotechnology-based drug delivery systems for control of microbial biofilms: a review. *Int J Nanomedicine* 2018;13:1179-1213.

(6) Ngandeu Neubi GM, Opoku-Damoah Y, Gu X, Han Y, Zhou J, Ding Y. Bio-inspired drug delivery systems: an emerging platform for targeted cancer therapy. *Biomater Sci* 2018. Available online.

(7) Blanco E, Shen H, Ferrari M. Principles of nanoparticle design for overcoming biological barriers to drug delivery. *Nat Biotechnol* 2015;33:941-951.

(8) Dilnawaz F, Acharya S, Sahoo SK. Recent trends of nanomedicinal approaches in clinics. *Int J Pharm* 2018;538:263-278.

(9) Sukhanova A, Bozrova S, Sokolov P, Berestovoy M, Karaulov A, Nabiev I. Dependence of Nanoparticle Toxicity on Their Physical and Chemical Properties. *Nanoscale Res Lett* 2018;13:44.

(10) Kassem AA. Nanotechnology inspired advanced engineering fundamentals for optimizing drug delivery. *Curr Drug Targets* 2018. Available online.

(11) Petros RA, DeSimone JM. Strategies in the design of nanoparticles for therapeutic applications. *Nat Rev Drug Discov* 2010;9:615-627.

(12) Azzopardi EA, Ferguson EL, Thomas DW. The enhanced permeability retention effect: a new paradigm for drug targeting in infection. *J Antimicrob Chemother* 2013;68:257-274.

(13) Maeda H, Nakamura H, Fang J. The EPR effect for macromolecular drug delivery to solid tumors: Improvement of tumor uptake, lowering of systemic toxicity, and distinct tumor imaging in vivo. *Adv Drug Deliv Rev* 2013;65:71-79.

(14) Duncan R, Gaspar R. Nanomedicine(s) under the microscope. *Mol Pharm* 2011;8:2101-2141.

(15) Mangues R, Vazquez E, Villaverde A. Targeting in Cancer Therapies. *Med Sci (Basel)* 2016;4:893-916.

(16) Bertrand N, Wu J, Xu X, Kamaly N, Farokhzad OC. Cancer nanotechnology: the impact of passive and active targeting in the era of modern cancer biology. *Adv Drug Deliv Rev* 2014;66:2-25.

(17) Yu MK, Park J, Jon S. Targeting strategies for multifunctional nanoparticles in cancer imaging and therapy. *Theranostics* 2012;2:3-44.

(18) Glasgow MD, Chougule MB. Recent Developments in Active Tumor Targeted Multifunctional Nanoparticles for Combination Chemotherapy in Cancer Treatment and Imaging. *J Biomed Nanotechnol* 2015;11:1859-1898.

(19) Toporkiewicz M, Meissner J, Matusewicz L, Czogalla A, Sikorski AF. Toward a magic or imaginary bullet? Ligands for drug targeting to cancer cells: principles, hopes, and challenges. *Int J Nanomedicine* 2015;10:1399-1414.

(20) Brown KC. Peptidic tumor targeting agents: the road from phage display peptide selections to clinical applications. *Curr Pharm Des* 2010;16:1040-1054.

(21) Zhang XX, Eden HS, Chen X. Peptides in cancer nanomedicine: drug carriers, targeting ligands and protease substrates. *J Control Release* 2012;159:2-13.

(22) Park K. Polysaccharide-based near-infrared fluorescence nanoprobes for cancer diagnosis. *Quant Imaging Med Surg* 2012;2:106-113.

(23) Nel AE, Madler L, Velegol D et al. Understanding biophysicochemical interactions at the nano-bio interface. *Nat Mater* 2009;8:543-557.

(24) Nguyen VH, Lee BJ. Protein corona: a new approach for nanomedicine design. *Int J Nanomedicine* 2017;12:3137-3151.

(25) Alexis F, Pridgen E, Molnar LK, Farokhzad OC. Factors affecting the clearance and biodistribution of polymeric nanoparticles. *Mol Pharm* 2008;5:505-515.

(26) D'souza AA, Shegokar R. Polyethylene glycol (PEG): a versatile polymer for pharmaceutical applications. *Expert Opin Drug Deliv* 2016;13:1257-1275.

(27) Harris JM, Chess RB. Effect of pegylation on pharmaceuticals. *Nat Rev Drug Discov* 2003;2:214-221.

(28) Zhao C, Deng H, Xu J et al. "Sheddable" PEG-lipid to balance the contradiction of PEGylation between long circulation and poor uptake. *Nanoscale* 2016;8:10832-10842.

(29) Hamidi M, Azadi A, Rafiei P. Pharmacokinetic consequences of pegylation. *Drug Deliv* 2006;13:399-409.

(30) Longmire M, Choyke PL, Kobayashi H. Clearance properties of nano-sized particles and molecules as imaging agents: considerations and caveats. *Nanomedicine (Lond)* 2008;3:703-717.

(31) Wang J, Liu G. Imaging Nano-Bio Interactions in the Kidney: Toward a Better Understanding of Nanoparticle Clearance. *Angew Chem Int Ed Engl* 2018;57:3008-3010.

(32) Garcia-Alvarez R, Hadjidemetriou M, Sanchez-Iglesias A, Liz-Marzan LM, Kostarelos K. In vivo formation of protein corona on gold nanoparticles. The effect of their size and shape. *Nanoscale* 2018;10:1256-1264.

(33) Piella J, Bastus NG, Puntes V. Size-Dependent Protein-Nanoparticle Interactions in Citrate-Stabilized Gold Nanoparticles: The Emergence of the Protein Corona. *Bioconjug Chem* 2017;28:88-97.

(34) Saikia J, Yazdimamaghani M, Hadipour Moghaddam SP, Ghandehari H. Differential Protein Adsorption and Cellular Uptake of Silica Nanoparticles Based on Size and Porosity. *ACS Appl Mater Interfaces* 2016;8:34820-34832.

(35) Gentile F, Chiappini C, Fine D et al. The effect of shape on the margination dynamics of non-neutrally buoyant particles in two-dimensional shear flows. *J Biomech* 2008;41:2312-2318.

(36) Geng Y, Dalhaimer P, Cai S et al. Shape effects of filaments versus spherical particles in flow and drug delivery. *Nat Nanotechnol* 2007;2:249-255.

(37) Champion JA, Mitragotri S. Role of target geometry in phagocytosis. *Proc Natl Acad Sci U S A* 2006;103:4930-4934.

(38) Champion JA, Mitragotri S. Shape induced inhibition of phagocytosis of polymer particles. *Pharm Res* 2009;26:244-249.

(39) Christian DA, Cai S, Garbuzenko OB et al. Flexible filaments for in vivo imaging and delivery: persistent circulation of filomicelles opens the

dosage window for sustained tumor shrinkage. *Mol Pharm* 2009;6:1343-1352.

(40) Zhang L, Cao Z, Li Y, Ella-Menye JR, Bai T, Jiang S. Softer zwitterionic nanogels for longer circulation and lower splenic accumulation. *ACS Nano* 2012;6:6681-6686.

(41) Kurrikoff K, Gestin M, Langel U. Recent in vivo advances in cell-penetrating peptide-assisted drug delivery. *Expert Opin Drug Deliv* 2016;13:373-387.

(42) Verma A, Stellacci F. Effect of surface properties on nanoparticle-cell interactions. *Small* 2010;6:12-21.

(43) Jiang W, Kim BY, Rutka JT, Chan WC. Nanoparticle-mediated cellular response is size-dependent. *Nat Nanotechnol* 2008;3:145-150.

(44) Gao H, Shi W, Freund LB. Mechanics of receptor-mediated endocytosis. *Proc Natl Acad Sci U S A* 2005;102:9469-9474.

(45) Rejman J, Oberle V, Zuhorn IS, Hoekstra D. Size-dependent internalization of particles via the pathways of clathrin- and caveolae-mediated endocytosis. *Biochem J* 2004;377:159-169.

(46) Langston Suen WL, Chau Y. Size-dependent internalisation of folate-decorated nanoparticles via the pathways of clathrin and caveolae-mediated endocytosis in ARPE-19 cells. *J Pharm Pharmacol* 2014;66:564-573.

(47) Xie X, Liao J, Shao X, Li Q, Lin Y. The Effect of shape on Cellular Uptake of Gold Nanoparticles in the forms of Stars, Rods, and Triangles. *Sci Rep* 2017;7:3827.

(48) Yameen B, Choi WI, Vilos C, Swami A, Shi J, Farokhzad OC. Insight into nanoparticle cellular uptake and intracellular targeting. *J Control Release* 2014;190:485-499.

(49) Liu X, Wu F, Tian Y et al. Size Dependent Cellular Uptake of Rod-like Bionanoparticles with Different Aspect Ratios. *Sci Rep* 2016;6:24567.

(50) Tkachenko AG, Xie H, Coleman D et al. Multifunctional gold nanoparticle-peptide complexes for nuclear targeting. *J Am Chem Soc* 2003;125:4700-4701.

(51) Medina-Kauwe LK, Xie J, Hamm-Alvarez S. Intracellular trafficking of nonviral vectors. *Gene Ther* 2005;12:1734-1751.

(52) Sun T, Zhang YS, Pang B, Hyun DC, Yang M, Xia Y. Engineered nanoparticles for drug delivery in cancer therapy. *Angew Chem Int Ed Engl* 2014;53:12320-12364.

(53) Wang Y, Sun S, Zhang Z, Shi D. Nanomaterials for Cancer Precision Medicine. *Adv Mater* 2018. Available online.

(54) Deci MB, Liu M, Dinh QT, Nguyen J. Precision engineering of targeted nanocarriers. *Wiley Interdiscip Rev Nanomed Nanobiotechnol* 2018. Available online.

(55) Rodriguez-Carmona E, Villaverde A. Nanostructured bacterial materials for innovative medicines. *Trends Microbiol* 2010;18:423-430.

(56) Ravindran S, Suthar JK, Rokade R et al. Pharmacokinetics, Metabolism, Distribution and Permeability of Nanomedicine. *Curr Drug Metab* 2018. Available online.

(57) Hassan S, Prakash G, Ozturk A et al. Evolution and Clinical Translation of Drug Delivery Nanomaterials. *Nano Today* 2017;15:91-106.

(58) Zhang L, Gu FX, Chan JM, Wang AZ, Langer RS, Farokhzad OC. Nanoparticles in medicine: therapeutic applications and developments. *Clin Pharmacol Ther* 2008;83:761-769.

(59) Ragelle H, Danhier F, Preat V, Langer R, Anderson DG. Nanoparticle-based drug delivery systems: a commercial and regulatory outlook as the field matures. *Expert Opin Drug Deliv* 2017;14:851-864.

(60) Miller KD, Siegel RL, Lin CC et al. Cancer treatment and survivorship statistics, 2016. *CA Cancer J Clin* 2016;66:271-289.

(61) Aggarwal S. Targeted cancer therapies. *Nat Rev Drug Discov* 2010;9(6):427–428.

(62) Da Silva CG, Peters GJ, Ossendorp F, Cruz LJ. The potential of multi-compound nanoparticles to bypass drug resistance in cancer. *Cancer Chemother Pharmacol* 2017;80:881-894.

(63) Li YJ, Lei YH, Yao N et al. Autophagy and multidrug resistance in cancer. *Chin J Cancer* 2017;36:52.

(64) Lee MS, Dees EC, Wang AZ. Nanoparticle-Delivered Chemotherapy: Old Drugs in New Packages. *Oncology (Williston Park)* 2017;31:198-208.

(65) Maeda H. Polymer therapeutics and the EPR effect. *J Drug Target* 2017;25:781-785.

(66) Torchilin VP. Cell penetrating peptide-modified pharmaceutical nanocarriers for intracellular drug and gene delivery. *Biopolymers* 2008;90:604-610.

(67) Fang J, Nakamura H, Maeda H. The EPR effect: Unique features of tumor blood vessels for drug delivery, factors involved, and limitations and augmentation of the effect. *Adv Drug Deliv Rev* 2011;63:136-151.

(68) Maeda H. Toward a full understanding of the EPR effect in primary and metastatic tumors as well as issues related to its heterogeneity. *Adv Drug Deliv Rev* 2015;91:3-6.

(69) Jain RK, Stylianopoulos T. Delivering nanomedicine to solid tumors. *Nat Rev Clin Oncol* 2010;7:653-664.

(70) Bae YH, Park K. Targeted drug delivery to tumors: myths, reality and possibility. *J Control Release* 2011;153:198-205.

(71) Sun T, Wu H, Li Y et al. Targeting transferrin receptor delivery of temozolomide for a potential glioma stem cell-mediated therapy. *Oncotarget* 2017;8:74451-74465.

(72) Lin R, Li Y, MacDonald T et al. Improving sensitivity and specificity of capturing and detecting targeted cancer cells with anti-biofouling polymer coated magnetic iron oxide nanoparticles. *Colloids Surf B Biointerfaces* 2017;150:261-270.

(73) Roy K, Patel YS, Kanwar RK, Rajkhowa R, Wang X, Kanwar JR. Biodegradable Eri silk nanoparticles as a delivery vehicle for bovine lactoferrin against MDA-MB-231 and MCF-7 breast cancer cells. *Int J Nanomedicine* 2016;11:25-44.

(74) Liang H, He L, Zhou B, Li B, Li J. Folate-functionalized assembly of low density lipoprotein/sodium carboxymethyl cellulose nanoparticles for targeted delivery. *Colloids Surf B Biointerfaces* 2017;156:19-28.

(75) Sampogna-Mireles D, Araya-Duran ID, Marquez-Miranda V, Valencia-Gallegos JA, Gonzalez-Nilo FD. Structural analysis of binding functionality of folic acid-PEG dendrimers against folate receptor. *J Mol Graph Model* 2017;72:201-208.

(76) Bwatanglang IB, Mohammad F, Yusof NA et al. In vivo tumor targeting and anti-tumor effects of 5-fluororacil loaded, folic acid targeted quantum dot system. *J Colloid Interface Sci* 2016;480:146-158.

(77) Cabezon I, Manich G, Martin-Venegas R, Camins A, Pelegri C, Vilaplana J. Trafficking of Gold Nanoparticles Coated with the 8D3 Anti-Transferrin Receptor Antibody at the Mouse Blood-Brain Barrier. *Mol Pharm* 2015;12:4137-4145.

(78) Altwerger G, Bonazzoli E, Bellone S et al. In vitro and in vivo activity of IMGN853, an Antibody-Drug Conjugate targeting Folate Receptor Alpha linked to DM4, in biologically aggressive endometrial cancers. *Mol Cancer Ther* 2018. Available online.

(79) Seidi K, Neubauer HA, Moriggl R, Jahanban-Esfahlan R, Javaheri T. Tumor target amplification: Implications for nano drug delivery systems. *J Control Release* 2018;275:142-161.

(80) Moulay G, Leborgne C, Mason AJ, Aisenbrey C, Kichler A, Bechinger B. Histidine-rich designer peptides of the LAH4 family promote cell delivery of a multitude of cargo. *J Pept Sci* 2017;23:320-328.

(81) Ferrer-Miralles N, Corchero JL, Kumar P et al. Biological activities of histidine-rich peptides; merging biotechnology and nanomedicine. *Microb Cell Fact* 2011;10:101.

(82) El-Sayed A, Futaki S, Harashima H. Delivery of macromolecules using arginine-rich cell-penetrating peptides: ways to overcome endosomal entrapment. *AAPS J* 2009;11:13-22.

(83) Ahmad A, Ranjan S, Zhang W, Zou J, Pyykko I, Kinnunen PK. Novel endosomolytic peptides for enhancing gene delivery in nanoparticles. *Biochim Biophys Acta* 2015;1848:544-553.

(84) Sanchez-Garcia L, Serna N, Mattanovich M et al. The fusogenic peptide HA2 impairs selectivity of CXCR4-targeted protein nanoparticles. *Chem Commun (Camb)* 2017;53:4565-4568.

(85) Liou JS, Liu BR, Martin AL, Huang YW, Chiang HJ, Lee HJ. Protein transduction in human cells is enhanced by cell-penetrating peptides fused with an endosomolytic HA2 sequence. *Peptides* 2012;37:273-284.

(86) Zhang W, Song J, Liang R et al. Stearylated antimicrobial peptide melittin and its retro isomer for efficient gene transfection. *Bioconjug Chem* 2013;24:1805-1812.

(87) Salomone F, Cardarelli F, Di LM et al. A novel chimeric cell-penetrating peptide with membrane-disruptive properties for efficient endosomal escape. *J Control Release* 2012;163:293-303.

(88) Van CE, Oliveira J. Advanced colorectal cancer: ESMO clinical recommendations for diagnosis, treatment and follow-up. *Ann Oncol* 2009;20 Suppl 4:61-63.

(89) Peitzsch C, Tyutyunnykova A, Pantel K, Dubrovska A. Cancer stem cells: The root of tumor recurrence and metastases. *Semin Cancer Biol* 2017;44:10-24.

(90) Vidal SJ, Rodriguez-Bravo V, Galsky M, Cordon-Cardo C, Domingo-Domenech J. Targeting cancer stem cells to suppress acquired chemotherapy resistance. *Oncogene* 2014;33:4451-4463.

(91) Chang JC. Cancer stem cells: Role in tumor growth, recurrence, metastasis, and treatment resistance. *Medicine (Baltimore)* 2016;95:S20-S25.

(92) Mishra J, Drummond J, Quazi SH et al. Prospective of colon cancer treatments and scope for combinatorial approach to enhanced cancer cell apoptosis. *Crit Rev Oncol Hematol* 2013;86:232-250.

(93) Medema JP. Targeting the Colorectal Cancer Stem Cell. *N Engl J Med* 2017;377:888-890.

(94) Zheng F, Zhang Z, Flamini V, Jiang WG, Cui Y. The Axis of CXCR4/SDF-1 Plays a Role in Colon Cancer Cell Adhesion Through Regulation of the AKT and IGF1R Signalling Pathways. *Anticancer Res* 2017;37:4361-4369.

(95) Cojoc M, Peitzsch C, Trautmann F, Polishchuk L, Telegeev GD, Dubrovska A. Emerging targets in cancer management: role of the CXCL12/CXCR4 axis. *Onco Targets Ther* 2013;6:1347-1361.

(96) Murakami T, Kawada K, Iwamoto M et al. The role of CXCR3 and CXCR4 in colorectal cancer metastasis. *Int J Cancer* 2013;132:276-287.

(97) Choi YJ, Chang WJ, Shin SW, Park KH, Kim ST, Kim YH. The prognostic role of serum C-X-C chemokine receptor type 4 in patients with metastatic or recurrent colorectal cancer. *Onco Targets Ther* 2016;9:3307-3312.

(98) Gassmann P, Haier J, Schluter K et al. CXCR4 regulates the early extravasation of metastatic tumor cells in vivo. *Neoplasia* 2009;11:651-661.

(99) Stanisavljevic L, Assmus J, Storli KE, Leh SM, Dahl O, Myklebust MP. CXCR4, CXCL12 and the relative CXCL12-CXCR4 expression as prognostic factors in colon cancer. *Tumour Biol* 2016;37:7441-7452.

(100) Fischer T, Nagel F, Jacobs S, Stumm R, Schulz S. Reassessment of CXCR4 chemokine receptor expression in human normal and neoplastic tissues using the novel rabbit monoclonal antibody UMB-2. *PLoS One* 2008;3:e4069.

(101) Katkoori VR, Basson MD, Bond VC, Manne U, Bumpers HL. Nef-M1, a peptide antagonist of CXCR4, inhibits tumor angiogenesis and epithelialtomesenchymal transition in colon and breast cancers. *Oncotarget* 2015;6:27763-27777.

(102) Trautmann F, Cojoc M, Kurth I et al. CXCR4 as biomarker for radioresistant cancer stem cells. *Int J Radiat Biol* 2014;90:687-699.

(103) Heckmann D, Maier P, Laufs S et al. CXCR4 Expression and Treatment with SDF-1alpha or Plerixafor Modulate Proliferation and Chemosensitivity of Colon Cancer Cells. *Transl Oncol* 2013;6:124-132.

(104) Ma L, Qiao H, He C et al. Modulating the interaction of CXCR4 and CXCL12 by low-molecular-weight heparin inhibits hepatic metastasis of colon cancer. *Invest New Drugs* 2012;30:508-517.

(105) Egusquiaguirre SP, Igartua M, Hernandez RM, Pedraz JL. Nanoparticle delivery systems for cancer therapy: advances in clinical and preclinical research. *Clin Transl Oncol* 2012;14:83-93.

(106) Lu ZR, Qiao P. Drug Delivery in Cancer Therapy, Quo Vadis? *Mol Pharm* 2018. Available online.

(107) Sharma A, Madhunapantula SV, Robertson GP. Toxicological considerations when creating nanoparticle-based drugs and drug delivery systems. *Expert Opin Drug Metab Toxicol* 2012;8:47-69.

(108) Strom CC, Andreasen HB. Comment on Neiser et al. Assessment of Dextran Antigenicity of Intravenous Iron Preparations with Enzyme-Linked Immunosorbent Assay (ELISA). Int. J. Mol. Sci. 2016, 17, 1185. *Int J Mol Sci* 2017;18.

(109) Neiser S, Koskenkorva TS, Schwarz K, Wilhelm M, Burckhardt S. Assessment of Dextran Antigenicity of Intravenous Iron Preparations with Enzyme-Linked Immunosorbent Assay (ELISA). *Int J Mol Sci* 2016;17.

(110) Duncan R, Izzo L. Dendrimer biocompatibility and toxicity. *Adv Drug Deliv Rev* 2005;57:2215-2237.

(111) Naahidi S, Jafari M, Edalat F, Raymond K, Khademhosseini A, Chen P. Biocompatibility of engineered nanoparticles for drug delivery. *J Control Release* 2013;166:182-194.

(112) Danhier F, Ansorena E, Silva JM, Coco R, Le BA, Preat V. PLGA-based nanoparticles: an overview of biomedical applications. *J Control Release* 2012;161:505-522.

(113) Semete B, Booysen L, Lemmer Y et al. In vivo evaluation of the biodistribution and safety of PLGA nanoparticles as drug delivery systems. *Nanomedicine* 2010;6:662-671.

(114) Gao W, Thamphiwatana S, Angsantikul P, Zhang L. Nanoparticle approaches against bacterial infections. *Wiley Interdiscip Rev Nanomed Nanobiotechnol* 2014;6:532-547.

(115) Spellberg B, Bartlett JG, Gilbert DN. The future of antibiotics and resistance. *N Engl J Med* 2013;368:299-302.

(116) Morens DM, Folkers GK, Fauci AS. The challenge of emerging and re-emerging infectious diseases. *Nature* 2004;430:242-249.

(117) Baltzer SA, Brown MH. Antimicrobial peptides: promising alternatives to conventional antibiotics. *J Mol Microbiol Biotechnol* 2011;20:228-235.

(118) Azzopardi EA, Ferguson EL, Thomas DW. The enhanced permeability retention effect: a new paradigm for drug targeting in infection. *J Antimicrob Chemother* 2013;68:257-274.

(119) Lee WL, Liles WC. Endothelial activation, dysfunction and permeability during severe infections. *Curr Opin Hematol* 2011;18:191-196.

(120) DiStasi MR, Ley K. Opening the flood-gates: how neutrophil-endothelial interactions regulate permeability. *Trends Immunol* 2009;30:547-556.

(121) Taylor SL, Wahl-Jensen V, Copeland AM, Jahrling PB, Schmaljohn CS. Endothelial cell permeability during hantavirus infection involves factor XII-dependent increased activation of the kallikrein-kinin system. *PLoS Pathog* 2013;9:e1003470.

(122) Boerman et al. Sterically stabilized liposomes labeled with indium-111 to image focal infection. J Nucl Med. 1995; 36, 1639-1644.

(123) Oyen WJ, et al. Detecting infection and inflammation with technetium-99m-labeled stealth(r) liposomes. J Nucl Med. 1996; 37, 1392-1397.

(124) Sundar S, Prajapati VK. Drug targeting to infectious diseases by nanoparticles surface functionalized with special biomolecules. *Curr Med Chem* 2012;19:3196-3202.

(125) Choi SK, Myc A, Silpe JE et al. Dendrimer-based multivalent vancomycin nanoplatform for targeting the drug-resistant bacterial surface. *ACS Nano* 2013;7:214-228.

(126) Choi KH, Lee HJ, Park BJ et al. Photosensitizer and vancomycin-conjugated novel multifunctional magnetic particles as photoinactivation agents for selective killing of pathogenic bacteria. *Chem Commun (Camb)* 2012;48:4591-4593.

(127) Chen J, Zhang C, Liu Q et al. Solanum tuberosum lectin-conjugated PLGA nanoparticles for nose-to-brain delivery: in vivo and in vitro evaluations. *J Drug Target* 2012;20:174-184.

(128) Umamaheshwari RB, Jain NK. Receptor mediated targeting of lectin conjugated gliadin nanoparticles in the treatment of Helicobacter pylori. *J Drug Target* 2003;11:415-423.

(129) Huang PJ, Tay LL, Tanha J, Ryan S, Chau LK. Single-domain antibody-conjugated nanoaggregate-embedded beads for targeted detection of pathogenic bacteria. *Chemistry* 2009;15:9330-9334.

(130) Tay LL, Huang PJ, Tanha J et al. Silica encapsulated SERS nanoprobe conjugated to the bacteriophage tailspike protein for targeted detection of Salmonella. *Chem Commun (Camb)* 2012;48:1024-1026.

(131) Duan N, Wu S, Chen X et al. Selection and characterization of aptamers against Salmonella typhimurium using whole-bacterium Systemic Evolution of Ligands by Exponential Enrichment (SELEX). *J Agric Food Chem* 2013;61:3229-3234.

(132) Chen F, Zhou J, Luo F, Mohammed AB, Zhang XL. Aptamer from whole-bacterium SELEX as new therapeutic reagent against virulent Mycobacterium tuberculosis. *Biochem Biophys Res Commun* 2007;357:743-748.

(133) Dillen K, Bridts C, Van d, V et al. Adhesion of PLGA or Eudragit/PLGA nanoparticles to Staphylococcus and Pseudomonas. *Int J Pharm* 2008;349:234-240.

(134) Nederberg F, Zhang Y, Tan JP et al. Biodegradable nanostructures with selective lysis of microbial membranes. *Nat Chem* 2011;3:409-414.

(135) Sambhy V, Peterson BR, Sen A. Antibacterial and hemolytic activities of pyridinium polymers as a function of the spatial relationship between the positive charge and the pendant alkyl tail. *Angew Chem Int Ed Engl* 2008;47:1250-1254.

(136) Liu L, Xu K, Wang H et al. Self-assembled cationic peptide nanoparticles as an efficient antimicrobial agent. *Nat Nanotechnol* 2009;4:457-463.

(137) Wang L, Hu C, Shao L. The antimicrobial activity of nanoparticles: present situation and prospects for the future. *Int J Nanomedicine* 2017;12:1227-1249.

(138) Chopra I. The increasing use of silver-based products as antimicrobial agents: a useful development or a cause for concern? *J Antimicrob Chemother* 2007;59:587-590.

(139) Grangeasse C, Obadia B, Mijakovic I, Deutscher J, Cozzone AJ, Doublet P. Autophosphorylation of the Escherichia coli protein kinase Wzc regulates tyrosine phosphorylation of Ugd, a UDP-glucose dehydrogenase. *J Biol Chem* 2003;278:39323-39329.

(140) Dakal TC, Kumar A, Majumdar RS, Yadav V. Mechanistic Basis of Antimicrobial Actions of Silver Nanoparticles. *Front Microbiol* 2016;7:1831.

(141) Duran N, Silveira CP, Duran M, Martinez DS. Silver nanoparticle protein corona and toxicity: a mini-review. *J Nanobiotechnology* 2015;13:55.

(142) Manivasagan P, Venkatesan J, Senthilkumar K, Sivakumar K, Kim SK. Biosynthesis, antimicrobial and cytotoxic effect of silver nanoparticles using a novel Nocardiopsis sp. MBRC-1. *Biomed Res Int* 2013;2013:287638.

(143) Gnanadhas DP, Ben TM, Thomas R, Raichur AM, Chakravortty D. Interaction of silver nanoparticles with serum proteins affects their antimicrobial activity in vivo. *Antimicrob Agents Chemother* 2013;57:4945-4955.

(144) Stone NR, Bicanic T, Salim R, Hope W. Liposomal Amphotericin B (AmBisome((R))): A Review of the Pharmacokinetics, Pharmacodynamics, Clinical Experience and Future Directions. *Drugs* 2016;76:485-500.

(145) Sharma A, Madhunapantula SV, Robertson GP. Toxicological considerations when creating nanoparticle-based drugs and drug delivery systems. *Expert Opin Drug Metab Toxicol* 2012;8:47-69.

(146) Dunn JS, Wyburn GM. The anatomy of the blood brain barrier: a review. *Scott Med J* 1972;17:21-36.

(147) Zhou Y, Peng Z, Seven ES, Leblanc RM. Crossing the blood-brain barrier with nanoparticles. *J Control Release* 2018;270:290-303.

(148) Dong X. Current Strategies for Brain Drug Delivery. *Theranostics* 2018;8:1481-1493.

(149) Kaushik A, Jayant RD, Bhardwaj V, Nair M. Personalized nanomedicine for CNS diseases. *Drug Discov Today* 2017;8:1341-1254.

(150) Eichler AF, Chung E, Kodack DP, Loeffler JS, Fukumura D, Jain RK. The biology of brain metastases-translation to new therapies. *Nat Rev Clin Oncol* 2011;8:344-356.

(151) Lajoie JM, Shusta EV. Targeting receptor-mediated transport for delivery of biologics across the blood-brain barrier. *Annu Rev Pharmacol Toxicol* 2015;55:613-631.

(152) Daneman R, Zhou L, Agalliu D, Cahoy JD, Kaushal A, Barres BA. The mouse blood-brain barrier transcriptome: a new resource for understanding the development and function of brain endothelial cells. *PLoS One* 2010;5:13741.

(153) Uchida Y, Ohtsuki S, Katsukura Y et al. Quantitative targeted absolute proteomics of human blood-brain barrier transporters and receptors. *J Neurochem* 2011;117:333-345.

(154) Kim JS, Shin DH, Kim JS. Dual-targeting immunoliposomes using angiopep-2 and CD133 antibody for glioblastoma stem cells. *J Control Release* 2018;269:245-257.

(155) Velasco-Aguirre C, Morales-Zavala F, Salas-Huenuleo E et al. Improving gold nanorod delivery to the central nervous system by conjugation to the shuttle Angiopep-2. *Nanomedicine (Lond)* 2017;12:2503-2517.

(156) Han W, Yin G, Pu X, Chen X, Liao X, Huang Z. Glioma targeted delivery strategy of doxorubicin-loaded liposomes by dual-ligand modification. *J Biomater Sci Polym Ed* 2017;28:1695-1712.

(157) Lu F, Pang Z, Zhao J et al. Angiopep-2-conjugated poly(ethylene glycol)-co- poly(epsilon-caprolactone) polymersomes for dual-targeting drug delivery to glioma in rats. *Int J Nanomedicine* 2017;12:2117-2127.

(158) Lu MJ, inventors. Peptide for transmigration across blood brain barrier and delivery systems comprising the same. 2014. Patent.

(159) Serna N, Cespedes MV, Saccardo P et al. Rational engineering of single-chain polypeptides into protein-only, BBB-targeted nanoparticles. *Nanomedicine* 2016;12:1241-1251.

(160) He Q, Liu J, Liang J et al. Towards Improvements for Penetrating the Blood-Brain Barrier-Recent Progress from a Material and Pharmaceutical Perspective. *Cells* 2018;7.

(161) Tsou YH, Zhang XQ, Zhu H, Syed S, Xu X. Drug Delivery to the Brain across the Blood-Brain Barrier Using Nanomaterials. *Small* 2017;13.

(162) Ishii T, Asai T, Oyama D et al. Treatment of cerebral ischemia-reperfusion injury with PEGylated liposomes encapsulating FK506. *FASEB J* 2013;27:1362-1370.

(163) Li Y, He H, Jia X, Lu WL, Lou J, Wei Y. A dual-targeting nanocarrier based on poly(amidoamine) dendrimers conjugated with transferrin and tamoxifen for treating brain gliomas. *Biomaterials* 2012;33:3899-3908.

(164) Somani S, Blatchford DR, Millington O, Stevenson ML, Dufes C. Transferrin-bearing polypropylenimine dendrimer for targeted gene delivery to the brain. *J Control Release* 2014;188:78-86.

(165) Ganta S, Deshpande D, Korde A, Amiji M. A review of multifunctional nanoemulsion systems to overcome oral and CNS drug delivery barriers. *Mol Membr Biol* 2010;27:260-273.

(166) Mahajan HS, Mahajan MS, Nerkar PP, Agrawal A. Nanoemulsion-based intranasal drug delivery system of saquinavir mesylate for brain targeting. *Drug Deliv* 2014;21:148-154.

(167) Peluffo H, Unzueta U, Negro-Demontel ML et al. BBB-targeting, protein-based nanomedicines for drug and nucleic acid delivery to the CNS. *Biotechnol Adv* 2015;33:277-287.

(168) Serna N, Sanchez-Garcia L, Unzueta U et al. Protein-Based Therapeutic Killing for Cancer Therapies. *Trends Biotechnol* 2018;36:318-335.

(169) Bobo D, Robinson KJ, Islam J, Thurecht KJ, Corrie SR. Nanoparticle-Based Medicines: A Review of FDA-Approved Materials and Clinical Trials to Date. *Pharm Res* 2016;33:2373-2387.

(170) Spicer CD, Davis BG. Selective chemical protein modification. *Nat Commun* 2014;5:4740.

(171) Tsuchikama K, An Z. Antibody-drug conjugates: recent advances in conjugation and linker chemistries. *Protein Cell* 2018;9:33-46.

(172) Polakis P. Antibody Drug Conjugates for Cancer Therapy. *Pharmacol Rev* 2016;68:3-19.

(173) Lohcharoenkal W, Wang L, Chen YC, Rojanasakul Y. Protein nanoparticles as drug delivery carriers for cancer therapy. *Biomed Res Int* 2014;2014:180549.

(174) Ko S, Gunasekaran S. Preparation of sub-100-nm beta-lactoglobulin (BLG) nanoparticles. *J Microencapsul* 2006;23:887-898.

(175) Duclairoir C, Orecchioni AM, Depraetere P, Nakache E. Alpha-tocopherol encapsulation and in vitro release from wheat gliadin nanoparticles. *J Microencapsul* 2002;19:53-60.

(176) Bilati U, Allemann E, Doelker E. Nanoprecipitation versus emulsion-based techniques for the encapsulation of proteins into biodegradable nanoparticles and process-related stability issues. *AAPS PharmSciTech* 2005;6:E594-E604.

(177) Gradishar WJ. Albumin-bound paclitaxel: a next-generation taxane. *Expert Opin Pharmacother* 2006;7:1041-1053.

(178) Lambert JM, Berkenblit A. Antibody-Drug Conjugates for Cancer Treatment. *Annu Rev Med* 2018;69:191-207.

(179) Dy GK, Adjei AA. Understanding, recognizing, and managing toxicities of targeted anticancer therapies. *CA Cancer J Clin* 2013;63:249-279.

(180) Richards DA, Maruani A, Chudasama V. Antibody fragments as nanoparticle targeting ligands: a step in the right direction. *Chem Sci* 2017;8:63-77.

(181) Doll TA, Raman S, Dey R, Burkhard P. Nanoscale assemblies and their biomedical applications. *J R Soc Interface* 2013;10:20120740.

(182) Schoonen L, van Hest JC. Functionalization of protein-based nanocages for drug delivery applications. *Nanoscale* 2014;6:7124-7141.

(183) Ferrer-Miralles N, Rodriguez-Carmona E, Corchero JL, Garcia-Fruitos E, Vazquez E, Villaverde A. Engineering protein self-assembling in protein-based nanomedicines for drug delivery and gene therapy. *Crit Rev Biotechnol* 2015;35:209-221.

(184) Lee LA, Wang Q. Adaptations of nanoscale viruses and other protein cages for medical applications. *Nanomedicine* 2006;2:137-149.

(185) He D, Marles-Wright J. Ferritin family proteins and their use in bionanotechnology. *N Biotechnol* 2015;32:651-657.

(186) Sana B, Johnson E, Lim S. The unique self-assembly/disassembly property of Archaeoglobus fulgidus ferritin and its implications on molecular release from the protein cage. *Biochim Biophys Acta* 2015;1850:2544-2551.

(187) Flenniken ML, Liepold LO, Crowley BE, Willits DA, Young MJ, Douglas T. Selective attachment and release of a chemotherapeutic agent from the interior of a protein cage architecture. *Chem Commun* 2005;447-449.

(188) Toita R, Murata M, Tabata S et al. Development of human hepatocellular carcinoma cell-targeted protein cages. *Bioconjug Chem* 2012;23:1494-1501.

(189) Poderycki MJ, Kickhoefer VA, Kaddis CS et al. The vault exterior shell is a dynamic structure that allows incorporation of vault-associated proteins into its interior. *Biochemistry* 2006;45:12184-12193.

(190) Matsumoto NM, Prabhakaran P, Rome LH, Maynard HD. Smart vaults: thermally-responsive protein nanocapsules. *ACS Nano* 2013;7:867-874.

(191) Douglas T, Young M. Viruses: making friends with old foes. *Science* 2006;312:873-875.

(192) Kushnir N, Streatfield SJ, Yusibov V. Virus-like particles as a highly efficient vaccine platform: diversity of targets and production systems and advances in clinical development. *Vaccine* 2012;31:58-83.

(193) Ghasparian A, Riedel T, Koomullil J et al. Engineered synthetic virus-like particles and their use in vaccine delivery. *Chembiochem* 2011;12:100-109.

(194) Grgacic EV, Anderson DA. Virus-like particles: passport to immune recognition. *Methods* 2006;40:60-65.

(195) Rohovie MJ, Nagasawa M, Swartz JR. Virus-like particles: Next-generation nanoparticles for targeted therapeutic delivery. *Bioeng Transl Med* 2017;2:43-57.

(196) Jariyapong P. Nodavirus-based biological container for targeted delivery system. *Artif Cells Nanomed Biotechnol* 2015;43:355-360.

(197) Manchester M, Singh P. Virus-based nanoparticles (VNPs): platform technologies for diagnostic imaging. *Adv Drug Deliv Rev* 2006;58:1505-1522.

(198) Seow Y, Wood MJ. Biological gene delivery vehicles: beyond viral vectors. *Mol Ther* 2009;17:767-777.

(199) Tasciotti E. Smart cancer therapy with DNA origami. *Nat Biotechnol* 2018;36:234-235.

(200) Gradisar H, Jerala R. Self-assembled bionanostructures: proteins following the lead of DNA nanostructures. *J Nanobiotechnology* 2014;12:4.

(201) Luo Q, Hou C, Bai Y, Wang R, Liu J. Protein Assembly: Versatile Approaches to Construct Highly Ordered Nanostructures. *Chem Rev* 2016;116:13571-13632.

(202) Lee EJ, Lee NK, Kim IS. Bioengineered protein-based nanocage for drug delivery. *Adv Drug Deliv Rev* 2016;106:157-171.

(203) Bromley EH, Channon K, Moutevelis E, Woolfson DN. Peptide and protein building blocks for synthetic biology: from programming biomolecules to self-organized biomolecular systems. *ACS Chem Biol* 2008;3:38-50.

(204) Taler-Vercic A, Kirsipuu T, Friedemann M et al. The role of initial oligomers in amyloid fibril formation by human stefin B. *Int J Mol Sci* 2013;14:18362-18384.

(205) Woolfson DN, Ryadnov MG. Peptide-based fibrous biomaterials: Some things old, new and borrowed. *Curr Opin Chem Biol* 2006;10:559-567.

(206) Ganesh S, Prakash S, Jayakumar R. Spectroscopic investigation on gel-forming beta-sheet assemblage of peptide derivatives. *Biopolymers* 2003;70:346-354.

(207) Dong H, Paramonov SE, Hartgerink JD. Self-assembly of alpha-helical coiled coil nanofibers. *J Am Chem Soc* 2008;130:13691-13695.

(208) Mason JM, Muller KM, Arndt KM. Considerations in the design and optimization of coiled coil structures. *Methods Mol Biol* 2007;352:35-70.

(209) Ryadnov MG, Woolfson DN. Engineering the morphology of a self-assembling protein fibre. *Nat Mater* 2003;2:329-332.

(210) Peng X, Jin J, Nakamura Y, Ohno T, Ichinose I. Ultrafast permeation of water through protein-based membranes. *Nat Nanotechnol* 2009;4:353-357.

(211) Ueda M, Makino A, Imai T, Sugiyama J, Kimura S. Rational design of peptide nanotubes for varying diameters and lengths. *J Pept Sci* 2011;17:94-99.

(212) Knowles TP, Oppenheim TW, Buell AK, Chirgadze DY, Welland ME. Nanostructured films from hierarchical self-assembly of amyloidogenic proteins. *Nat Nanotechnol* 2010;5:204-207.

(213) Gour N, Mondal S, Verma S. Synthesis and self-assembly of a neoglycopeptide: morphological studies and ultrasound-mediated DNA encapsulation. *J Pept Sci* 2011;17:148-153.

(214) Banwell EF, Abelardo ES, Adams DJ et al. Rational design and application of responsive alpha-helical peptide hydrogels. *Nat Mater* 2009;8:596-600.

(215) Raman S, Machaidze G, Lustig A, Aebi U, Burkhard P. Structure-based design of peptides that self-assemble into regular polyhedral nanoparticles. *Nanomedicine* 2006;2:95-102.

(216) Vazquez E, Villaverde A. Engineering building blocks for self-assembling protein nanoparticles. *Microb Cell Fact* 2010;9:101.

(217) Nikitin MP, Zdobnova TA, Lukash SV, Stremovskiy OA, Deyev SM. Protein-assisted self-assembly of multifunctional nanoparticles. *Proc Natl Acad Sci U S A* 2010;107:5827-5832.

(218) Ferrer-Miralles N, Rodriguez-Carmona E, Corchero JL, Garcia-Fruitos E, Vazquez E, Villaverde A. Engineering protein self-assembling in protein-based nanomedicines for drug delivery and gene therapy. *Crit Rev Biotechnol* 2015;35:209-221.

(219) Unzueta U, Cespedes MV, Vazquez E, Ferrer-Miralles N, Mangues R, Villaverde A. Towards protein-based viral mimetics for cancer therapies. *Trends Biotechnol* 2015;33:253-258.

(220) Sanchez-Garcia L, Martin L, Mangues R, Ferrer-Miralles N, Vazquez E, Villaverde A. Recombinant pharmaceuticals from microbial cells: a 2015 update. *Microb Cell Fact* 2016;15:33.

(221) Rosano GL, Ceccarelli EA. Recombinant protein expression in Escherichia coli: advances and challenges. *Front Microbiol* 2014;5:172.

(222) Jenkins N. Modifications of therapeutic proteins: challenges and prospects. *Cytotechnology* 2007;53:121-125.

(223) Walsh G, Jefferis R. Post-translational modifications in the context of therapeutic proteins. *Nat Biotechnol* 2006;24:1241-1252.

(224) Lau BT, Malkus P, Paulsson J. New quantitative methods for measuring plasmid loss rates reveal unexpected stability. *Plasmid* 2013;70:353-361.

(225) Martinez-Alonso M, Gonzalez-Montalban N, Garcia-Fruitos E, Villaverde A. Learning about protein solubility from bacterial inclusion bodies. *Microb Cell Fact* 2009;8:4.

(226) Garcia-Fruitos E, Sabate R, de Groot NS, Villaverde A, Ventura S. Biological role of bacterial inclusion bodies: a model for amyloid aggregation. *FEBS J* 2011;278:2419-2427.

(227) Mamat U, Wilke K, Bramhill D et al. Detoxifying Escherichia coli for endotoxin-free production of recombinant proteins. *Microb Cell Fact* 2015;14:57.

(228) Low KO, Muhammad MN, Md IR. Optimisation of signal peptide for recombinant protein secretion in bacterial hosts. *Appl Microbiol Biotechnol* 2013;97:3811-3826.

(229) Ferrer-Miralles N, Villaverde A. Bacterial cell factories for recombinant protein production; expanding the catalogue. *Microb Cell Fact* 2013;12:113.

(230) Corchero JL, Gasser B, Resina D et al. Unconventional microbial systems for the cost-efficient production of high-quality protein therapeutics. *Biotechnol Adv* 2013;31:140-153.

(231) Rueda F, Cespedes MV, Sanchez-Chardi A et al. Structural and functional features of self-assembling protein nanoparticles produced in endotoxin-free Escherichia coli. *Microb Cell Fact* 2016;15:59.

(232) Cano-Garrido O, Sanchez-Chardi A, Pares S et al. Functional protein-based nanomaterial produced in microorganisms recognized as safe: A new platform for biotechnology. *Acta Biomater* 2016;43:230-239.

(233) Cano-Garrido O, Seras-Franzoso J, Garcia-Fruitos E. Lactic acid bacteria: reviewing the potential of a promising delivery live vector for biomedical purposes. *Microb Cell Fact* 2015;14:137.

(234) Cespedes MV, Unzueta U, Tatkiewicz W et al. In vivo architectonic stability of fully de novo designed protein-only nanoparticles. *ACS Nano* 2014;8:4166-4176.

(235) Unzueta U, Ferrer-Miralles N, Cedano J et al. Non-amyloidogenic peptide tags for the regulatable self-assembling of protein-only nanoparticles. *Biomaterials* 2012;33:8714-8722.

(236) Pesarrodona M, Ferrer-Miralles N, Unzueta U et al. Intracellular targeting of CD44+ cells with self-assembling, protein only nanoparticles. *Int J Pharm* 2014;473:286-295.

(237) Unzueta U, Cespedes MV, Ferrer-Miralles N et al. Intracellular CXCR4(+) cell targeting with T22-empowered protein-only nanoparticles. *Int J Nanomedicine* 2012;7:4533-4544.

(238) Sharma A, Madhunapantula SV, Robertson GP. Toxicological considerations when creating nanoparticle-based drugs and drug delivery systems. *Expert Opin Drug Metab Toxicol* 2012;8:47-69.

(239) Lagasse HA, Alexaki A, Simhadri VL et al. Recent advances in (therapeutic protein) drug development. *F1000Res* 2017;6:113.

(240) Cragg GM, Newman DJ. Natural products: a continuing source of novel drug leads. *Biochim Biophys Acta* 2013;1830:3670-3695.

(241) La Spada AR, Weydt P. Targeting toxic proteins for turnover. *Nat Med* 2005;11:1052-1053.

(242) Yin L, Chen X, Vicini P, Rup B, Hickling TP. Therapeutic outcomes, assessments, risk factors and mitigation efforts of immunogenicity of therapeutic protein products. *Cell Immunol* 2015;295:118-126.

(243) Hertler AA, Frankel AE. Immunotoxins: a clinical review of their use in the treatment of malignancies. *J Clin Oncol* 1989;7:1932-1942.

(244) Bergonzi MC, Guccione C, Grossi C et al. Albumin Nanoparticles for Brain Delivery: A Comparison of Chemical versus Thermal Methods and in vivo Behavior. *ChemMedChem* 2016;11:1840-1849.

(245) Patra S, Basak P, Tibarewala DN. Synthesis of gelatin nano/submicron particles by binary nonsolvent aided coacervation (BNAC) method. *Mater Sci Eng C Mater Biol Appl* 2016;59:310-318.

(246) Elzoghby AO. Gelatin-based nanoparticles as drug and gene delivery systems: reviewing three decades of research. *J Control Release* 2013;172:1075-1091.

(247) Lu HD, Zhao HQ, Wang K, Lv LL. Novel hyaluronic acid-chitosan nanoparticles as non-viral gene delivery vectors targeting osteoarthritis. *Int J Pharm* 2011;420:358-365.

(248) Gradisar H, Jerala R. Self-assembled bionanostructures: proteins following the lead of DNA nanostructures. *J Nanobiotechnology* 2014;12:4.

(249) Maham A, Tang Z, Wu H, Wang J, Lin Y. Protein-based nanomedicine platforms for drug delivery. *Small* 2009;5:1706-1721.

(250) Collins L, Parker AL, Gehman JD et al. Self-assembly of peptides into spherical nanoparticles for delivery of hydrophilic moieties to the cytosol. *ACS Nano* 2010;4:2856-2864.

(251) Hassouneh W, Zhulina EB, Chilkoti A, Rubinstein M. Elastin-like Polypeptide Diblock Copolymers Self-Assemble into Weak Micelles. *Macromolecules* 2015;48:4183-4195.

(252) Molino NM, Wang SW. Caged protein nanoparticles for drug delivery. *Curr Opin Biotechnol* 2014;28:75-82.

(253) van VR, Pieters RJ, Breukink E. Site-specific functionalization of proteins and their applications to therapeutic antibodies. *Comput Struct Biotechnol J* 2014;9:e201402001.

(254) Basle E, Joubert N, Pucheault M. Protein chemical modification on endogenous amino acids. *Chem Biol* 2010;17:213-227.

(255) Petschauer JS, Madden AJ, Kirschbrown WP, Song G, Zamboni WC. The effects of nanoparticle drug loading on the pharmacokinetics of anticancer agents. *Nanomedicine (Lond)* 2015;10:447-463.

(256) Kristensen M, Birch D, Morck NH. Applications and Challenges for Use of Cell-Penetrating Peptides as Delivery Vectors for Peptide and Protein Cargos. *Int J Mol Sci* 2016;17.

(257) Zhikun Xu, et al. Targeting low-density lipoprotein receptors with protein-only nanoparticles. *Journal of Nanoparticle Research*. 2018. Available online.

(258) Cespedes MV, Unzueta U, Tatkiewicz W et al. In vivo architectonic stability of fully de novo designed protein-only nanoparticles. *ACS Nano* 2014;8:4166-4176.

(259) McCully M, Sanchez-Navarro M, Teixido M, Giralt E. Peptide Mediated Brain Delivery of Nano- and Submicroparticles: a Synergistic Approach. *Curr Pharm Des* 2017;33:134-142.

(260) Unzueta U, Saccardo P, Ferrer-Miralles N et al. Improved performance of protein-based recombinant gene therapy vehicles by tuning downstream procedures. *Biotechnol Prog* 2013;29:1458-1463.

(261) Domingo-Espin J, Petegnief V, de VN et al. RGD-based cell ligands for cell-targeted drug delivery act as potent trophic factors. *Nanomedicine* 2012;8:1263-1266.

(262) Garberg P, Ball M, Borg N et al. In vitro models for the blood-brain barrier. *Toxicol In Vitro* 2005;19:299-334.

(263) Zhang GM, Wang MY, Liu YN et al. Functional variants in the low-density lipoprotein receptor gene are associated with clear cell renal cell carcinoma susceptibility. *Carcinogenesis* 2017;38:1241-1248.

(264) Chung NS, Sachs-Barrable K, Lee SD, Wasan KM. Suitability of LLC-PK1 pig kidney cells for the study of drug action on renal cell cholesterol uptake: identification and characterization of low-density lipoprotein receptors. *J Pharmacol Toxicol Methods* 2005;51:139-145.

(265) King GF. Venoms as a platform for human drugs: translating toxins into therapeutics. *Expert Opin Biol Ther* 2011;11:1469-1484.

(266) Harvey AL. Toxins and drug discovery. *Toxicon* 2014;92:193-200.

(267) De Groot AS, Scott DW. Immunogenicity of protein therapeutics. *Trends Immunol* 2007;28:482-490.

(268) Deslouches B, Di YP. Antimicrobial peptides with selective antitumor mechanisms: prospect for anticancer applications. *Oncotarget* 2017;8:46635-46651.

(269) Huang Z. Bcl-2 family proteins as targets for anticancer drug design. *Oncogene* 2000;19:6627-6631.

(270) Baeuerle PA, Murry JA. Human therapies as a successful liaison between chemistry and biology. *Chem Biol* 2014;21:1046-1054.

(271) Sellers WR, Fisher DE. Apoptosis and cancer drug targeting. *J Clin Invest* 1999;104:1655-1661.

(272) Soderquist S, Eastman A. BCL2 Inhibitors as Anticancer Drugs: A Plethora of Misleading BH3 Mimetics. *Mol Cancer Ther* 2016;15:2011-2017.

(273) Delbridge AR, Strasser A. The BCL-2 protein family, BH3-mimetics and cancer therapy. *Cell Death Differ* 2015;22:1071-1080.

(274) Vandenberg CJ, Cory S. ABT-199, a new Bcl-2-specific BH3 mimetic, has in vivo efficacy against aggressive Myc-driven mouse lymphomas without provoking thrombocytopenia. *Blood* 2013;121:2285-2288.

(275) Chiappori AA, Schreeder MT, Moezi MM et al. A phase I trial of pan-Bcl-2 antagonist obatoclax administered as a 3-h or a 24-h infusion in combination with carboplatin and etoposide in patients with extensive-stage small cell lung cancer. *Br J Cancer* 2012;106:839-845.

(276) Orzechowska EJ, Kozlowska E, Czubaty A, Kozlowski P, Staron K, Trzcinska-Danielewicz J. Controlled delivery of BID protein fused with TAT peptide sensitizes cancer cells to apoptosis. *BMC Cancer* 2014;14:771.

(277) Eric P.Holinger, et al. Bak BH3 Peptides Antagonize Bcl-xL Function and Induce Apoptosis through Cytochrome c-independent Activation of Caspases. *Journal of Biological Chemistry* 1999;274:13298-304.

(278) Azar Y, Lorberboum-Galski H. GnRH-Bik/Bax/Bak chimeric proteins target and kill adenocarcinoma cells; the general use of pro-apoptotic proteins of the Bcl-2 family as novel killing components of targeting chimeric proteins. *Apoptosis* 2000;5:531-542.

(279) Antignani A, Youle RJ. A chimeric protein induces tumor cell apoptosis by delivering the human Bcl-2 family BH3-only protein Bad. *Biochemistry* 2005;44:4074-4082.

(280) Wang F, Ren J, Qiu XC et al. Selective cytotoxicity to HER2-positive tumor cells by a recombinant e23sFv-TD-tBID protein containing a furin cleavage sequence. *Clin Cancer Res* 2010;16:2284-2294.

(281) Leshchiner ES, Braun CR, Bird GH, Walensky LD. Direct activation of full-length proapoptotic BAK. *Proc Natl Acad Sci U S A* 2013;110:E986-E995.

(282) Senft D, Weber A, Saathoff F et al. In non-transformed cells Bak activates upon loss of anti-apoptotic Bcl-XL and Mcl-1 but in the absence of active BH3-only proteins. *Cell Death Dis* 2015;6:1996.

(283) Chen HC, Kanai M, Inoue-Yamauchi A et al. An interconnected hierarchical model of cell death regulation by the BCL-2 family. *Nat Cell Biol* 2015;17:1270-1281.

(284) Dai H, Pang YP, Ramirez-Alvarado M, Kaufmann SH. Evaluation of the BH3-only protein Puma as a direct Bak activator. *J Biol Chem* 2014;289:89-99.

(285) Edwards AL, Gavathiotis E, LaBelle JL et al. Multimodal interaction with BCL-2 family proteins underlies the proapoptotic activity of PUMA BH3. *Chem Biol* 2013;20:888-902.

(286) Chen YL, Li JH, Yu CY et al. Novel cationic antimicrobial peptide GW-H1 induced caspase-dependent apoptosis of hepatocellular carcinoma cell lines. *Peptides* 2012;36:257-265.

(287) Chou HT, Kuo TY, Chiang JC et al. Design and synthesis of cationic antimicrobial peptides with improved activity and selectivity against Vibrio spp. *Int J Antimicrob Agents* 2008;32:130-138.

(288) Sandvig K, Torgersen ML, Engedal N, Skotland T, Iversen TG. Protein toxins from plants and bacteria: probes for intracellular transport and tools in medicine. *FEBS Lett* 2010;584:2626-2634.

(289) Huang HW. Free energies of molecular bound states in lipid bilayers: lethal concentrations of antimicrobial peptides. *Biophys J* 2009;96:3263-3272.

(290) Lee H, Iglewski WJ. Cellular ADP-ribosyltransferase with the same mechanism of action as diphtheria toxin and Pseudomonas toxin A. *Proc Natl Acad Sci U S A* 1984;81:2703-2707.

(291) Onda M, Beers R, Xiang L et al. Recombinant immunotoxin against B-cell malignancies with no immunogenicity in mice by removal of B-cell epitopes. *Proc Natl Acad Sci U S A* 2011;108:5742-5747.

(292) Kreitman RJ, Pastan I. Importance of the glutamate residue of KDEL in increasing the cytotoxicity of Pseudomonas exotoxin derivatives and for increased binding to the KDEL receptor. *Biochem J* 1995;307:29-37.

(293) Wang T, Zhao J, Ren JL et al. Recombinant immunoproapoptotic proteins with furin site can translocate and kill HER2-positive cancer cells. *Cancer Res* 2007;67:11830-11839.

(294) Sandvig K, Torgersen ML, Engedal N, Skotland T, Iversen TG. Protein toxins from plants and bacteria: probes for intracellular transport and tools in medicine. *FEBS Lett* 2010;584:2626-2634.

(295) Unzueta U, Serna N, Sanchez-Garcia L et al. Engineering multifunctional protein nanoparticles by in vitro disassembling and reassembling of heterologous building blocks. *Nanotechnology* 2017;28:505102.

(296) Unzueta U, Seras-Franzoso J, Cespedes MV et al. Engineering tumor cell targeting in nanoscale amyloidal materials. *Nanotechnology* 2017;28:015102.

(297) Vazquez E, Cubarsi R, Unzueta U et al. Internalization and kinetics of nuclear migration of protein-only, arginine-rich nanoparticles. *Biomaterials* 2010;31:9333-9339.

(298) Ansari AM, Ahmed AK, Matsangos AE et al. Cellular GFP Toxicity and Immunogenicity: Potential Confounders in in Vivo Cell Tracking Experiments. *Stem Cell Rev* 2016;12:553-559.

(299) Wilson MR, Jones DS, Andrews GP. The development of sustained release drug delivery platforms using melt-extruded cellulose-based polymer blends. *J Pharm Pharmacol* 2017;69:32-42.

(300) Unzueta U, et al. Release of targeted protein nanoparticles from functional bacterial amyloids: A death star-like approach. 2018; *Journal of Controlled Release.* Available online.

(301) Rinas U, Garcia-Fruitos E, Corchero JL, Vazquez E, Seras-Franzoso J, Villaverde A. Bacterial Inclusion Bodies: Discovering Their Better Half. *Trends Biochem Sci* 2017;42:726-737.

(302) Villaverde A, Corchero JL, Seras-Franzoso J, Garcia-Fruitos E. Functional protein aggregates: just the tip of the iceberg. *Nanomedicine (Lond)* 2015;10:2881-2891.

(303) Cano-Garrido O, Rodriguez-Carmona E, Diez-Gil C et al. Supramolecular organization of protein-releasing functional amyloids solved in bacterial inclusion bodies. *Acta Biomater* 2013;9:6134-6142.

(304) Cespedes MV, Fernandez Y, Unzueta U et al. Bacterial mimetics of endocrine secretory granules as immobilized in vivo depots for functional protein drugs. *Sci Rep* 2016;6:35765.

(305) Balouiri M, Sadiki M, Ibnsouda SK. Methods for in vitro evaluating antimicrobial activity: A review. *J Pharm Anal* 2016;6:71-79.

(306) Wiegand I, Hilpert K, Hancock RE. Agar and broth dilution methods to determine the minimal inhibitory concentration (MIC) of antimicrobial substances. *Nat Protoc* 2008;3:163-175.

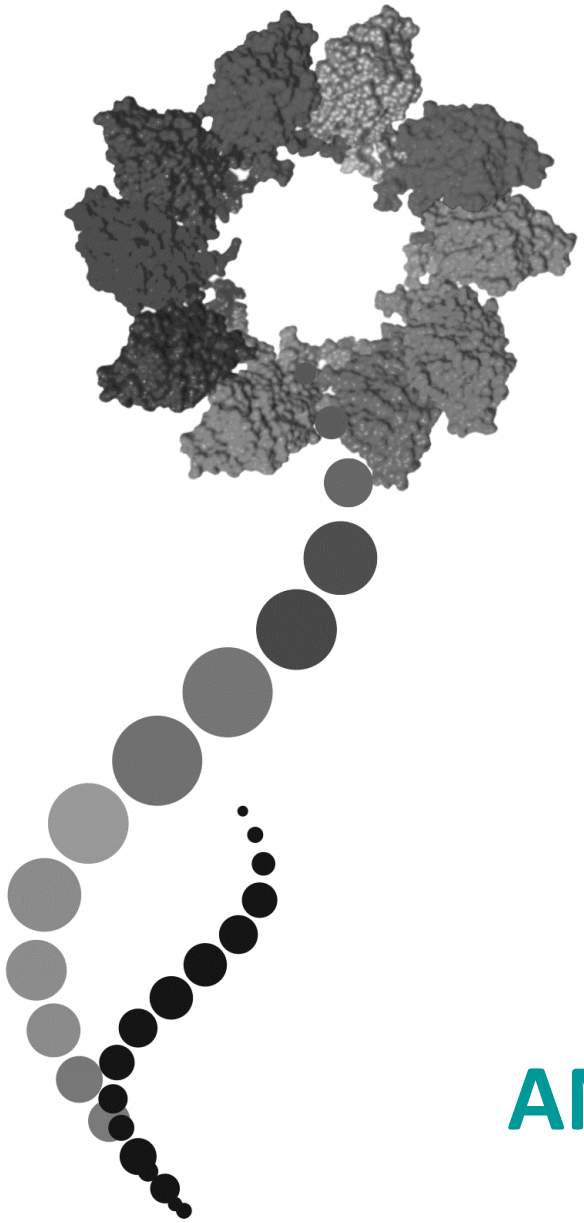

ANNEXES

ANNEX 1: ARTICLE 4

Self-assembling toxin-based nanoparticles as self-delivered antitumoral drugs.

Laura Sánchez-García[1] , Naroa Serna[1] , Patricia Álamo, Rita Sala, María Virtudes Céspedes, Mònica Roldan, Alejandro Sánchez-Chardi, Ugutz Unzueta, Isolda Casanova, Ramón Mangues, Esther Vázquez, Antonio Villaverde.

[1]Equally contributed.

Journal of Controlled Release. 2018. 274: 81-92.

Impact factor: 7.786. Quartile: Q1. Decile: D1.

Journal of Controlled Release 274 (2018) 81–92

Contents lists available at ScienceDirect

Journal of Controlled Release

journal homepage: www.elsevier.com/locate/jconrel

Self-assembling toxin-based nanoparticles as self-delivered antitumoral drugs

Laura Sánchez-García[a,b,c,1], Naroa Serna[a,b,c,1], Patricia Álamo[c,d,e], Rita Sala[c,d], María Virtudes Céspedes[c,d], Mònica Roldan[f], Alejandro Sánchez-Chardi[g], Ugutz Unzueta[c,d], Isolda Casanova[c,d,e], Ramón Mangues[c,d,e,*], Esther Vázquez[a,b,c], Antonio Villaverde[a,b,c,*]

[a] Institut de Biotecnologia i de Biomedicina, Universitat Autònoma de Barcelona, Bellaterra, 08193 Barcelona, Spain
[b] Departament de Genètica i de Microbiologia, Universitat Autònoma de Barcelona, Bellaterra, 08193 Barcelona, Spain
[c] CIBER de Bioingeniería, Biomateriales y Nanomedicina (CIBER-BBN), Spain
[d] Institut d'Investigacions Biomèdiques Sant Pau, Hospital de la Santa Creu i Sant Pau, 08025 Barcelona, Spain
[e] Josep Carreras Research Institute, Hospital de la Santa Creu i Sant Pau, Barcelona, Spain
[f] Unitat de Microscòpia Confocal, Servei d'Anatomia Patològica, Institut Pediàtric de Malalties Rares (IPER), Hospital Sant Joan de Déu, Edifici Consultes Externes, Passeig Sant Joan de Déu, 2, Planta 0, 08950, Esplugues de Llobregat, Barcelona, Spain
[g] Servei de Microscòpia, Universitat Autònoma de Barcelona, Bellaterra, 08193 Barcelona, Spain

ARTICLE INFO

Keywords:
Protein materials
Nanoparticles
Drug delivery
Cell-targeting
Recombinant proteins

ABSTRACT

Loading capacity and drug leakage from vehicles during circulation in blood is a major concern when developing nanoparticle-based cell-targeted cytotoxics. To circumvent this potential issue it would be convenient the engineering of drugs as self-delivered nanoscale entities, devoid of any heterologous carriers. In this context, we have here engineered potent protein toxins, namely segments of the diphtheria toxin and the *Pseudomonas aeruginosa* exotoxin as self-assembling, self-delivered therapeutic materials targeted to CXCR4$^+$ cancer stem cells. The systemic administration of both nanostructured drugs in a colorectal cancer xenograft mouse model promotes efficient and specific local destruction of target tumor tissues and a significant reduction of the tumor volume. This observation strongly supports the concept of intrinsically functional protein nanoparticles, which having a dual role as drug and carrier, are designed to be administered without the assistance of heterologous vehicles.

1. Introduction

Natural protein toxins are produced by different species of unicellular and pluricellular organisms and are extremely potent functional molecules [1]. Toxins occur alone or as venom components with roles in predation and defense or during tissue colonization in bacterial infections and show a wide spectrum of mechanisms of action that target vital physiological processes. The biological properties of protein toxins can be exploited in a therapeutic context, because they are usually preserved in versions produced by recombinant DNA technologies. This fact allows the industry-oriented, large-scale bioproduction and further formulation of protein toxins as medicines. A few toxin-based drugs have been already approved for use in humans by the medicament agencies, including Captopril for hypertension, Prialt for chronic pain, Integrilin for coronary angioplasty, Byetta for type 2 diabetes, Botox for neuromuscular disorders and Contulakin-G as an analgesic [2–6]. Many others are currently under development or in clinical trials [7–9]. A major therapeutic value of toxins relies on their ability to kill exposed cells through molecular events that are devoid, in general, of cell type specificity. The high potency exhibited by some toxins enables toxin-mediated cell killing to be explored in oncology to replace or complement conventional chemotherapies [10,11]. However, not only efficient but selective cell killing should be envisaged when developing antitumoral drugs, to minimize the undesired adverse effects and potentially severe toxicity associated to conventional chemotherapies. As an example, in the drug Denileukin diftitox, cell targeting is provided by the human interleukin-2. Fused to the fragments A and B of the *Corynebacterium diphtheriae* exotoxin (diphtheria toxin), this cytokine allows binding of the whole fusion to the IL-2 receptor, overexpressed in cutaneous T cell lymphoma cells. Ideally, toxins for use in oncology should be targeted by highly specific ligands of tumoral surface markers [12–15] and administered in stable formulations ensuring

* Corresponding authors.
E-mail addresses: rmangues@santpau.cat (R. Mangues), antoni.Villaverde@uab.es (A. Villaverde).
[1] Equally contributed.

https://doi.org/10.1016/j.jconrel.2018.01.031
Received 17 September 2017; Received in revised form 21 January 2018; Accepted 29 January 2018
Available online 31 January 2018

bioavailability and minimizing renal filtration. This would be achieved by presenting them in sizes over the renal clearance threshold (~8 nm), through the use of nanoscale carriers. Regarding the extremely high potency of toxins, possible drug leakage from the vehicle during blood circulation represents an important risk that limits the development of toxin-based nanoconjugates. In addition, the intrinsic potential toxicity of the nanoparticle used as carrier, is a matter of additional concern at both individual and environmental levels [16,17]. In this regard, the current trends towards developing self-delivery nanoscale drugs devoid of heterologous vehicles [18] might potentially expand the fields or applicability of toxins and other cytotoxic protein drugs in safer ways. However, the first prototypes in this line have resulted in very complex combinations of different types of molecules, that devoid of true nanoscale vehicles, require instead the assistance of accompanying molecular systems to provide the required functions. For instance, self-assembling therapeutic siRNA has been combined with polymeric metformin, condensed with hyaluronic acid and the nanoparticles covered with 1,2-dioleoyl-3-tri-methylammonium-propane chloride and cholesterol and functionalized with a sigma receptor ligand [19]. As another recent example, the anticancer agent epigallocatechin gallate was induced to self-assemble in combination with the antitumoral proteins herceptin or interferon alpha-2a (IFN-α 2a), followed by coating with polyethylene glycol [20].

In contrast to the chemical heterogeneity of these constructs, that are observed as representative of vehicle-free nanomedicines [18], the emerging concept of self-delivered nanoscale drugs could be fully achieved by functional recruitment in single molecular species that such as proteins, can oligomerize as chemically homogeneous nanoscale entities with predefined properties [21]. Importantly, nanoscale size in drug formulations is of high clinical relevance as cell penetrability and drug stability are favoured, the enhanced permeability and retention (EPR) effect stimulated and renal clearance largely minimized [18,22]. Recently [23], we have proposed a biological principle to promote self-assembling of fusion proteins as stable protein-only nanoparticles using cationic end-terminal tags. In addition, we have proved that short protein segments, such as pro-apoptotic or antimicrobial peptides, might retain their therapeutic potential when fused to carrier proteins such as GFP and once organized in oligomers [24]. Then, a protein toxin might be genetically instructed, by the addition of architectonic and cell targeting tags, to self-assemble into stable nanoparticles acting as intrinsically functional, cell-targeted protein materials with self-delivery properties. In this context, we have here engineered two potent toxins as CXCR4-targeted self-assembling nanoparticles for the systemic treatment of $CXCR4^+$ colorectal cancer. These proteins are the active fragments of the diphtheria toxin and of the *Pseudomonas aeruginosa* exotoxin, that perform ADP-ribosylation of the elongation factor 2 (EF-2), resulting in the irreversible inhibition of protein synthesis and cell death [25,26]. In addition, we designed these drug biomaterials to proteolytically discharge the targeting agent and other non-relevant protein segments upon cell internalization, for the cytotoxic activity being solely executed by the precise protein drug domain.

2. Materials and methods

2.1. Protein design, production, purification and characterization

Synthetic genes encoding the self-assembling modular proteins T22-DITOX-H6 and T22-PE24-H6 respectively were designed in-house (Fig. 1A) and provided by Geneart (ThermoFisher). DITOX contains the translocation and catalytic domains of the diphtheria toxin from *Corynebacterium diphtheriae*. PE24 is based in the de-immunized catalytic domain of *Pseudomonas aeruginosa* exotoxin A in which point mutations that disrupt B and T cell epitopes have been incorporated. Moreover, it has been added a KDEL sequence in the C-terminus of T22-PE24-H6, which enables the binding to KDEL receptors more efficiently at the Golgi apparatus during subsequent intracellular trafficking [27]. Furin-cleavage sites were inserted between the CXCR4 ligand T22 and the functional toxin (Fig. 1A) to release the amino terminal peptide once internalized into target cells. This has been designed so as the natural version of both toxins act with free amino termini [26,28], and the recombinant versions proved to be active also show this terminal end in absence of additional peptide segments [29,30]. Both gene fusions were inserted into the plasmid pET22b, and the recombinant versions of the vector were transformed by heat shock in *Escherichia coli* Origami B (BL21, $OmpT^-$, Lon^-, $TrxB^-$, Gor^-, Novagen, Darmstadt, Germany). Transformed cells were grown at 37 °C overnight in LB medium supplemented with 100 μg/ml ampicillin, 12.5 μg/ml tetracycline and 15 μg/ml kanamycin. The encoded proteins were produced at 20 °C overnight upon addition of 0.1 and 1 mM IPTG (isopropyl-β-D-thiogalactopyranoside) for T22-DITOX-H6 and T22-PE24-H6 respectively, when the OD_{550} of the cell culture reached around 0.5–0.7. Bacterial cells were centrifuged during 15 min (5000*g* at 4 °C) and kept at −80 °C until use. Pellets were thaw and resuspended in Wash buffer (20 mM Tris-HCl pH 8.0, 500 mM NaCl, 10 mM imidazole) in presence of protease inhibitors (Complete EDTA-Free, Roche Diagnostics, Indianapolis, IN, USA). Cell disruption was performed by French Press (Thermo FA-078A) at 1200 psi. The lysates were then centrifuged for 45 min (15,000*g* at 4 °C), and the soluble fraction was filtered using a pore diameter of 0.2 μm.

Proteins were then purified through the His-tag by Immobilized Metal Affinity Chromatography (IMAC) using a HiTrap Chelating HP 1 ml column (GE Healthcare, Piscataway, NJ, USA) with an AKTA purifier FPLC (GE Healthcare). Elution was achieved using a lineal gradient of Elution buffer (20 mM Tris-HCl pH 8.0, 500 mM NaCl and 500 mM imidazole). The eluted fractions were collected, dialyzed against carbonate buffer (166 mM $NaCO_3H$ pH 8) and centrifuged for 15 min (15,000*g* at 4 °C) to remove insoluble aggregates. The integrity and purity of the proteins was analyzed by mass spectrometry (MALDI-TOF), SDS-PAGE and Western blotting using anti-His monoclonal antibody (Santa Cruz Biotechnology, Santa Cruz, CA, USA). Protein concentration was determined by Bradford's assay. The nomenclature used for the fusion proteins has been established according to their modular organization.

2.2. Furin cleavage design and detection

To promote the intracellular release of ligand-free toxins, two different furin cleavage sites, naturally acting in the respective toxin precursors to activate translocation, were included in T22-DITOX-H6 and T22-PE24-H6 (Fig. 1A). Efficiency of cleavage in the platform was assessed in T22-DITOX-H6, since the expected fragments should exhibit fully distinguishable molecular masses suitable for quantitative analysis. For that, HeLa cell extracts exposed to 1 μM protein for 24 h were submitted to a Western Blot analysis. After protein incubation, cells were collected, centrifuged, suspended in DPBS and disrupted by sonication. The Western Blot bands were quantified using Image Lab Software version 5.2.1. Two additional modular proteins were also constructed in which these engineered furin cleavage sites were not included, namely T22-DITOX-H6 F^- and T22-PE24-H6 F^-. Their amino acid sequence exactly matched that of the equivalent constructs T22-DITOX-H6 and T22-PE24-H6 at exception of the boldface dark blue peptide (Fig. 1 A), corresponding to the protease target site. These non-cleavable constructs were used for a comparative analysis of protein cytotoxicity.

2.3. Fluorescence labelling and dynamic light scattering

T22-DITOX-H6 and T22-PE24-H6 were labelled with ATTO 488 (Sigma Aldrich, Buchs, Switzerland) to track their internalization when performing *in vitro* and *in vivo* experiments. The conjugation was performed at a molar ratio of 1:2 at room temperature in darkness. The

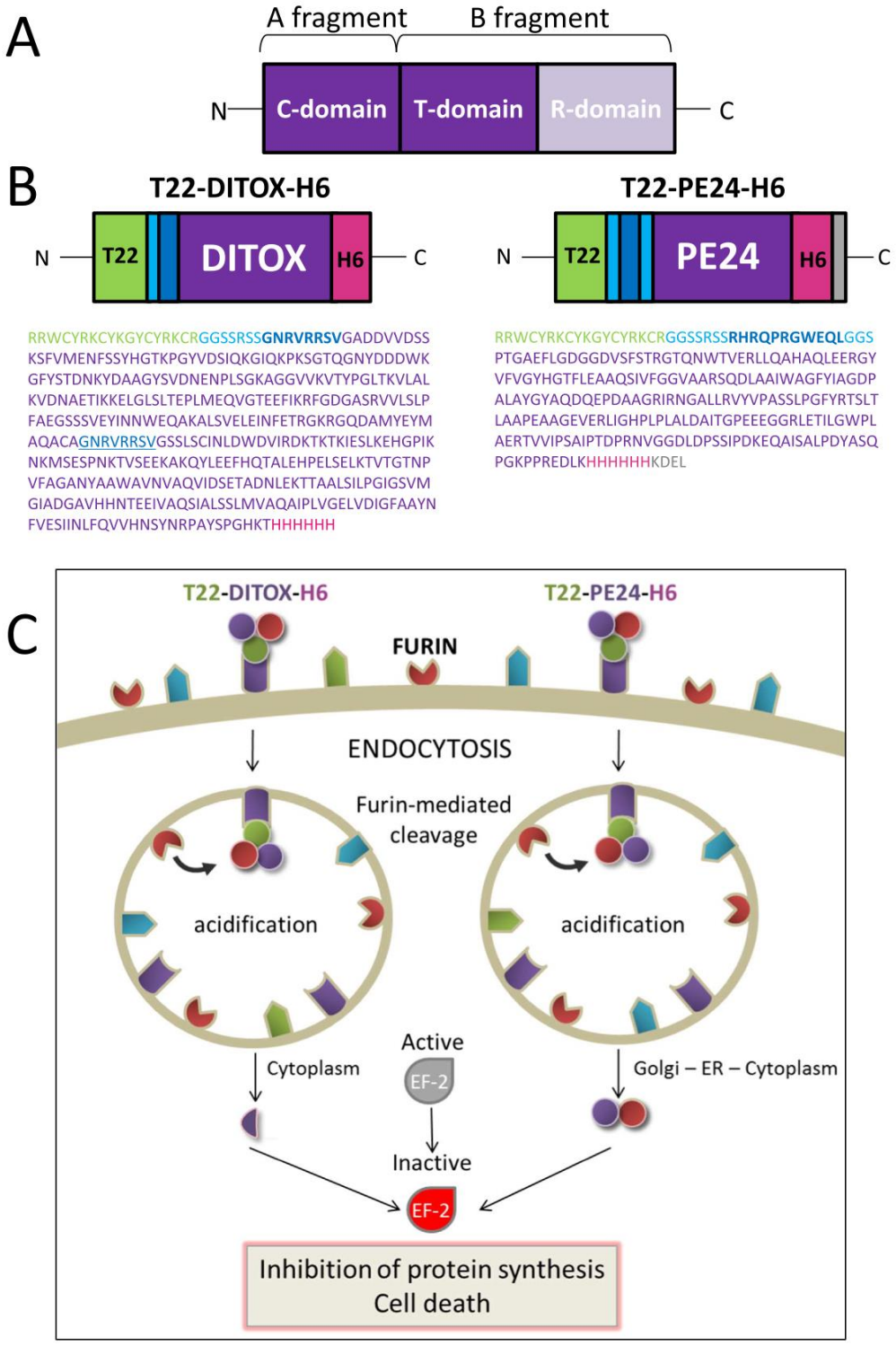

Fig. 1. A. Native structure of A-B toxins such as diphtheria toxin (*Corynebacterium diphtheriae*) or exotoxin A (*Pseudomonas aeruginosa*). The native toxin is divided in two fragments (A and B). Fragment A includes the catalytic domain (C-domain), whereas the fragment B comprises the translocation and the receptor binding domain (T- and R-domain). The selected domains for the construction of the recombinant nanoparticles are coloured in dark purple (T22-PE24-H6 construct does not include the T-domain). B. Modular organization of T22-DITOX-H6 and T22-PE24-H6, in which T22 acts as both CXCR4 ligand and as an architectonic tag. Functional segments are intersected by linker regions (light blue) and furin-cleavage sites (dark blue, boldface). A natural furin-cleavage site also occurs within DITOX (dark blue, underlined), that separates the amino terminal catalytic domain from the carboxy terminal translocation domain. A KDEL peptide has been incorporated neighboring the H6 region in T22-PE24-H6. Box sizes are only indicative. Two additional proteins, namely T22-DITOX-H6 F^- and T22-PE24-H6 F^- were constructed for comparative purposes, precisely lacking the engineered furin cleavage sites (boldface dark blue regions). C. Expected pathway for the cytotoxicity of T22-DITOX-H6 and T22-PE24-H6 nanoparticles over $CXCR4^+$ target cells, upon intracellular furin-mediated release of protein domains useful for biodistribution and cell penetration steps but irrelevant for cell killing. (For interpretation of the references to color in this figure legend, the reader is referred to the web version of this article.)

reaction mixture was gently stirred every 15 min during 1 h, centrifuged for 15 min (15,000*g* at 4 °C) and dialyzed overnight in the original buffer (166 mM $NaCO_3H$ pH 8) to eliminate free ATTO. Fluorescence of the nanoparticles at 0.1 mg/ml was determined by a Varian Cary Eclipse fluorescence spectrophotometer (Agilent Technologies, Mulgrave, Australia) at 523 nm using an excitation wavelength of 488 nm. For comparative analyses, the intensity of fluorescence was corrected by protein amounts to render specific emission values. Stability of dye conjugation was assessed through the incubation of T22-DITOX-H6* at a final concentration of 0.5 μg/μl in human serum (S2257-5ML, Sigma, St Louis, MO, USA) for 48 h at 37 °C, with gentle agitation. Then, the sample was dialyzed in 300 ml of carbonate buffer (166 mM $NaCO_3H$, pH 8) for 2 h to remove the free ATTO that might have been released from the nanoparticle. In parallel a positive control was dialyzed containing the same amount of free ATTO. The fluorescence of buffers obtained after the dialysis was measured in the fluorimeter. The volume size distribution of all nanoparticles was determined by dynamic light scattering (DLS) at 633 nm (Zetasizer Nano ZS, Malvern Instruments Limited, Malvern, Worcestershire, UK).

2.4. Ultrastructural characterization

Size and shape of T22-DITOX-H6 and T22-PE24-H6 nanoparticles at nearly native state were evaluated with a field emission scanning electron microscope (FESEM) Zeiss Merlin (Zeiss, Oberkochen, Germany) operating at 1 kV. Drops of 3 μl of each protein sample were directly deposited on silicon wafers (Ted Pella Inc., Reading, CA, USA) for 1 min, excess blotted with Whatman filter paper number 1 (GE Healthcare, Piscataway, NJ, USA), air dried, and observed without coating with a high resolution in-lens secondary electron detector. For each sample, representative images of different fields were captured at magnifications from 120,000× to 200,000×.

2.5. Cell culture and flow cytometry

$CXCR4^+$ cervical, colorectal and pancreatic cancer cell lines were used to study the performance of the recombinant proteins *in vitro* (HeLa ATCC-CCL-2, SW1417 ATCC-CCL-238 and Panc-1 ATCC-CCL-1469). HeLa cells were maintained in Eagle's Minimum Essential Medium (Gibco®, Rockville, MD, USA), whereas SW1417 and Panc-1 in Dulbecco's Modified Eagle's Medium (Gibco®). All of them were supplemented with 10% foetal bovine serum (Gibco®) and incubated in a humidified atmosphere at 37 °C and 5% of CO_2 (at 10% for SW1417 cells).

In order to monitor protein internalization, HeLa cells were cultured on 24-well plates at $3 \cdot 10^4$ cells/well for 24 h until reaching 70% confluence. Proteins were incubated for 1 h at different concentrations (100, 500 and 1000 nM) in presence of OptiPRO™ SFM supplemented with L-glutamine. Additionally, specific internalization through CXCR4 receptor was proved adding a specific antagonist, AMD3100 [31,32], which is expected to inhibit the interaction with T22. This chemical inhibitor was added 1 h prior protein incubation at a ratio of 1:10. Furthermore, kinetics of the internalization was performed at a concentration of 1 μM, after different periods of incubation (0, 20, 30, 60, 120, and 240 min). After protein exposure, cells were detached using 1 mg/ml Trypsin-EDTA (Gibco®) for 15 min at 37 °C, a harsh protocol designed to remove externally attached protein [33]. The obtained samples were analyzed by a FACS-Canto system (Becton Dickinson, Franklin Lakes, NJ, USA) using a 15 mW air-cooled argon ion laser at 488 nm excitation. Experiments were performed in duplicate.

2.6. Confocal laser scanning microscopy

For confocal microscopy HeLa cells were grown on Mat-Tek plates (MatTek Corporation, Ashland, MA, USA). Upon exposure to the materials cell nuclei were labelled with 5 μg/ml Hoechst 33342 (ThermoFischer, Waltham, MA, USA) and the plasma membrane with 2.5 μg/ml CellMask™ Deep Red (ThermoFischer) for 10 min at room temperature. Cells were then washed in PBS buffer (Sigma-Aldrich, Steinheim, Germany). The confocal images of the HeLa cells were collected on an inverted TCS SP5 Leica Spectral confocal microscope (Leica Microsystems, Wetzlar, Germany) using 63× (1.4 NA) oil immersion objective lenses. Excitation was reached *via* a 405 nm blue diode laser (nucleic acids), 488 nm line of an argon ion laser (nanoparticles) and 633 nm line of a HeNe laser (Cell membrane). Optimized emission detection bandwidths were configured to avoid inter-channel crosstalk and multitrack sequential acquisition setting were used. The confocal pinhole was set to 1 Airy unit and z-stacks acquisition intervals were selected to satisfy Nyquist sampling criteria. Three-dimensional images were processed using the Surpass Module in Imaris X64 v.7.2.1. software (Bitplane, Zürich, Switzerland).

2.7. Cell viability assays

The CellTiter-Glo® Luminescent Cell Viability Assay (Promega, Madison, WI, USA) was used to determine the cytotoxicity of T22-DITOX-H6, T22-PE24-H6, T22-DITOX-H6 F^- and T22-PE24-H6 F^- nanoparticles on HeLa, SW1417 $CXCR4^+$ or SW1417 $CXCR4^-$ cell lines. Cells were cultured in opaque-walled 96-well plates at 3500 or 6000 cells/well during 24 h at 37 °C until reaching 70% confluence. All protein incubations were performed in the corresponding medium according to the cell line used. Inhibition of cell death was analyzed by adding AMD3100, a chemical antagonist of CXCR4 [34,35], at a ratio of 1:10, 1 h prior to protein incubation. T22-GFP-H6, a non-functional T22-bearing protein [36] was also used as a competitor of T22-empowered toxins at a final concentration of 2 μM. After protein incubation, a single reagent provided by the manufacturer was added to cultured cells, which prompted lysis and generated a luminescent signal proportional to the amount of ATP present in the sample. The ATP generated is directly related to the quantity of living cells that remain in the well. Then, plates were measured in a conventional luminometer, Victor3 (Perkin Elmer, Waltham, MA, USA). Viability of Panc-1 cells, that overexpress luciferase, was determined with an alternative non fluorescence kit (EZ4U) under the same experimental conditions. The cell viability experiments were performed in triplicate.

2.8. Biodistribution, pharmacokinetics and apoptotic induction analyses in $CXCR4^+$ colorectal cancer mouse model after single dose administration of nanoparticles

All *in vivo* experiments were approved by the institutional animal Ethics Committee of Hospital Sant Pau. We used 5 week-old female Swiss Nu/Nu mice, weighing 18–20 g (Charles River, L'Abresle, France), maintained in specific pathogen-free conditions. To generate the subcutaneous (SC) mouse model, we implanted subcutaneously 10 mg of the patient-derived M5 colorectal (CCR) tumor tissue from donor animals in the mouse subcutis. At day 15, when tumors reached approximately 500 mm^3, mice received 50 μg single i.v. bolus of T22-DITOX-H6* (n = 3) or 300 μg single i.v. bolus of T22-PE24-H6* (n = 3) in $NaCO_3H$, pH = 8 buffer. Control animals received the same buffer (n = 3) or 0.25 μg of free ATTO 488 (n = 2). At 5, 24 and 48 h mice were euthanized and subcutaneous tumors and organs (brain, lung, liver, kidney and heart) were collected. Biodistribution of ATTO-labelled nanoparticles in tumor and non-tumor organs was determined by measuring the emitted fluorescence in *ex vivo* tissue sections (3 mm thick) using the IVIS® Spectrum (Perkin Elmer, Santa Clara, CA, USA) platform. The fluorescent signal (FLI), which correlates to the amount of administered protein accumulated in each tissue, was first digitalized, displayed as a pseudocolor overlay, and expressed as radiant efficiency [$(p/s/cm^2/sr)/\mu W/cm^2$]. The FLI values were calculated subtracting FLI signal from experimental mice by FLI auto-fluorescence of control mice. Samples were first fixed with 4% formaldehyde in PBS for

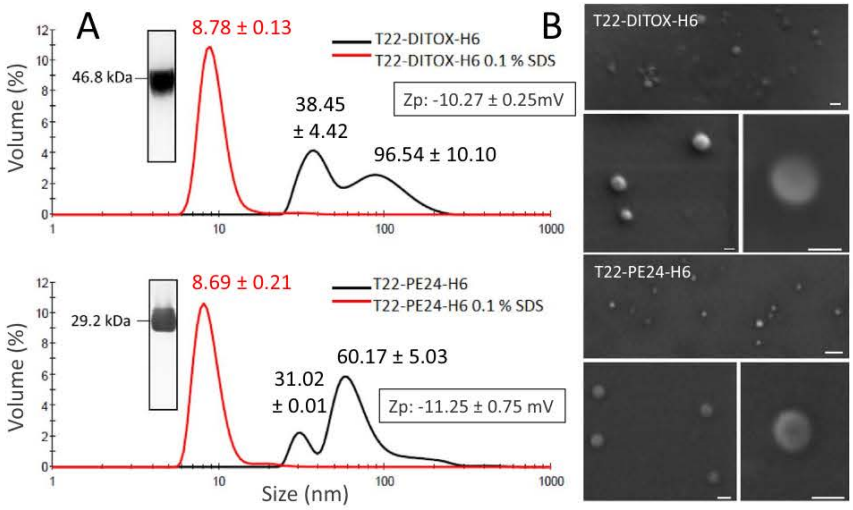

Fig. 2. Nanoarchitecture of toxin-based proteins. A. Size and SDS-mediated disassembling of T22-DITOX-H6 and T22-PE24-H6 nanoparticles determined by DLS. Values of peak sizes (mode) are indicated in bold (in nm, ± SEM). *Z*-potential (Zp) values of the nanoparticles are also indicated. The molecular mass of proteins upon purification is shown by Western Blot upon PAGE-SDS. B. FESEM examination of purified T22-DITOX-H6 and T22-PE24-H6 materials. Bars indicate 50 nm.

24 h to be embedded in paraffin for histopathological evaluation and apoptotic index analyses.

Pharmacokinetic analyses were performed after a 300 μg single i.v. bolus administration of T22-PE24-H6* in 12 Swiss nude mice, or after a 50 μg single bolus administration of T22-DITOX-H6* also in 12 animals. We sacrificed three mice per each time point, at 0, 1, 2, 5, 24 and 48 h after the administration and obtained approximately 1 ml of blood EDTA anticoagulated collection tubes. We measured the exact volume of plasma obtained and the fluorescent emission at each time point, and calculated the concentration of nanoparticle as referred to the fluorescence emitted and concentration of the administered dose.

Apoptotic induction analyses were performed in 4 μm sections of tumors and normal organs (liver, lung, spleen, heart, kidney and brain) stained with hematoxylin and eosin (H&E), which were histopathologically analyzed by two independent observers. Apoptotic induction was evaluated by both, the presence of cell death bodies in H&E stained and Hoechst stained tumor slices. Triton X-100 (0.5%) permeabilized sections were then stained with Hoechst 33258 (Sigma-Aldrich) diluted, 1:5000 in PBS, for 1 h, rinsed with water, mounted and analyzed under fluorescence microscope (λex = 334 nm/λem = 465 nm). The number of apoptotic cell bodies was quantified by recording the number of condensed and/or defragmented nuclei per 10 high-power fields (magnification 400×), in blinded samples evaluated by two independent researchers, using Cell∧B s.

2.9. Antitumor effect in a CXCR4$^+$ CRC model after nanoparticle repeated dose administration

To generate the CXCR4$^+$ colorectal xenograft mouse models, we used the patient-derived M5 colorectal tumor tissue. Ten mg fragments obtained from donor animals were implanted in the subcutis of Swiss nu/nu mice to generate subcutaneous (SC) tumors as described above (n = 9). Once tumors reached approximately 120 mm^3, mice were randomized in Control, T22-PE24-H6 and T22-DITOX-H6 groups and received intravenous doses of T22-PE24-H6 or T22-DITOX-H6, both at a repeated dose regime of 10 μg, 3 times a week, per 8 doses. The control group received buffer using the same administration schedule. Mouse body weight was registered over the experimental period 3 times a week. Seventeen days after the initiation of nanoparticle administration, mice were euthanized and the subcutaneous tumors were taken to measure their final tumor volume and to count the number of apoptotic figures in 5 high-power fields (magnification 400×), of H&E stained tumor sections as described above.

2.10. Statistical analysis

The specificity of nanoparticle-promoted cell death and the pairwise data comparisons were checked with a one-way ANOVA and Tukey's tests, respectively. Pairwise divergences of internalization and cell death were evaluated using Student's *t*-tests, whereas Mann–Whitney *U* tests were used to pairwise comparisons of the number of apoptotic bodies. Differences between groups were considered significant at $p < 0.05$ and differences between relevant data are indicated by letters or as ¥ for $0.01 < p < 0.05$ and § for $p < 0.01$ in the Figures. All statistical analyses were performed using SPSS version 11.0 package (IBM, NY, USA), and values were expressed as mean ± standard error of the mean (SEM).

3. Results

Active fragments of the diphtheria toxin (DITOX) and the *Pseudomonas aeruginosa* exotoxin (PE24) were produced in *Escherichia coli* as the modular fusion proteins T22-DITOX-H6 and T22-PE24-H6 (Fig. 1A, B), intended to induce targeted cell death through the activity of the catalytic fragments of the protein drug (Fig. 1C). The cationic peptide T22, placed at the amino terminus of the whole construct and cooperating with carboxy terminal histidines, promotes both oligomerization into regular nanoparticles [37] and binding to the cell-surface chemokine receptor CXCR4 (overexpressed in many aggressive human cancers [38–41]). In this way, it has been proved efficient in endorsing the endosomal penetration of payload GFP and IRFP into CXCR4$^+$ cancer stem cells [23]. Then, T22-DITOX-H6 spontaneously self-assembled into 38 and 90 nm-nanoparticles (Pdi = 0.25 ± 0.01 nm) and T22-PE24-H6 into ~60 nm-nanoparticles (Pdi = 0.22 ± 0.01, Fig. 2A), always within the size range considered as optimal for efficient cell uptake [22,42,43]. A secondary population of protein material was observed in the case of T22-PE24-H6, being always minority. Nanoparticles were effectively disassembled by 0.1% SDS, resulting in monodisperse building blocks peaking at ~6 nm (Pdi = 0.60 ± 0.01 and 0.30 ± 0.07 respectively), compatible with the expected size of the monomeric protein. However, both protein nanoparticles were fully stable in several physiological buffers in medium term incubation and also when exposed to high salt content buffer (up to 1 M NaCl, not shown), what prompted us expecting high stability *in vivo*. In addition, nanoparticles were found stable after one-year storage at −80 °C and upon repeated cycles of freezing and thawing (not shown). The assembled proteins appeared as toroid materials (Fig. 2B), with ultrastructural morphometry (round shape and

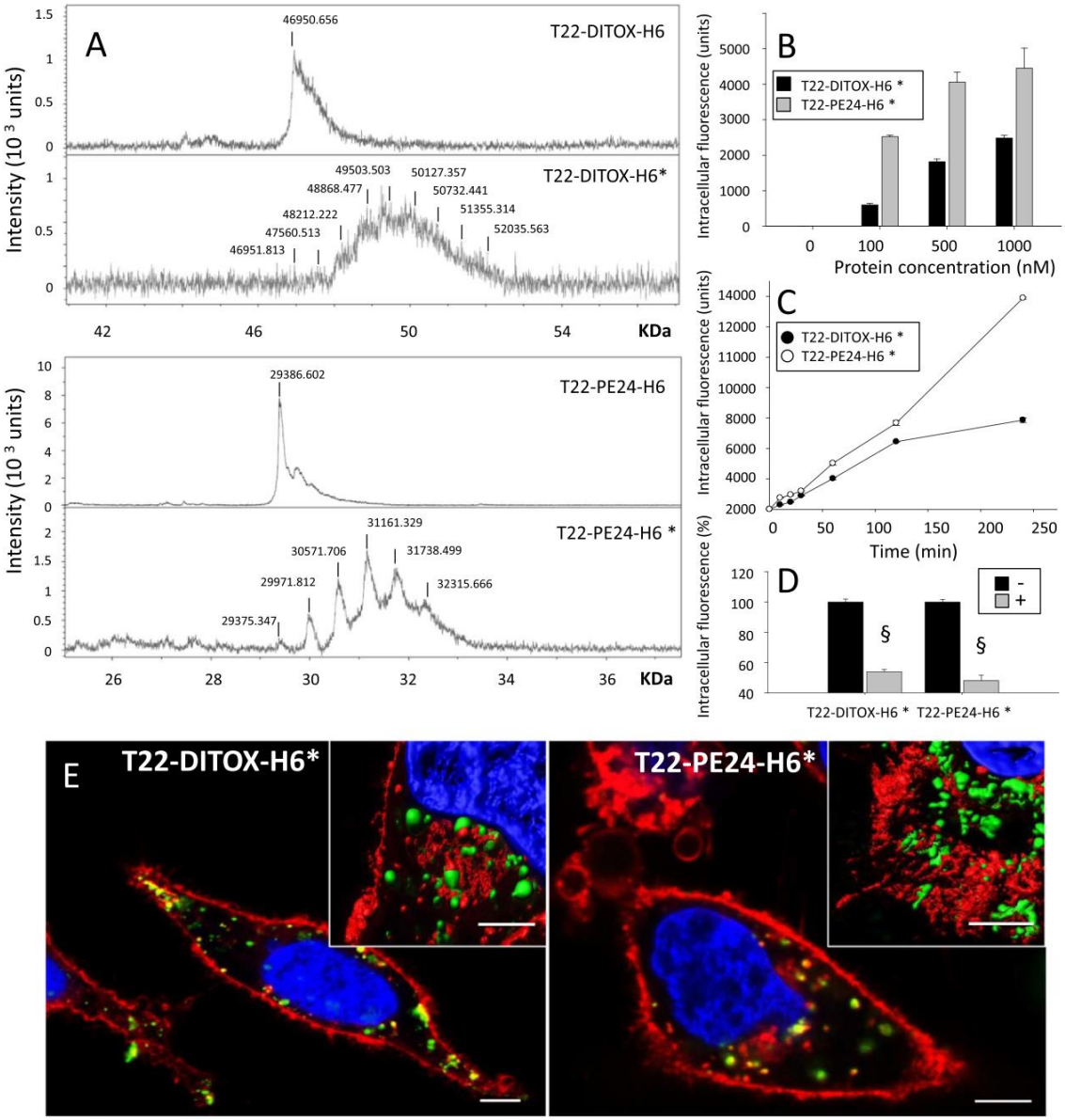

Fig. 3. Internalization of toxin-based nanoparticles in CXCR4$^+$ cells. A. Mass spectroscopy of pure unlabeled and ATTO-labelled (*) T22-DITOX-H6 and T22-PE24-H6 proteins. B. Dose-dependent uptake of T22-DITOX-H6* and T22-PE24-H6* nanoparticles in CXCR4$^+$ HeLa cells upon 1 h of exposure. C. Time course kinetics of cell internalization of T22-DITOX-H6* and T22-PE24-H6* nanoparticles (1 μM) in CXCR4$^+$ HeLa cells. Note the short error bars in the plot. D. Protein (100 nM) uptake inhibition by the CXCR4 antagonist AMD3100 (+) upon 1 h of exposure. Significant differences between relevant data pairs are indicated as § for $p < 0.01$. All A, B and C data are presented as mean ± SEM (n = 2). E. Confocal microscopy of HeLa cells exposed for 5 h to T22-DITOX-H6* and T22-PE24-H6* nanoparticles (1 μM). The Cell Mask membrane staining (red) was added together with nanoparticles to observe the endosomal membrane. Nanoparticles are visualized in green and nuclear regions in blue. The yellow spots indicate merging of red and green signals. In the insets, 3D Imaris reconstructions of confocal stacks. Bars indicate 5 μm. (For interpretation of the references to colour in this figure legend, the reader is referred to the web version of this article.)

clear size populations) that confirmed the size range observed by DLS. The same regular architecture had been previously described for the related T22-GFP-H6 construct, in which the GFP-based sub-units (with a molecular size similar to that of T22-DITOX-H6 and T22-PE24-H6) organized in toroid entities, whose organization has been modelled *in silico* [44] and confirmed by sophisticated analytical methods such as SAXS or high resolution electron microscopy imaging techniques [45].

Purified T22-DITOX-H6 and T22-PE24-H6 nanoparticles were tested for internalization into cultured CXCR4$^+$ cells, upon chemically labelling with the fluorescent dye ATTO 488 (tagged with *, Fig. 3A). Both kinds of labelled nanoparticles (Fig. 3A) penetrated target HeLa cells in a dose-dependent manner (Fig. 3B) and accumulated intracellularly with a kinetics characteristic of receptor-mediated uptake (with a faster slope in the case of T22-PE24-H6*, Fig. 3C). The CXCR4 specificity of the penetration was confirmed through its inhibition by the CXCR4 antagonist AMD3100 [34] (Fig. 3D). Internalized nanoparticles were observed as engulfed into endosomes, especially in cytoplasm areas close to the cell membrane, but they tended to be visualized as membrane-free entities when approaching the perinuclear regions (Fig. 3E), suggesting important endosomal escape. No cell-attached extracellular fluorescence was observed in any case.

Once the internalization was assessed, we tested if the furin cleavage sites introduced in the constructs to release the toxin segments from the building blocks were active in the oligomers. The expected

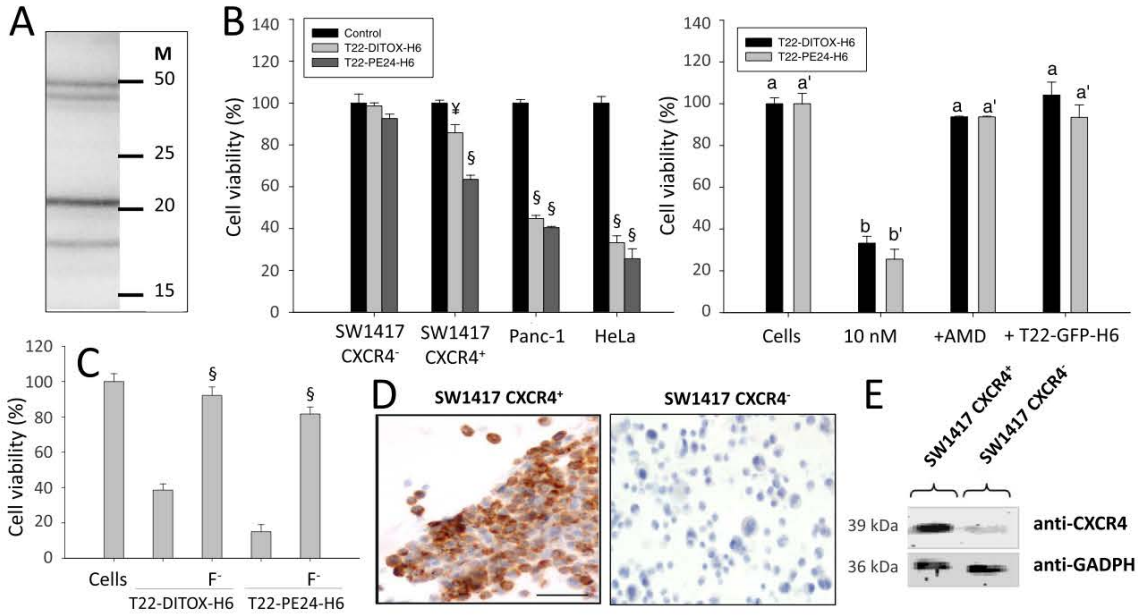

Fig. 4. Specific cytotoxicity of toxin-based nanoparticles in CXCR4$^+$ cells. A. Detection of intracellular T22-DITOX-H6 by Western blot analysis of HeLa cell extracts, after exposure of the cell cultures to nanoparticles (1 μM protein) for 24 h. M indicates the migration of molecular weight markers. B. Left: Cell death induced by T22-DITOX-H6 and T22-PE24-H6 nanoparticles (10 nM) over a SW1417 CXCR4$^-$ cell line and different CXCR4$^+$ cell lines (including an isogenic, CXCR4$^+$ SW1417 version), 48 h after exposure (72 h for SW1417 cell line). Significant differences between relevant data pairs are indicated as ¥ $0.01 < p < 0.05$ and § $p < 0.01$. Right: inhibition of HeLa cell death (induced by 10 nM of protein nanoparticles) by either the CXCR4 antagonist AMD3100 or by 2 μM protein T22-GFP-H6. Significant differences between relevant data are indicated as a change in the letter, from "a" to "b". All the significant results were $p < 0.01$. All data are presented as mean ± SEM (n = 3). C. HeLa cell death promoted by T22-DITOX-H6 F$^-$ and by T22-PE24-H6 F$^-$, compared to the related T22-DITOX-H6 and by T22-PE24-H6 respectively. Cells were exposed to 10 nM of each protein for 48 h. Data and statistics are as in panel B. D. Immunocytochemistry staining showing the lack of CXCR4 expression in the isogenic SW1417 CXCR4$^-$ cells as compared with the high CXCR4 expression in SW1417 CXCR4$^+$ cells. Bar indicates 50 μm. E. Differential CXCR4 protein expression in these cells assessed by an immunoblotting assay. Glyceraldehyde-3-phosphate dehydrogenase (GADPH) was used as protein loading control.

intracellular hydrolysis should enhance the cytotoxic properties of the toxin domains, which would then benefit from lower load of superfluous protein sequences. For that, we explored the sensitivity of the multiple cleavage sites in the construct T22-DITOX-H6 that would offer, upon intracellular digestion, fully distinguishable protein fragments. Unlike the extracellular protein that appears as one single protein species (Figs. 2A and 3A), the His tag immunodetection of the cell-engulfed protein showed the protein as digested by different alternative sites, matching the molecular weight of the expected products for each furin cleavage site. In particular, the release of the T22 peptide through the *de novo* incorporated cleavage site was proved *in vivo* in cell-internalized protein by the shift from the 48.65 kDa full-length protein to the 44.21 kDa fragment, analyzing cell extracts upon exposure to the nanoparticles for 24 h (Fig. 4A). The rest of fragments corresponded to the progressive digestion intermediates that still kept the carboxy terminal tag, by which the protein is immunodetected. The natural cleavage at the internal furin site, which releases the catalytic domain from the translocation domain, is also proved by the occurrence of the major 20.60 kDa segment. Therefore, the catalytic segment alone is expected to occur inside the target cells, among other biologically active versions, at reasonable amounts.

When exploring the cytotoxic effects, both T22-DITOX-H6 and T22-PE24-H6 were effective in killing cultured HeLa cells, with low IC50 values (0.78 nM and 0.99 nM respectively, not shown). The cytotoxic effect was clearly detectable in several CXCR4-expressing cell lines, including SW1417 CXCR4$^+$ but not in the isogenic SW1417 CXCR4$^-$ line (Fig. 4B, left). Cytotoxicity was mostly abolished by AMD3100 and by the T22-displaying biologically inner protein T22-GFP-H6 (Fig. 4B, right), thus confirming again the specificity of the entrance of the nanoparticles, the intracellular nature of the nanoparticle-mediated toxicity and the expected CXCR4 receptor mediation in cell killing. Besides, it has been observed a reversion effect of T22-DITOX-H6 (90%) when adding chloroquine, which inhibits endosomal acidification (not shown). This fact confirms that the mechanism of action is pH-dependent as described above (Fig. 1). In this context, we also evaluated the relevance of the removal of accessory protein segments (mediated by furin) on the cytotoxicity of the nanoparticles. For that, versions of T22-DITOX-H6 and T22-PE24-H6 without the engineered cleavage sites (labelled as F$^-$) were constructed and tested for biological activity. The comparative analyses of HeLa cell death mediated by these proteins revealed a dramatic drop of cytotoxicity in T22-DITOX-H6 F$^-$ and T22-PE24-H6 F$^-$ nanoparticles compared to the original materials (Fig. 4 C). On the other hand, the differential CXCR4 expression in the isogenic SW1417 cells was fully assessed by immunocytochemistry and Western blot (Fig. 4 D,E). Interestingly, the capacity of T22-DITOX-H6 and T22-PE24-H6 to promote cell death was not lost after one-year storage at −80 °C and also upon 4 cycles of freezing and thawing (not shown).

Due to the high CXCR4$^+$ specific cytotoxicity observed in cell culture, we next tested the performance of the toxin-based materials *in vivo* using a CXCR4-linked disease model. For that, we explored the biodistribution, antitumor activity and potential side toxicity of both T22-DITOX-H6* and T22-PE24-H6* nanoparticles in a CXCR4 overexpressing subcutaneous colorectal cancer model. As expected, after a single dose i.v. administration the protein materials accumulated in tumor in the studied time range (Fig. 5). Other organs such as brain, lung or heart were completely free of fluorescence. However, significant levels of emission associated to both nanoparticles were found in liver and kidney. To discard that significant amounts of ATTO might had been released from the nanoparticles during circulation in blood and generate artefacts in the biodistribution analysis, we evaluated the stability of the dye in T22-DITOX-H6* nanoparticles incubated in commercial serum. At 48 h, only a very minor fraction of fluorescence was released from nanoparticles (5%, Supplementary Fig. 1A). In addition, the administration of free ATTO did not resulted in detectable

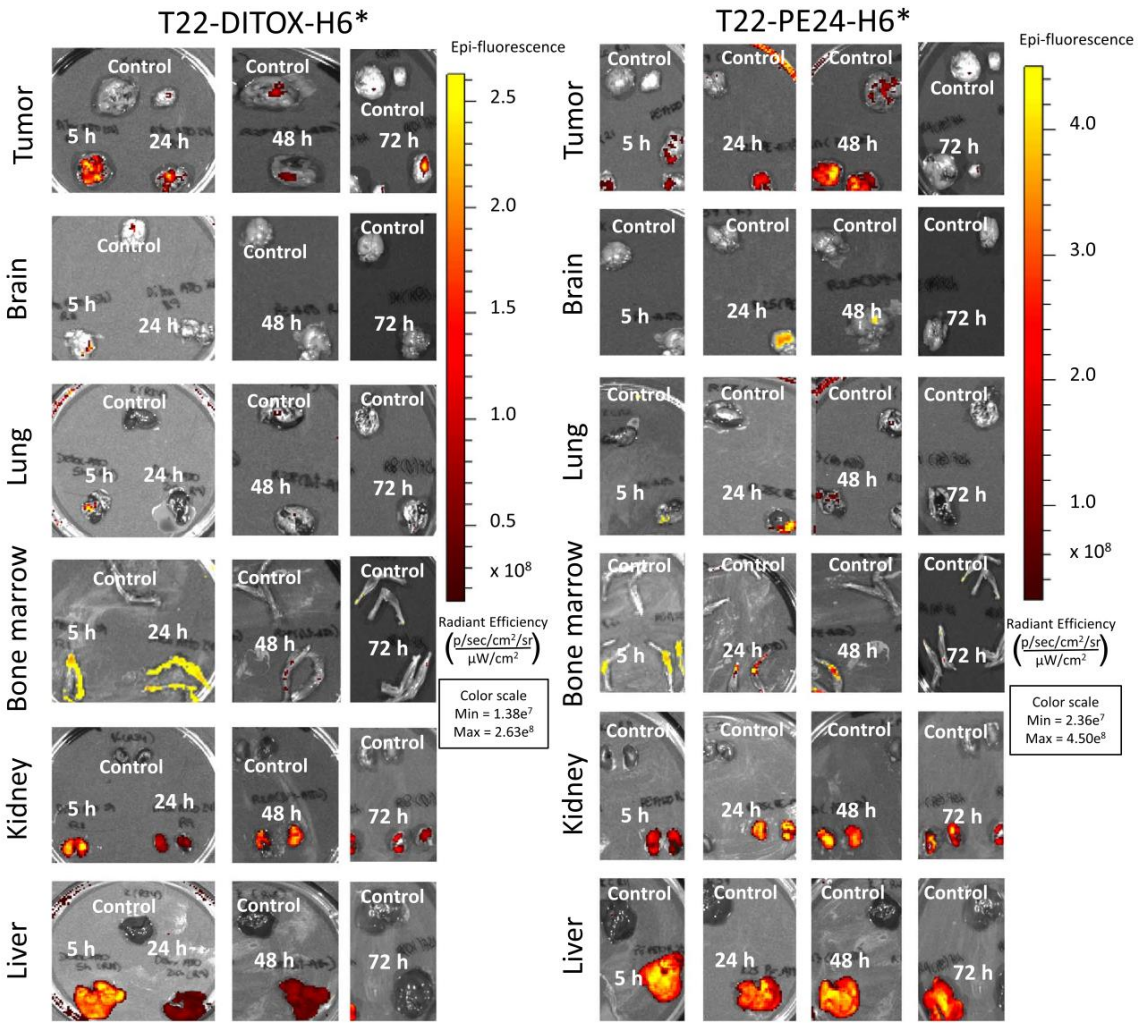

Fig. 5. Biodistribution kinetics of T22-DITOX-H6* and T22-PE24-H6* nanoparticles in a CXCR4$^+$ colorectal cancer mouse model. *Ex vivo* fluorescence emitted by subcutaneous tumor and relevant organs in buffer-administered (control) and T22-DITOX-H6*- and T22-PE24-H6*-treated mice at 5, 24, 48 and 72 h after 50 µg or 300 µg single dose i.v. administration. Emission scales are shown as radiant efficiency units (see methods section).

accumulation in tumor (Supplementary Fig. 1B), and the absence of dye signal in major organs was indicative of a fast urine secretion (as expected for a small molecule of 981 Da). These data fully supported the biodistribution of labelled nanoparticles shown in Fig. 5.

The presence of nanoparticles in liver was observed as worthy of a deeper analysis, since hepatic occurrence and damage is a severe concern in conventional and innovative cancer therapies, even in nanoconjugates or antibody-based drugs that show tissue-specific targeting [46–51]. Then, since it would be of crucial interest to discriminate between mere occurrence of fluorescence and toxin-induced damage in these organs, we comparatively investigated cell damage in tumor, liver and kidney. In this regard, we observed a high level of apoptosis induced by both nanoparticles in tumoral tissue, what was especially intense in T22-PE24-H6*-treated animals at 48 h post administration (Fig. 6). In contrast, apoptosis was undetectable in liver or kidney (Fig. 6), and most of the hepatic tissues were histologically normal except for a few and scattered small inflammation foci (Fig. 6) that can be attributed to non-specific extracellular retention of the drug in off-target tissues. This alteration was resolved after 72 h returning to normal histology. Probably, the intracellular activation of the toxins promoted by the furin-mediated release of accessory peptides (Fig. 4) does not occur in hepatic tissue, which does not overexpress CXCR4.

To discard that ATTO might have a positive contribution in the cytotoxicity of the materials in tumor after single dose administration we checked local apoptosis in animals treated with the non-labelled protein versions T22-DITOX-H6 and T22-PE24-H6. This was done at the times, among those tested, showing the highest potency (24 and 48 h respectively). As observed, local apoptosis was still present (Fig. 6) at values even higher than those induced by the labelled protein versions. This result was indicative that the observed antitumoral effect was intrinsically associated to the protein material. Then, data supported the notion that in spite of the occurrence of the protein drug in liver and kidney, this did not translate in a relevant uptake of any of the two nanoparticles in the parenchyma of these tissues. Our observations suggest that both labelled protein drugs underwent transient circulation through the fenestrated hepatic sinusoids and renal glomeruli despite their nanometric size (in contrast to other normal tissues) as reported for other nanoparticles [52]. Moreover, their lack of toxicity in kidney or liver suggest their inability to internalize into the parenchymal cells in these organs because of their negligible CXCR4 expression, in comparison for instance to spleen or bone marrow which despite showing low nanoparticle accumulation express CXCR4 [53]. This is a finding similar to that reported for CXCR4-targeted imaging agents [54]. Then, both T22-DITOX-H6 and T22-PE24-H6 appear to have a therapeutic

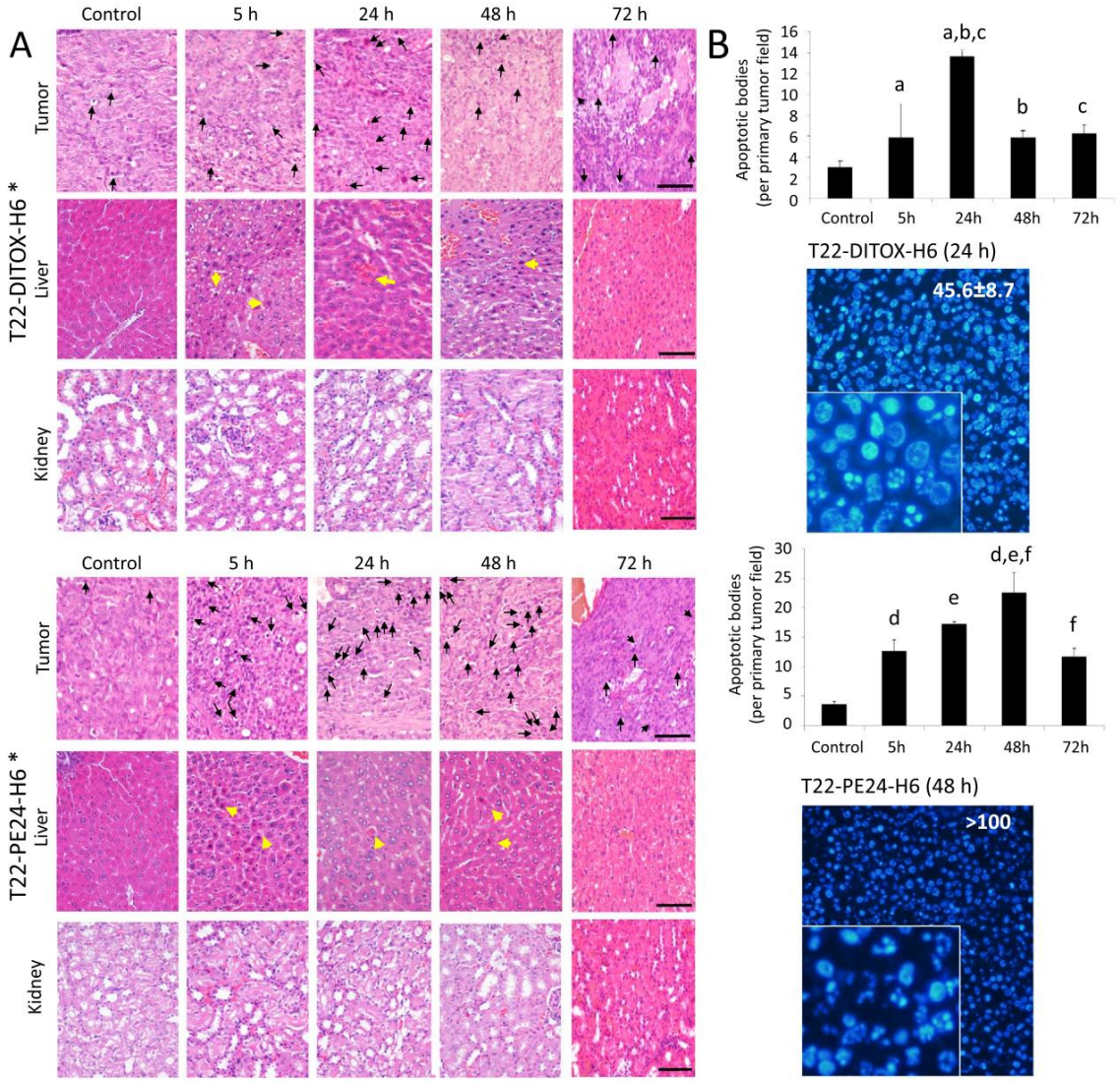

Fig. 6. Local induction of apoptosis in tumor by ATTO-labelled and unlabeled T22-DITOX-H6 (50 μg) and T22-PE24-H6 (300 μg) nanoparticles. A. Representative H&E staining of subcutaneous tumors showing apoptotic figures (black arrows). No significant apoptosis was detected in liver tissue at the studied times. Few and small inflammation foci in this organ were observed and are indicated by yellow arrows, which were resolved at 72 h, returning to histologically normal parenchyma. Note the absence of histological alterations in kidneys. Bar: 50 μm. B. Number of apoptotic cell bodies in H&E tumor slices per ten high-power fields (400× magnification) are plotted for each nanoparticle. For the experimental times showing higher number of apoptotic lesions we also show representative Hoechst staining of subcutaneous tumors in animals treated with unlabeled protein versions, at different magnifications. All data are presented as mean ± SEM (n = 3). Statistical significance: $^{a}p = 0.008$; $^{b}p = 0.027$; $^{c}p = 0.010$; $^{d,e,f}p = 0.001$.

index high enough to validate (i) their potential use for the treatment of CXCR4^{+} tumors but more importantly, and (ii) the wide applicability of the transversal concept supporting the self-assembling self-driving protein drugs based on chemically homogenous building blocks.

In order to evaluate further the therapeutic potential of the engineered toxins and the concepts that support the design of toxin-based nanoparticles we also assessed the pharmacokinetics in blood mouse samples after a single dose of 50 μg for T22-DITOX-H6* or 300 μg for T22-PE24-H6*. This was done through registering their fluorescence emission at 0, 1, 2, 5, 24 and 48 h after administration. We observed a biphasic decline in plasma concentration from Cmax, with a fast nanoparticle biodistribution limited to the plasma compartment for both tested proteins (Vd = 3.9 ml T22-PE-H6* and Vd = 3.2 ml for T22-DITOX-H6*). This fast biodistribution was followed by a second and slow elimination phase, with a half-life of $t_{1/2}$ = 30 h for both nanoparticles (Fig. 7A). This kinetic behavior is similar to the one we previously reported for pharmacologically inactive protein nanoparticles [23], and also similar to that described for antibody-drug conjugates or large nanometric size therapeutic proteins, which show a comportment similar to the unconjugated antibody [55].

In a step further, we assessed the antitumor effect of each nanoparticle in a CXCR4^{+} subcutaneous CRC mouse model after repeated dose administration. After a dosage schedule of 10 μg of T22-DITOX-H6, three times a week, per 8 doses, we observed at the end of the experiment a 5.8-fold reduction in tumor volume, as compared to buffer-treated mice ($p = 0.05$). This was associated with a 3.0-fold increase in apoptoptic figures in tumor tissue ($p < 0.001$) (Fig. 7B), with no significant differences in body weight between toxin-treated and control groups (Fig. 7C). Similarly, and after a dosage schedule in mice of 10 μg of T22-PE24-H6, three times a week, per 8 doses, we observed at the end of the experiment a 2.3-fold reduction in tumor volume, as compared to buffer-treated mice ($p = 0.034$), associated with a 3.8-fold

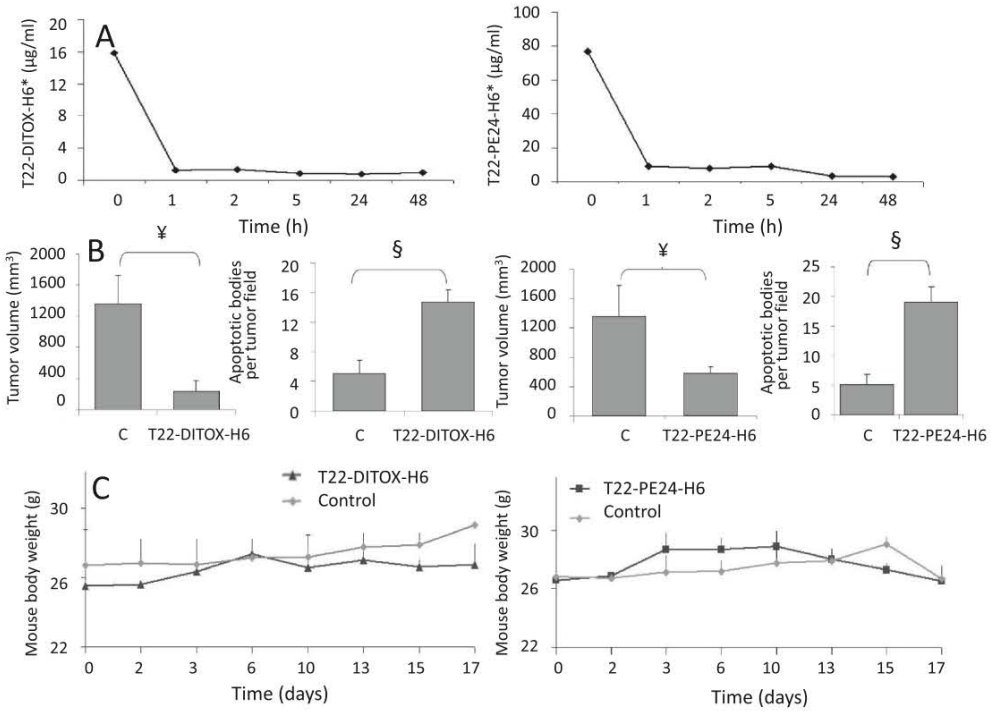

Fig. 7. Pharmacokinetics, antitumoral effect and mouse body weight after T22-DITOX-H6 and T22-PE24-H6 administration. A. Pharmacokinetics of T22-DITOX-H6* and T22-PE24-H6* after a 50 μg or 300 μg intravenous bolus administration respectively. Fluorescence was recorded in plasma obtained after blood centrifugation at time 0, 1, 2, 5, 24 and 48 h (n = 3 per time point). B. Antitumor effect of T22-DITOX-H6 and T22-PE24-H6 measured by the analysis of tumor volume and number of apoptotic bodies at the end of the experiment, after repeated dose administration for each nanoparticle (10 μg, three times a week, × 8 doses). C. Evolution of mouse body weight after the described repeated dose regime for the protein nanoparticles. Statistics are ¥ for $0.01 < p < 0.05$ and § for $p < 0.01$. All data are presented as mean ± SEM, n = 3.

increase in the number of apoptotic figures in tumor tissue ($p = 0.001$) (Fig. 7B). Again, no significant differences in body weight between experimental and control groups were observed (Fig. 7C).

4. Discussion

This set of data is in the line of new nanomedical concepts in targeted drug delivery in which the drugs itself act, in addition to their therapeutic functionalities, as self-assembled and self-delivered entities [18]. Conveniently engineered, the protein drugs developed here have been successfully produced and purified in bacteria, and self-organize as toroid nanoparticles of 30–90 nm (Fig. 2). In this form, they penetrate $CXCR4^+$ target cells (Fig. 3) and promote receptor specific cell killing both *in vitro* (Fig. 4) and *in vivo* (Fig. 6), resulting in significant programmed cell death induction and in destruction of tumoral tissue after single dose administration (Fig. 6). Moreover, after repeated dose administration the nanostructured toxins increase apoptosis in tumor tissue associated with a significant reduction of tumor volume, with no alteration of mouse body weight (Fig. 7). These data prove the realistic feasibility of the application of these nanostructured toxins in a true therapeutic context. In comparison with similar approaches to generate self-assembling peptidic drugs (as pro-apoptotic and antimicrobial agents) [24,56], the concept explored here (i) does not use supporting irrelevant proteins such as GFP, thus minimizing the amount of bulk inactive material in the drug and enhancing nominal productivity in cell factories and (ii) allows the releasing of the active proteins in the cell cytoplasm by the controlled discharging of accessory protein segments that had been exploited for self-assembling of the building blocks and for the biodistribution and cell-targeted internalization of the nanoparticles. In this regard, the intrinsic cytotoxicity of the protein drugs is dramatically enhanced by the occurrence of the active domain free from siding accessory peptides (Fig. 4). This is achieved by the appropriate incorporation of intracellular cleavage sites in the fusion protein that allow protein activation once in the right cell compartment and promotes the cytotoxic activity being executed solely by the minimal functional protein domain. As a generic concept, removing the vehicle in cell-targeted nanomedicines [18], would replace the otherwise promoted nanoconjugate strategies [57] through the design of new generations of chemically homogeneous nanoscale drugs. This would not only allow a heavy reduction of fabrication costs, but it will also minimize off-target drug effects, smoother regulatory constraints to drug approval and reduce the concerns about individual and environmental toxicity of inappropriate materials used as carriers. In this regard, other examples of self-assembling, self-delivered drugs are based on the combination of different types of molecules to achieve their function. Note the aggregation of VEGF siRNA, PolyMet (polymeric metmorfine), polyethylenimine, dicyandiamide, hyaluronic acid, DOTAP, cholesterol, DOTAP and a pegylated targeting ligand [19], or of EGCG, PEG, and herceptin or interferon α-2a [20] in self-delivered materials (summarized in [18]). The exceptional but technologically simple functional recruitment offered by proteins in single polypeptide chains [21] allows not only purifying the drug from recombinant cell factories in a single step by fully standardized recombinant DNA technologies [9], but globally, it also conduces to the simple design of self-assembling nanoparticles that can be easily fabricated in promising endotoxin-free bacterial systems [58,59].

5. Conclusions

We provide here data that fully supports an emerging groundbreaking concept in nanomedicine that is the generation of self-assembled, self-delivered drugs that act in absence of any external vehicle

[18]. The approach presented here, based on modular recombinant proteins, allows the single-step biological production of nanostructured protein materials that exhibit intrinsic therapeutic properties and show an appropriate cell targeting and biodistribution upon systemic administration. This is linked to a specific biological impact (tumor tissue destruction leading to tumor shrinkage) at the local level, because of the cell targeting domains included in the nanoparticle. These functional stretches, useful for biodistribution and during the delivery process, are self-removed from the protein nanoparticles once they have reached the target cell compartment. Then, the cytotoxic protein domain acts very efficiently free from any accessory protein segment. The design of self-organizing, cell-targeted protein drugs at the nanoscale level represents a step forward towards chemically homogeneous nanomedicines that should allow to full discard additional, potentially deleterious carriers.

Supplementary data to this article can be found online at https://doi.org/10.1016/j.jconrel.2018.01.031.

Competing interests

LSG, NS, UU, MSC, IC, RM, EV and AV are con-inventors of the patent application EP17169722.0 on the use of self-structured protein drugs.

Acknowledgments

We are indebted to Agencia Estatal de Investigación (AEI) and to Fondo Europeo de Desarrollo Regional (FEDER) (grant BIO2016-76063-R, AEI/FEDER, UE), AGAUR (2014SGR-132) and CIBER-BBN (project NANOPROTHER) granted to AV, Marató de TV3 Foundation (TV32013-3930) and ISCIII (PI15/00272 co-founding FEDER) to EV and ISCIII (PI15/00378 and PIE15/00028, co-founding FEDER), Marató de TV3 foundation (TV32013-2030) and AGAUR2014-PROD0005 to RM. Protein production has been partially performed by the ICTS "NANBIOSIS", more specifically by the Protein Production Platform of CIBER-BBN/IBB (http://www.nanbiosis.es/unit/u1-protein-production-platform-ppp/). Biodistribution studies were performed in the NANBIOSIS Nanotoxicology Unit and particle characterization was partially done at the NANBIOSIS Biomaterial Processing and Nanostructuring Unit. We are also indebted to SCAC (UAB) for cell culture facilities and assistance. LSG was supported by AGAUR (2017FI_B100063), NS by a predoctoral fellowship from the Government of Navarra, UU received a Sara Borrell postdoctoral fellowship and MVC is supported by Miguel Servet contract, both from ISCIII and AV an ICREA ACADEMIA award.

References

[1] J.J. Calvete, L. Sanz, Y. Angulo, B. Lomonte, J.M. Gutierrez, Venoms, venomics, antivenomics, FEBS Lett. 583 (2009) 1736–1743.
[2] C.Y. Koh, R.M. Kini, From snake venom toxins to therapeutics—cardiovascular examples, Toxicon 59 (2012) 497–506.
[3] P. Russo, A. Del Bufalo, M. Fini, Deep sea as a source of novel-anticancer drugs: update on discovery and preclinical/clinical evaluation in a systems medicine perspective, EXCLI J. 14 (2015) 228–236.
[4] B.G. Livett, K.R. Gayler, Z. Khalil, Drugs from the sea: conopeptides as potential therapeutics, Curr. Med. Chem. 11 (2004) 1715–1723.
[5] M. D'Incalci, M. Simone, M. Tavecchio, G. Damia, A. Garbi, E. Erba, New drugs from the sea, J. Chemother. 16 (Suppl. 4) (2004) 86–89.
[6] J.W. Fox, S.M. Serrano, Approaching the golden age of natural product pharmaceuticals from venom libraries: an overview of toxins and toxin-derivatives currently involved in therapeutic or diagnostic applications, Curr. Pharm. Des. 13 (2007) 2927–2934.
[7] S. Kotova, R.M. Wong, R.B. Cameron, New and emerging therapeutic options for malignant pleural mesothelioma: review of early clinical trials, Cancer Manag. Res. 7 (2015) 51–63.
[8] N.B. Finnerup, N. Attal, S. Haroutounian, E. McNicol, R. Baron, R.H. Dworkin, et al., Pharmacotherapy for neuropathic pain in adults: a systematic review and meta-analysis, Lancet Neurol. 14 (2015) 162–173.
[9] L. Sanchez-Garcia, L. Martin, R. Mangues, N. Ferrer-Miralles, E. Vazquez, A. Villaverde, Recombinant pharmaceuticals from microbial cells: a 2015 update, Microb. Cell Factories 15 (2016) 33.
[10] C. Sarfo-Poku, O. Eshun, K.H. Lee, Medical application of scorpion venom to breast cancer: a mini-review, Toxicon 122 (2016) 109–112.
[11] J. Chaisakul, W.C. Hodgson, S. Kuruppu, N. Prasongsook, Effects of animal venoms and toxins on hallmarks of cancer, J. Cancer 7 (2016) 1571–1578.
[12] C. Zhan, C. Li, X. Wei, W. Lu, W. Lu, Toxins and derivatives in molecular pharmaceutics: drug delivery and targeted therapy, Adv. Drug Deliv. Rev. 90 (2015) 101–118.
[13] C. Bachran, S.H. Leppla, Tumor targeting and drug delivery by anthrax toxin, Toxins 8 (2016).
[14] Y.M. Li, W.A. Hall, Targeted toxins in brain tumor therapy, Toxins 2 (2010) 2645–2662.
[15] N.G. Rainov, A. Soling, Clinical studies with targeted toxins in malignant glioma, Rev. Recent Clin. Trials 1 (2006) 119–131.
[16] A. Elsaesser, C.V. Howard, Toxicology of nanoparticles, Adv. Drug Deliv. Rev. 64 (2012) 129–137.
[17] C. Haynes, Editorial—analytical toxicology of nanoparticles, Analyst 139 (2014) 868–869.
[18] J. Shen, J. Wolfram, M. Ferrari, H. Shen, Taking the vehicle out of drug delivery, Mater. Today 20 (2017) 95–97.
[19] Y. Zhao, W. Wang, S. Guo, Y. Wang, L. Miao, Y. Xiong, et al., PolyMetformin combines carrier and anticancer activities for in vivo siRNA delivery, Nat. Commun. 7 (2016) 11822.
[20] J.E. Chung, S. Tan, S.J. Gao, N. Yongvongsoontorn, S.H. Kim, J.H. Lee, et al., Self-assembled micellar nanocomplexes comprising green tea catechin derivatives and protein drugs for cancer therapy, Nat. Nanotechnol. 9 (2014) 907–912.
[21] E. Vazquez, R. Mangues, A. Villaverde, Functional recruitment for drug delivery through protein-based nanotechnologies, Nanomedicine 11 (2016) 1333–1336.
[22] R. Duncan, R. Gaspar, Nanomedicine(s) under the microscope, Mol. Pharm. 8 (2011) 2101–2141.
[23] M.V. Cespedes, U. Unzueta, W. Tatkiewicz, A. Sanchez-Chardi, O. Conchillo-Sole, P. Alamo, et al., In vivo architectonic stability of fully de novo designed protein-only nanoparticles, ACS Nano 8 (2014) 4166–4176.
[24] N. Serna, M.V. Céspedes, L. Sánchez-García, U. Unzueta, R. Sala, A. Sánchez-Chardi, F. Cortés, N. Ferrer-Miralles, R. Mangues, E. Vázquez, A. Villaverde, Peptide-based nanostructured materials with intrinsic proapoptotic activities in CXCR4$^+$ solid tumors, Adv. Funct. Mater. 27 (2017) (1700919).
[25] R.J. Collier, Understanding the mode of action of diphtheria toxin: a perspective on progress during the 20th century, Toxicon 39 (2001) 1793–1803.
[26] M. Michalska, P. Wolf, Pseudomonas exotoxin a: optimized by evolution for effective killing, Front. Microbiol. 6 (2015) 963.
[27] S. Seetharam, V.K. Chaudhary, D. FitzGerald, I. Pastan, Increased cytotoxic activity of *Pseudomonas* exotoxin and two chimeric toxins ending in KDEL, J. Biol. Chem. 266 (1991) 17376–17381.
[28] R.K. Holmes, Biology and molecular epidemiology of diphtheria toxin and the tox gene, J. Infect. Dis. 181 (Suppl. 1) (2000) S156–67.
[29] B.Y. Wong, S.A. Gregory, N.H. Dang, Denileukin diftitox as novel targeted therapy for lymphoid malignancies, Cancer Investig. 25 (2007) 495–501.
[30] F. Bauss, M. Lechmann, B.F. Krippendorff, R. Staack, F. Herting, M. Festag, et al., Characterization of a re-engineered, mesothelin-targeted *Pseudomonas* exotoxin fusion protein for lung cancer therapy, Mol. Oncol. 10 (2016) 1317–1329.
[31] H.Y. Kim, J.Y. Hwang, S.W. Kim, H.J. Lee, H.J. Yun, S. Kim, et al., The CXCR4 antagonist AMD3100 has dual effects on survival and proliferation of myeloma cells in vitro, Cancer Res. Treat. 42 (2010) 225–234.
[32] J.S. Song, C.M. Kang, H.H. Kang, H.K. Yoon, Y.K. Kim, K.H. Kim, et al., Inhibitory effect of CXC chemokine receptor 4 antagonist AMD3100 on bleomycin induced murine pulmonary fibrosis, Exp. Mol. Med. 42 (2010) 465–472.
[33] J.P. Richard, K. Melikov, E. Vives, C. Ramos, B. Verbeure, M.J. Gait, et al., Cell-penetrating peptides. A reevaluation of the mechanism of cellular uptake, J. Biol. Chem. 278 (2003) 585–590.
[34] J. Kim, K.L. Connelly, E.M. Unterwald, S.M. Rawls, Chemokines and cocaine: CXCR4 receptor antagonist AMD3100 attenuates cocaine place preference and locomotor stimulation in rats, Brain Behav. Immun. 62 (2017) 30–34.
[35] Y.H. Jung, D.Y. Lee, W. Cha, B.H. Kim, M.W. Sung, K.H. Kim, et al., Antitumor effect of CXCR4 antagonist AMD3100 on the tumorigenic cell line of BHP10-3 papillary thyroid cancer cells, Head Neck 38 (2016) 1479–1486.
[36] U. Unzueta, M.V. Cespedes, N. Ferrer-Miralles, I. Casanova, J. Cedano, J.L. Corchero, et al., Intracellular CXCR4(+) cell targeting with T22-empowered protein-only nanoparticles, Int. J. Nanomedicine 7 (2012) 4533–4544.
[37] U. Unzueta, N. Ferrer-Miralles, J. Cedano, X. Zikung, M. Pesarrodona, P. Saccardo, et al., Non-amyloidogenic peptide tags for the regulatable self-assembling of protein-only nanoparticles, Biomaterials 33 (2012) 8714–8722.
[38] T. Koshiba, R. Hosotani, Y. Miyamoto, J. Ida, S. Tsuji, S. Nakajima, et al., Expression of stromal cell-derived factor 1 and CXCR4 ligand receptor system in pancreatic cancer: a possible role for tumor progression, Clin. Cancer Res. 6 (2000) 3530–3535.
[39] H. Kulbe, N.R. Levinson, F. Balkwill, J.L. Wilson, The chemokine network in cancer—much more than directing cell movement, Int. J. Dev. Biol. 48 (2004) 489–496.
[40] T. Murakami, A.R. Cardones, S.T. Hwang, Chemokine receptors and melanoma metastasis, J. Dermatol. Sci. 36 (2004) 71–78.
[41] F. Barbieri, A. Bajetto, T. Florio, Role of chemokine network in the development and progression of ovarian cancer: a potential novel pharmacological target, J. Oncol. 2010 (2010) 426956.
[42] A. Albanese, P.S. Tang, W.C. Chan, The effect of nanoparticle size, shape, and surface chemistry on biological systems, Annu. Rev. Biomed. Eng. 14 (2012) 1–16.
[43] B.D. Chithrani, A.A. Ghazani, W.C. Chan, Determining the size and shape

dependence of gold nanoparticle uptake into mammalian cells, Nano Lett. 6 (2006) 662–668.
[44] F. Rueda, M.V. Cespedes, O. Conchillo-Sole, A. Sanchez-Chardi, J. Seras-Franzoso, R. Cubarsi, et al., Bottom-up instructive quality control in the biofabrication of smart protein materials, Adv. Mater. 27 (2015) 7816–7822.
[45] M. Pesarrodona, E. Crosas, R. Cubarsi, A. Sanchez-Chardi, P. Saccardo, U. Unzueta, et al., Intrinsic functional and architectonic heterogeneity of tumor-targeted protein nanoparticles, Nanoscale 9 (2017) 6427–6435.
[46] B. Vincenzi, G. Armento, M. Spalato Ceruso, G. Catania, M. Leakos, D. Santini, et al., Drug-induced hepatotoxicity in cancer patients - implication for treatment, Expert Opin. Drug Saf. 15 (2016) 1219–1238.
[47] P. Sarges, J.M. Steinberg, J.H. Lewis, Drug-induced liver injury: highlights from a review of the 2015 literature, Drug Saf. 39 (2016) 801–821.
[48] G. Damodar, T. Smitha, S. Gopinath, S. Vijayakumar, Y. Rao, An evaluation of hepatotoxicity in breast cancer patients receiving injection Doxorubicin, Ann. Med. Health Sci. Res. 4 (2014) 74–79.
[49] J. Wang, Y. Wu, M. Dong, X. He, Z. Wang, J. Li, et al., Observation of hepatotoxicity during long-term gefitinib administration in patients with non-small-cell lung cancer, Anti-Cancer Drugs 27 (2016) 245–250.
[50] W. Wang, P. Lie, M. Guo, J. He, Risk of hepatotoxicity in cancer patients treated with immune checkpoint inhibitors: a systematic review and meta-analysis of published data, Int. J. Cancer 141 (2017) 1018–1028.
[51] I.S. Elefsiniotis, K.D. Pantazis, A. Ilias, L. Pallis, A. Mariolis, I. Glynou, et al., Tamoxifen induced hepatotoxicity in breast cancer patients with pre-existing liver steatosis: the role of glucose intolerance, Eur. J. Gastroenterol. Hepatol. 16 (2004) 593–598.
[52] N. Bertrand, J.C. Leroux, The journey of a drug-carrier in the body: an anatomo-physiological perspective, J. Control. Release 161 (2012) 152–163.
[53] J.B. Regard, I.T. Sato, S.R. Coughlin, Anatomical profiling of G protein-coupled receptor expression, Cell 135 (2008) 561–571.
[54] I.D. Weiss, O. Jacobson, Molecular imaging of chemokine receptor CXCR4, Theranostics 3 (2013) 76–84.
[55] A. Deslandes, Comparative clinical pharmacokinetics of antibody-drug conjugates in first-in-human Phase 1 studies, MAbs 6 (2014) 859–870.
[56] N. Serna, L. Sanchez-Garcia, A. Sanchez-Chardi, U. Unzueta, M. Roldan, R. Mangues, et al., Protein-only, antimicrobial peptide-containing recombinant nanoparticles with inherent built-in antibacterial activity, Acta Biomater. 60 (2017) 256–263.
[57] A.Z. Wang, R. Langer, O.C. Farokhzad, Nanoparticle delivery of cancer drugs, Annu. Rev. Med. 63 (2012) 185–198.
[58] F. Rueda, M.V. Cespedes, A. Sanchez-Chardi, J. Seras-Franzoso, M. Pesarrodona, N. Ferrer-Miralles, et al., Structural and functional features of self-assembling protein nanoparticles produced in endotoxin-free *Escherichia coli*, Microb. Cell Factories 15 (2016) 59.
[59] O. Cano-Garrido, M.V. Cespedes, U. Unzueta, P. Saccardo, M. Roldan, A. Sanchez-Chardi, et al., CXCR4(+)-targeted protein nanoparticles produced in the food-grade bacterium *Lactococcus lactis*, Nanomedicine 11 (2016) 2387–2398.

ANNEX 2: DRAFT 1

Toxin-based nanoparticles are effective tools against human colon cancer stem cells.

Naroa Serna, Patricia Álamo, Daria Vinokurova, Prashanthi Ramesh, Laura Sánchez, Ugutz Unzueta, Mª Virtudes Céspedes, Ramón Mangues, Esther Vázquez, Antonio Villaverde and Jan Paul Medema.

.

Toxin-based nanoparticles are effective tools against human colon cancer stem cells.

Naroa Serna[1,2,3], Patricia Álamo[3,4], Daria Vinokurova[5,6], Prashanthi Ramesh[5,6], Laura Sánchez[1,2,3], Ugutz Unzueta[1,2,3], Mª Virtudes Céspedes, Ramón Mangues, Esther Vázquez[1,2,3], Antonio Villaverde[1,2,3,*] and Jan Paul Medema[5,6,7,*].

*Corresponding authors.

[1] Institut de Biotecnologia i de Biomedicina, Universitat Autònoma de Barcelona, Bellaterra, 08193 Barcelona, Spain.

[2] Departament de Genètica i de Microbiologia, Universitat Autònoma de Barcelona, Bellaterra, 08193 Barcelona, Spain.

[3] CIBER de Bioingeniería, Biomateriales y Nanomedicina (CIBER-BBN), Bellaterra, 08193 Barcelona, Spain.

[4] Biomedical Research Institute Sant Pau (IIB-Sant Pau) and Josep Carreras Research Institute, Hospital de la Santa Creu i Sant Pau, 08025 Barcelona, Spain.

[5] Laboratory for Experimental Oncology and Radiobiology (LEXOR), Center for Experimental Molecular Medicine (CEMM), Academic Medical Center (AMC), University of Amsterdam, 1105AZ, Amsterdam, The Netherlands.

[6] Cancer Center Amsterdam and Cancer Genomics Center, Amsterdam, The Netherlands.

[7] Academic Medical Center, Meibergdreef 9, 1105AZ, Amsterdam, The Netherlands.

Abstract

Current therapies fail to eradicate colorectal cancer stem cells (CSCs) and therefore selecting a resistant cell subset that is able to facilitate tumor recurrences and metastases. In this study, we have explored the potency of CXCR4-targeted self-assembling toxin-based nanoparticles to target, kill and circumvent resistance presented by colon-CSCs to traditional therapy. For that, we used 3D spheroid colon-CSCs cultures directly derived from patients with colorectal cancer. Results set the basis for further developement of more efficient therapies focused on CSCs targeting and represent a pre-clinical proof of concept for the use of toxins as protein drugs for colon-CSC therapy.

1 Introduction

Cancer stem cells (CSCs) are the tumorigenic root of cancers due to their clonogenic and high self-renewal capacity [1-3]. CSCs are suggested to be selectively resistant to conventional therapy [4,5] and recent studies have highlighted their principal role in tumor recurrence, relapse and metastatic dissemination [4,6]. The development of treatment strategies that can specifically target and eliminate CSCs are therefore expected to enable a long-lasting clinical response controlling metastatic process [7-10].

Hepatic metastases are the principal reason of the mortality in colon cancer patients [11]. Nowadays, stage 3 patients are routinely treated with co-adjuvant chemotherapy (5-fluorourocil (5-FU), oxaliplatin and Irinotecan) after radical resection of the primary tumor. However, after a period of remission cancer recurs in nearly 35% of all cases [12-14], possibly because these drugs do not promote efficient destruction of colon-CSCs. Thus we hypothesize that there is an urgent need to develop new drugs that can specifically target and kill colon-CSCs [7], which must be necessarily based on developing new concepts for advanced drug design.

Tumor spheroids are one of the most versatile scaffold-free methods for three-dimensional (3D) cell culture that have gained increasing interest in drug discovery for research [15,16]. These cultures provide highly relevant physiological information regarding cell-cell interactions, hypoxia, drug penetration, response and resistance, being a powerful tool for CSC therapy research [17]. The colon CSCs within colon carcinomas can be propagated in vitro as spheroid cultures retaining tumorigenic capacity under specific conditions.

Recent identification of surface markers in colon cancer allows for the proper design of effective targeted drug treatments [1]. Colon-CSCs have been found to overexpress the chemokine receptor CXCR4, which plays a critical role in determining the metastatic destination to the liver, bone and lungs where its ligand SDF-1 is abundant [18-23]. Indeed, patients with high CXCR4-expressing tumors have increased risk of local recurrence and distant metastases [21,24], and also CXCR4 expression is higher in the metastases compared to primary tumors [25]. This offers preclinical evidence that

blockade of the SDF-1/CXCR4 and depletion of CXCR4+ cell population is a promising therapeutic strategy to achieve metastatic control in colon cancer [26-29].

The use of nanoparticles as vehicles for targeted drug delivery significantly increases efficiency of the delivery of payload drug to the target cells and mitigates side effects of conventional chemotherapy[30,31]. The architectonic control of nanoparticle size allows achieving an optimal structure in order to avoid renal clearance[32,33]. Self-assembling protein domains such a cationic stretches offer unique opportunities to generate protein only- nanostructured materials that promote oligomerization of the whole polypeptide[34-36]. In this context, these self-assembling domains can be fused to cytotoxic proteins to generate protein-only, fully stable nanoparticles with intrinsic therapeutic activities[37]. Among cytotoxic peptides, toxins are highly bioactive molecules that inhibit protein synthesis on cells leading to cell death. Previously, we have engineered the catalytic site of the diphtheria toxin (DITOX) and the *Pseudomonas aeruginosa* exotoxin (PE24) as self-assembling therapeutic materials targeted to CXCR4 for the systemic treatment of CXCR4 over-expressing tumors such a breast, colon and pancreatic cancers[37]. The systemic administration of both nanostructured drugs in a primary colorectal cancer xenograft mouse model promotes specific local destruction of target tumor tissues. As conventional treatments, such as chemotherapy and radiation, can kill bulk tumor cells, but fail to induce durable clinical results potentially because they are not effective at eliminating CSCs, the cytotoxic effect of toxin based nanoparticles on colon CSCs should be further explored.

In this study, we have explored whether CXCR4-targeted self-assembling toxin-based nanoparticles were able to circumvent resistance of colon CSCs and could be valuable tools for colon-CSC-specific therapy. We used 3D spheroid colon-CSCs cultures directly derived from patients with colorectal cancer and a colon CSCs mouse model. Results set the basis for further developement of more efficient therapies focused on CSCs targeting. In addition it represents a pre-clinical proof of concept for the use of T22-DITOX-H6 and T22-PE24-H6 as potential “all in one” drug and delivery platform.

2 Materials and Methods.

2.1 Protein nanoparticles.

The synthetic genes were designed in house inserted into the prokaryotic expression pET-22b vector and obtained from Genscript (Piscataway, USA). The encoded proteins were produced in Escherichia coli Origami B (BL21, OmpT- , Lon- , TrxB- , Gor- , Novagen) and purified by His-tag affinity chromatography as described before. Fusion proteins T22-DITOX-H6 and T22-PE24-H6 were named according to their modular organization.

2.2 Cell lines and culture.

Cancer stem cell cultures (CSC) were isolated from patients with colon cancer and classified based on gene expression data according to the consensus molecular stratification: Da13, RC511, Co147 (consensus molecular subtype (CMS) 4), GTG7 (CMS2). Colon CSC cultures were maintained in serum-free medium supplemented with EGF (50 ng/ml) and FGF (4ng/ml) under low-adherent condition (Poly-HEMA coating, Sigma-Aldrich). Routine passaging implied enzymatic dissociation of spheres using accutase (Da13, RC511, Co147) or trypsin-EDTA (GTG7) solution.

2.3 CXCR4 expression: Flow cytometry and qRT-PCR.

Flow cytometry was performed on dissociated CSC cultures. Cell surface expression of CXCR4 in CSCs was determined with APC anti-human CD184 antibody clone 12G5 (BioLegend). Dead cells were excluded using 7-AAD (BD Biosciences).

For qRT-PCR, total RNA from CSC cultures was extracted according to the manufacturer's protocol (NucleoSpin® RNA, Macherey Nagel) and reverse transcribed into cDNA. qRT–PCR was performed using SYBR Green (Roche) and a Roche Light Cycler 480 II. Primer sequences included CXCR4 (forward: 5'-AGCATGACGGACAAGTACAGG-3'; reverse: 5'-GATGAAGTCGGGAATAGTCAGC-3'), CXCL12 - intron-spanning (forward: 5'-AGAGCCAACGTCAAGCATCT-3'; reverse: 5'-CTTTAGCTTCGGGTCAATGC-3'). Levels of target genes are reported as relative values *to GAPDH.*

2.4 Clonogenic assay.

To check the correlation between CXCR4 expression and clonogenic potential CSCs were stained with APC anti-human CD184 antibody and 10% cell fractions with highest and lowest expression of CXCR4 were used in clonogenic assay. Cells were seeded into 96-well plates in density 1, 1, 2, 2, 4, 4, 8, 8, 12, 16, 32, 64 cells/well, dead cells were excluded using 7-AAD. Positive results for each dose were scored after 14 days. Estimation of clonogenic cell frequency was perfomed using ELDA webtool (http://bioinf.wehi.edu.au/software/elda/index.html).

2.5 Internalization assay.

CXCR4+ Da13 and CXCR4- GTG7 spheroid cultures were used to study the performance of the toxin nanoparticles. GTG7 and Da13 spheroid cultures were dissociated with 0.1 mg/ml trypsin-EDTA (Gibco) and 0.1 mg/ml accutase (Gibco) respectively and seeded as single cells on an adherent cell culture 24-well plate (Greiner). Cells were cultured overnight at 40.000 cells/well until reaching 70% confluence. Nanoparticles were added at 0.1uM to the cell culture during 24 h and additionally, specific internalization through CXCR4 receptor was measured adding specific antagonist AMD3100 1h prior nanoparticle incubation at a ratio of 1:10. Cell samples were analyzed on a FACSCanto system (BD biosciences) using a laser at 488 nm excitation. ATTO488 fluorescence emission was measured with a detector D (530/30 nm band pass filter) after treatment with 1 mg/ml trypsin-EDTA (Gibco) for 15 min. Experiments were performed in duplicate.

2.6 Cell viability assay.

For the cytotoxicity analysis of T22-DITOX-H6 and T22-PE24-H6, the CellTiter-Blue Luminescent Cell Viability Assay (Promega) was used. Da13 and GTG7 spheroid cultures were dissociated as explained before and seeded as single cells on an adherent cell culture 96-well plate (Greiner) at 2000 cells/well overnight. Nanoparticle treatment was performed at different concentrations during 48h. Inhibition of cell death was analyzed by adding AMD3100 at a ratio of 1:10, 1h prior to nanoparticles

incubation at 0.1uM. After nanoparticle incubation, 20 µl/well of cell titer blue reagent (Promega) was add and subsequently, cells were incubated for 4 h and fluorescence was measured on a Biotek HT synergy plate reader (BioTek).

2.7 Cell survival assay.

Da13 cancer spheroid cultures were dissociated with accutase and seeded as single cells on an adherent cell culture 12-well plate (Greiner) overnight. Adherent cells were treated with chemotherapeutic drugs and nanoparticles during 24h. After treatment, cells were harvested and 2000 cells were transferred into ultra-low adherent 96-well plates (Corning). Cell survival was measured at different days (0, 2, 5 and 8 days) by adding 20 µl/well of cell titer blue reagent (Promega). Subsequently, cells were incubated for 4 h and fluorescence was measured on a Biotek HT synergy plate reader (BioTek).

2.8 Apoptosis assay and FACS analysis.

In colorectal cancer CSCs were identified by different markers, such as the cell surface molecule CD133, LGR5 expression and Wnt pathway activity. Wnt pathway has been demonstrated to be a stemness marker in GTG7 cell line and therefore, can be used to discriminate cancer stem cells from more differentiated progenity by employing a Wnt reporter construct (TOP-GFP) that directs the expression of green fluorescent protein. Thus, cells expressing high TOP-GFP levels (high TOP-GFP) are shown to be the CSCs and cells with low Wnt pathway activity (low TOP-GFP) correspond to more diffentiated cells. Using these TOP-GFP spheroid cultures we compared the effect of T22-DITOX-H6 to treatment with Oxaliplatin and 5-FU within the CSC population and compare it to the more differentiated tumor cells by the expression of the early apoptosis marker Annexin-V.

GTG7 cancer spheroid cultures were dissociated with trypsin-EDTA (Gibco) and seeded as single cells on an adherent cell culture 12-well plate (Greiner) overnight. The next day, adherent cells were treated with 1uM of chemotherapeutic drugs and different concentrations of T22-DITOX-H6 (1, 0.5, 0.3 and 0.1uM). After 48h treatment, cell death was measured by Annexin-V staining and analyzed by flow cytometry

(FACSCanto, BD biosciences). In summary, spheroid cultured cells were stained with Annexin V-APC (BD biosciences) and 7-AAD (BD biosciences) for 15 min at RT. During FACS, the CSCs were identified by gating on the TOP-GFPhigh, whereas the differentiated cells were determinated simultaneously by gating on the TOP-GFPlow cells.

3 Results.

3.1 Analysis of CXCR4 in colon-CSC spheroid cultures.

To explore the role of CXCR4 in colon CSC biology, we first determined the expression levels of this tumoral marker using flow cytometry. For that, we used four colon cancer spheroid cell lines directly derived from patients that contain stem-like features. Differential CXCR4 expression in CSC cultures was observed with the highest level in Da13 cell line and negative results for RC511 and GTG7 cell lines (Figure 1A). This differential expression was confirmed by qPCR (Figure 1B). For further analyses we decided to select CXCR4+ Da13 and CXCR4- GTG7 cell lines for comparative purposes.

To check the association of CXCR4 marker expression with clonogenecity, CXCR4+ Da13 and CXCR4- GTG7 cells were sorted for population with highest and lowest expression of the receptor followed by limiting dilution assay to compare clonogenic capacity of these populations. Clonogenic assay revealed that Da13 cells with highest CXCR4 expression have more clonogenic potential (Figure 1C). These results suggest that CXCR4 is involved in stem cell function in Da13 spheroids.

3.2 Nanoparticles are specific of CXCR4+ Colon CSCs.

We tested the ability of protein nanoparticles to bind and penetrate, in a receptor-dependent way, CXCR4+ cancer stem cells. The assembled T22-DITOX-H6 and T22-PE24-H6, upon labelling with the fluorescent dye ATTO488 (named as T22-DITOX-H6* and T22-PE24-H6* respectively), efficiently entered CXCR4+ Da13 cells but were not able to internalize into CXCR4- GTG7 cell line. Moreover, the CXCR4-dependent uptake was demonstrated through the inhibition of T22-CXCR4 interaction by AMD3100 that

strongly reduced the intracellular fluorescence in Da13 cells upon exposure (Figure 2A).

Once the internalization was evaluated, we explored toxin nanoparticles mediated cytotoxicity in both cell lines. Cytotoxicity was clearly detectable in CXCR4+ Da13 cell line but it was abolished upon treatment with AMD3100. In addition, toxicity was not observed in CXCR4- GTG7 cell line, revealing the role of the receptor and therapeutic domain in cell death (Figure 2B).

Because of the potent cytotoxic activities of protein toxins, we also checked cell viability in healthy human colon organoids that were generated by culturing colon stem cells derived from a healthy patient submerged in Matrigel. First, we analyzed the CXCR4 expression in these cells. As expected, cells did not express the receptor (data not shown). More importantly, toxicity was not detected in cells treated with funcional nanoparticles (Figure 2B).

3.3 Validation of toxin-based nanoparticles for colon-CSCs therapy.

-Colon CSCs are very efficiently killed by targeted toxin nanoparticles when compared with chemotherapeutic compounds:

Due to the better internalization and cytotoxicity of T22-DITOX-H6 over the spheroids than T22-PE24-H6, we selected this nanoparticle for the following *in vitro* experiments. When CXCR4+ Da13 spheroid cultures were treated with Oxaliplatin and 5-FU chemotherapeutic compounds and nanoparticles at the same concentration (1µM), we observed a strong initial decrease in cell viability in the first 2 days for all treatments. However, when we measured the growth of the cultures over time (up to 8 days), we detected that cells treated with chemotherapeutics regained proliferative potential in the days after, suggesting that clonogenic colon CSCs survived the therapy. In contrast, treatment with T22-DITOX-H6 inhibited this revival strongly (Figure 3A). Importantly, at 100nM, at which receptor mediated internalization of the nanoparticles was observed (Figure 3A), T22-DITOX-H6 remained more effective than the other drugs (Figure 3A).

This indicates that targeting CXCR4+ CSCs with toxin protein fusions is a promising approach for colon-CSC therapy.

-Treatment with toxin functional domains overcomes the resistance of colon-CSCs to chemotherapeutics:

Resistance to chemotherapy induced apoptosis in colorectal cancer (CRC) tumors seem to be due to an increased block of the intrinsic apoptotic pathway in cancer stem cells. Toxins promote cell death by diverse mechanisms besides stimulation of apoptotic pathway. We wondered if they were able to circumvent this resistance, independently of the targeting moiety, for their translational application in the engineering of cytotoxic proteins against cancer stem cells. As these spheroid cultures do not only contain CSCs, but also more differentiated cells, as shown previously by our group, we decided to analyze cell death in the CSC population and compare it with the more differentiated tumor cells simultaneously and under the same conditions in CXCR4- cell line, GTG7.

First, we tested the toxicity over GTG7 culture at different concentrations of nanoparticles to select the appropriate one for the comparative study with chemotherapeutics (Figure 3B). Of course, we assume that increasing dosage does result in death linked to a CXCR4 independent internalization of toxins. We decided to select a concentration of 1µM at which nanoparticle mediated cell death was clear.

As expected, treatment of 3D cultures with 5-FU and Oxaliplatin induced apoptosis in the more differentiated cells, whereas CSCs were resistant. In contrast, T22-DITOX-H6 induces cell death in both population (Figure 3C), indicating that colon CSCs do not display any resistance to it.

4 Discussion.

First-line chemotherapeutic treatment of CRC comprises intravenous 5-FU in combination with oxaliplatin, increasing the response to therapy up to 50% compared with 15% for 5-FU monotherapy[13,14]. Unfortunately, traditional therapy induces tumor cell death and shrinkage but is suggested to grow back due to selective

resistance of a subset of cells that have CSC potential.

There is evidence that CSCs are more resistant to current chemotherapy than other subpopulations of cells within the tumor[5,38]. Slow rate of division, high expression of drug-efflux pumps, an increased blockage of apoptotic pathways and high capacity for DNA repair are CSC specific properties involved in drug resistance. In colon-CSCs, the most relevant resistance mechanisms to oxaliplatin-based combinations are upregulation of GSTP1, a subclass of Glutathione S-transferases, which is involved in the detoxification process, also the autocrine response to the immune cytokine interleukin 4 (IL-4) that entails growth stimulation effects and a blocking of the apoptotic pathway. For instance, a decrease in BAK and BAX levels and an increase of some anti-apoptotic proteins such a Bcl-2 have been reported in colon-CSCs and low expression of BAX has been shown to correlate to 5-FU resistance[39]. Thus, compounds able to overcome these anti-apoptotic defenses makes such agents especially valuable for the effective death of colon CSC.

In this context, major therapeutic values of toxins rely on their ability to kill exposed cells through molecular events that are devoid, in general, of cell type specificity and also, on their incredible killing potency. Interestingly, the evolutionary analysis has revealed a modular architecture of many toxins that offers additional versatility in the engineering of these agents as multifunctional drugs.

Recombinant T22-DITOX-H6 and T22-PE24-H6 proteins kill cells by binding to a CXCR4 receptor, internalizing via a coated pit, translocating its active fragment into the cytosol, and enzymatically ADP-ribosylating elongation factor-2[37]. In turn, both inhibit protein synthesis and cells die by diverse mechanisms that include induction of apoptosis. Remarkably, a single molecule of those toxins is lethal to a cell in some model systems. This cytotoxic potency together with the ability to trigger diverse cell death pathways upon inhibition of protein synthesis may minimize the emergence of specific resistance in cells.

In addition to toxin driven cytotoxicity, T22 ligand has been shown to also induce cell death[36,40]. T22 is a peptide ligand that acts extracellularly by competing with SDF-1α for binding to the CXCR4 receptor. This peptide triggers the inhibition of signal

transduction downstream of CXCR4 leading to proliferative blocking, apoptotic induction and tumor growth.

The insufficient therapeutic effect of chemotherapeutic compounds such as 5-FU or Oxaliplatin is also related to their small molecular size, that being below renal filtration cut-off (around 7 nm) are excreted from the kidney, what result in short circulation time[8,32]. Moreover, those not targeted drugs are regularly systemically administered to patients leading to life-threatening side effects involving the damage of active, fast growing healthy cells such as bone marrow, gastrointestinal or liver cells. In this regard, toxin-based NPs are likely to provide higher circulation times, escape renal clearance and show multivalent display of a CXCR4 ligand, enhancing accumulation in tumor and therefore reducing the required doses.

Importantly no toxicity was detected in cultures derived from healthy human colon tissue suggesting a quite specific action of the protein drug against malignant cells and thus reducing off-target deleterious effects.

Nowadays, there are no available effective colon CSC-targeted therapies that prevent dissemination and metastasis. Therefore, it is important to develop new treatments able to target and efficiently kill this chemotherapy-refractory population in colon tumors[10]. Results obtained here show that CXCR4-targeted toxin nanoparticles not only target and effectively kill tumor colon CSCs, but also, they are able to overcome the resistance presented by colon-CSCs to traditional therapy.

For a clinical point of view, it has been shown that differentiated cancer cells can re-acquire stemness through factors secreted from fibroblasts. Shimokawa et al. propose that killing cancer stem cells would free the niche and allow differentiated tumor cells to fill the space to become cancer stem cells[41]. Importantly, this induced CSC state coincides with re-acquisition of resistance to chemotherapy. Interestingly, in contrast to cancer at the primary site, metastatic cells do not have the capacity to induce de novo cancer stem cells. Therefore, efficient cancer therapy which can target CSCs together with conventional chemotherapy seem to be the more intelligent treatment strategy to eradicate primary tumor and metastatic foci.

In conclusion, toxin-based protein only-nanoparticles, alone or in combinatorial

therapy, are presented as especially valuable tools for the treatment of colon cancer overcoming issues of improve therapeutic efficacy, drug resistance and metastasis.

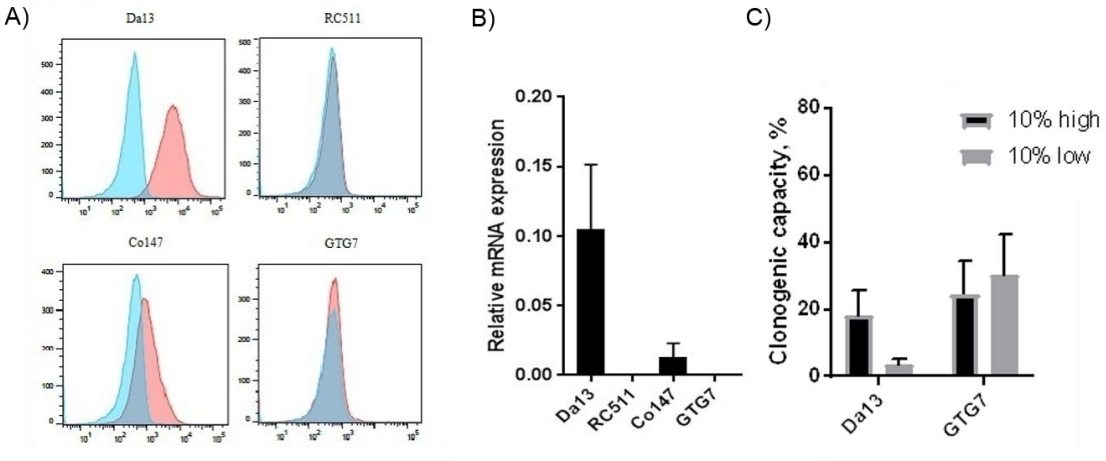

Figure 1: CXCR4 expression in CSC cultures. (A) FACS analysis of CXCR4 expression. (B) Expression of CXCR4 evaluated by quantitative RT-PCR, error bars represent s.d. (n = 2). (C) Correlation of CXCR4 expression with clonogenic potential.

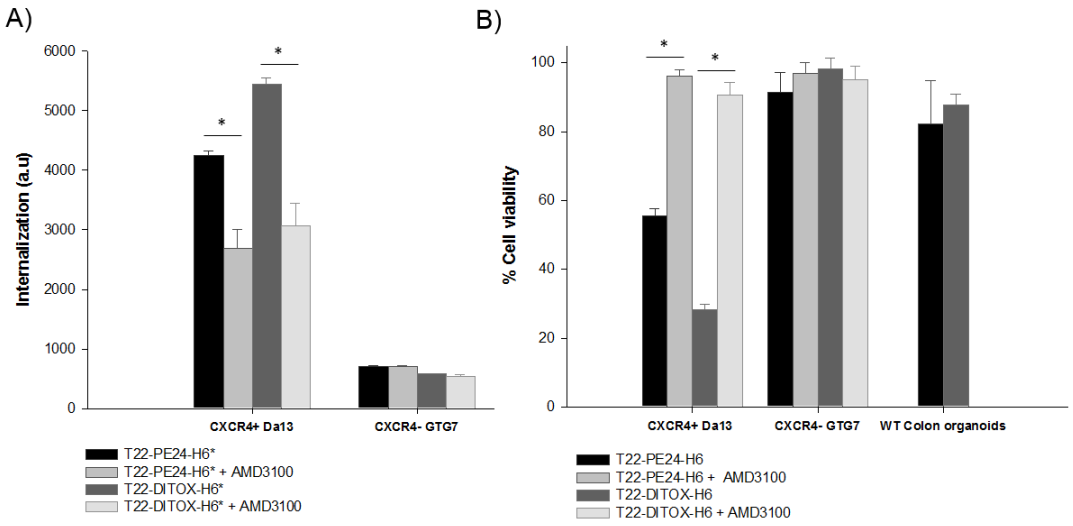

Figure 2: (A) Internalization of 100nM of T22-DITOX-H6* and T22-PE24-H6* upon 2h of exposure and uptake inhibition by AMD3100 in spheroid cultures. (B) Cell death induced by 100nM of toxin-based nanoparticles in CXCR4+/- colon CSCs spheroids and WT colon organoids 48 after exposure. Correlation of CXCR4 expression with clonogenic potential. Significan differences between relevant data pairs are indicated as * $p<0.01$.

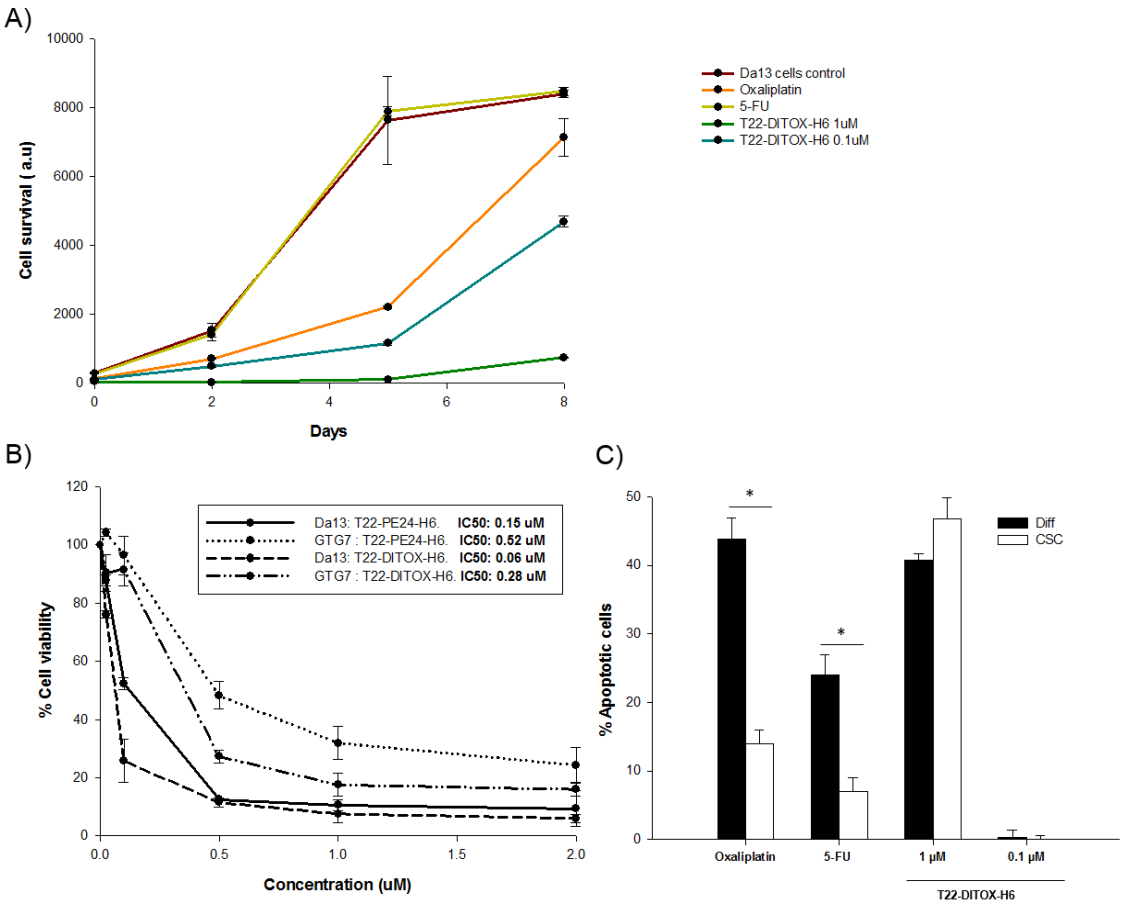

Figure 3: (A) Da13 spheroid cultures were treated with 1uM of chemotherapeutics and 1 and 0.1uM of T22-DITOX-H6 for 24h and cell numbers were measured at various time points. (B) Cell death induced by T22-DITOX-H6 at different concentrations over a CXCR4+ Da13 and CXCR4- GTG7 spheroids 48 after exposure. (C) GTG7 spheroids were treated for 48h with 1uM of chemotherapeutics and 1 and 0.1uM of T22-DITOX-H6. Next, early marker of apoptosis, Annexin-V staining was measured in differentiated cancer cells and CSCs. Significant differences between relevant data pairs are indicated as * $p<0.01$.

References

[1] K. Mabert, M. Cojoc, C. Peitzsch, I. Kurth, S. Souchelnytskyi, and A. Dubrovska, Cancer biomarker discovery: current status and future perspectives, Int. J. Radiat. Biol., 90 (2014) 659-677.

[2] J. P. Medema, Cancer stem cells: the challenges ahead, Nat. Cell Biol., 15 (2013) 338-344.

[3] P. R. Prasetyanti and J. P. Medema, Intra-tumor heterogeneity from a cancer stem cell perspective, Mol. Cancer, 16 (2017) 41.

[4] J. C. Chang, Cancer stem cells: Role in tumor growth, recurrence, metastasis, and treatment resistance, Medicine (Baltimore), 95 (2016) S20-S25.

[5] S. Colak and J. P. Medema, Cancer stem cells--important players in tumor therapy resistance, FEBS J., 281 (2014) 4779-4791.

[6] C. Peitzsch, A. Tyutyunnykova, K. Pantel, and A. Dubrovska, Cancer stem cells: The root of tumor recurrence and metastases, Semin. Cancer Biol., 44 (2017) 10-24.

[7] M. Todaro, M. G. Francipane, J. P. Medema, and G. Stassi, Colon cancer stem cells: promise of targeted therapy, Gastroenterology, 138 (2010) 2151-2162.

[8] D. L. Dragu, L. G. Necula, C. Bleotu, C. C. Diaconu, and M. Chivu-Economescu, Therapies targeting cancer stem cells: Current trends and future challenges, World J. Stem Cells, 7 (2015) 1185-1201.

[9] S. J. Vidal, V. Rodriguez-Bravo, M. Galsky, C. Cordon-Cardo, and J. Domingo-Domenech, Targeting cancer stem cells to suppress acquired chemotherapy resistance, Oncogene, 33 (2014) 4451-4463.

[10] R. J. Winquist, D. M. Boucher, M. Wood, and B. F. Furey, Targeting cancer stem cells for more effective therapies: Taking out cancer's locomotive engine, Biochem. Pharmacol., 78 (2009) 326-334.

[11] A. K. Croker and A. L. Allan, Cancer stem cells: implications for the progression and treatment of metastatic disease, J. Cell Mol. Med., 12 (2008) 374-390.

[12] D. Cunningham, Y. Humblet, S. Siena, D. Khayat, H. Bleiberg, A. Santoro, D. Bets, M. Mueser, A. Harstrick, C. Verslype, I. Chau, and C. E. Van, Cetuximab monotherapy and cetuximab plus irinotecan in irinotecan-refractory metastatic colorectal cancer, N. Engl. J. Med., 351 (2004) 337-345.

[13] J. Mishra, J. Drummond, S. H. Quazi, S. S. Karanki, J. J. Shaw, B. Chen, and N. Kumar, Prospective of colon cancer treatments and scope for combinatorial approach to enhanced cancer cell apoptosis, Crit Rev. Oncol. Hematol., 86 (2013) 232-250.

[14] C. E. Van and J. Oliveira, Advanced colorectal cancer: ESMO clinical recommendations for diagnosis, treatment and follow-up, Ann. Oncol., 20 Suppl 4 (2009) 61-63.

[15] Y. Fang and R. M. Eglen, Three-Dimensional Cell Cultures in Drug Discovery and Development, SLAS. Discov., 22 (2017) 456-472.

[16] S. Sant and P. A. Johnston, The production of 3D tumor spheroids for cancer drug discovery, Drug Discov. Today Technol., 23 (2017) 27-36.

[17] L. P. Pereira, P. Silva, M. Duarte, L. Rodrigues, C. M. Duarte, C. Albuquerque, and A. T. Serra, Targeting Colorectal Cancer Proliferation, Stemness and Metastatic Potential Using Brassicaceae Extracts Enriched in Isothiocyanates: A 3D Cell Model-Based Study, Nutrients., 9 (2017).

[18] M. Cojoc, C. Peitzsch, F. Trautmann, L. Polishchuk, G. D. Telegeev, and A. Dubrovska, Emerging targets in cancer management: role of the CXCL12/CXCR4 axis, Onco. Targets. Ther., 6 (2013) 1347-1361.

[19] P. Gassmann, J. Haier, K. Schluter, B. Domikowsky, C. Wendel, U. Wiesner, R. Kubitza, R. Engers, S. W. Schneider, B. Homey, and A. Muller, CXCR4 regulates the early extravasation of metastatic tumor cells in vivo, Neoplasia., 11 (2009) 651-661.

[20] T. Murakami, K. Kawada, M. Iwamoto, M. Akagami, K. Hida, Y. Nakanishi, K. Kanda, M. Kawada, H. Seno, M. M. Taketo, and Y. Sakai, The role of CXCR3 and CXCR4 in colorectal cancer metastasis, Int. J. Cancer, 132 (2013) 276-287.

[21] L. Stanisavljevic, J. Assmus, K. E. Storli, S. M. Leh, O. Dahl, and M. P. Myklebust, CXCR4, CXCL12 and the relative CXCL12-CXCR4 expression as prognostic factors in colon cancer, Tumour. Biol., 37 (2016) 7441-7452.

[22] S. S. Zhang, Z. P. Han, Y. Y. Jing, S. F. Tao, T. J. Li, H. Wang, Y. Wang, R. Li, Y. Yang, X. Zhao, X. D. Xu, E. D. Yu, Y. C. Rui, H. J. Liu, L. Zhang, and L. X. Wei, CD133(+)CXCR4(+) colon cancer cells exhibit metastatic potential and predict poor prognosis of patients, BMC. Med., 10 (2012) 85.

[23] F. Zheng, Z. Zhang, V. Flamini, W. G. Jiang, and Y. Cui, The Axis of CXCR4/SDF-1 Plays a Role in Colon Cancer Cell Adhesion Through Regulation of the AKT and IGF1R Signalling Pathways, Anticancer Res., 37 (2017) 4361-4369.

[24] Y. J. Choi, W. J. Chang, S. W. Shin, K. H. Park, S. T. Kim, and Y. H. Kim, The prognostic role of serum C-X-C chemokine receptor type 4 in patients with metastatic or recurrent colorectal cancer, Onco. Targets. Ther., 9 (2016) 3307-3312.

[25] S. Chatterjee, A. B. Behnam, and S. Nimmagadda, The intricate role of CXCR4 in cancer, Adv. Cancer Res., 124 (2014) 31-82.

[26] M. J. Cutler, E. L. Lowthers, C. L. Richard, D. M. Hajducek, P. A. Spagnuolo, and J. Blay, Chemotherapeutic agents attenuate CXCL12-mediated migration of colon cancer cells by selecting for CXCR4-negative cells and increasing peptidase CD26, BMC. Cancer, 15 (2015) 882.

[27] D. Heckmann, P. Maier, S. Laufs, F. Wenz, W. J. Zeller, S. Fruehauf, and H. Allgayer, CXCR4 Expression and Treatment with SDF-1alpha or Plerixafor Modulate Proliferation and Chemosensitivity of Colon Cancer Cells, Transl. Oncol., 6 (2013) 124-132.

[28] V. R. Katkoori, M. D. Basson, V. C. Bond, U. Manne, and H. L. Bumpers, Nef-M1, a peptide antagonist of CXCR4, inhibits tumor angiogenesis and epithelialtomesenchymal transition in colon and breast cancers, Oncotarget., 6 (2015) 27763-27777.

[29] L. Ma, H. Qiao, C. He, Q. Yang, C. H. Cheung, J. R. Kanwar, and X. Sun, Modulating the interaction of CXCR4 and CXCL12 by low-molecular-weight heparin inhibits hepatic metastasis of colon cancer, Invest New Drugs, 30 (2012) 508-517.

[30] M. S. Lee, E. C. Dees, and A. Z. Wang, Nanoparticle-Delivered Chemotherapy: Old Drugs in New Packages, Oncology (Williston. Park), 31 (2017) 198-208.

[31] K. D. Miller, R. L. Siegel, C. C. Lin, A. B. Mariotto, J. L. Kramer, J. H. Rowland, K. D. Stein, R. Alteri, and A. Jemal, Cancer treatment and survivorship statistics, 2016, CA Cancer J. Clin., 66 (2016) 271-289.

[32] R. Mangues, E. Vazquez, and A. Villaverde, Targeting in Cancer Therapies, Med. Sci. (Basel), 4 (2016).

[33] L. Zhang, F. X. Gu, J. M. Chan, A. Z. Wang, R. S. Langer, and O. C. Farokhzad, Nanoparticles in medicine: therapeutic applications and developments, Clin. Pharmacol. Ther., 83 (2008) 761-769.

[34] N. Ferrer-Miralles, E. Rodriguez-Carmona, J. L. Corchero, E. Garcia-Fruitos, E. Vazquez, and A. Villaverde, Engineering protein self-assembling in protein-based nanomedicines for drug delivery and gene therapy, Crit Rev. Biotechnol., 35 (2015) 209-221.

[35] E. Vazquez and A. Villaverde, Engineering building blocks for self-assembling protein nanoparticles, Microb. Cell Fact., 9 (2010) 101.

[36] U. Unzueta, N. Ferrer-Miralles, J. Cedano, X. Zikung, M. Pesarrodona, P. Saccardo, E. Garcia-Fruitos, J. Domingo-Espin, P. Kumar, K. C. Gupta, R. Mangues, A. Villaverde, and E. Vazquez, Non-amyloidogenic peptide tags for the regulatable self-assembling of protein-only nanoparticles, Biomaterials, 33 (2012) 8714-8722.

[37] L. Sanchez-Garcia, N. Serna, P. Alamo, R. Sala, M. V. Cespedes, M. Roldan, A. Sanchez-Chardi, U. Unzueta, I. Casanova, R. Mangues, E. Vazquez, and A. Villaverde, Self-assembling toxin-based nanoparticles as self-delivered antitumoral drugs, J. Control Release, 274 (2018) 81-92.

[38] J. C. Chang, Cancer stem cells: Role in tumor growth, recurrence, metastasis, and treatment resistance, Medicine (Baltimore), 95 (2016) S20-S25.

[39] S. Colak, C. D. Zimberlin, E. Fessler, L. Hogdal, P. R. Prasetyanti, C. M. Grandela, A. Letai, and J. P. Medema, Decreased mitochondrial priming determines chemoresistance of colon cancer stem cells, Cell Death. Differ., 21 (2014) 1170-1177.

[40] U. Unzueta, M. V. Cespedes, N. Ferrer-Miralles, I. Casanova, J. Cedano, J. L. Corchero, J. Domingo-Espin, A. Villaverde, R. Mangues, and E. Vazquez, Intracellular CXCR4(+) cell targeting with T22-empowered protein-only nanoparticles, Int. J. Nanomedicine., 7 (2012) 4533-4544.

[41] M. Shimokawa, Y. Ohta, S. Nishikori, M. Matano, A. Takano, M. Fujii, S. Date, S. Sugimoto, T. Kanai, and T. Sato, Visualization and targeting of LGR5(+) human colon cancer stem cells, Nature, 545 (2017) 187-192.

ANNEX 3: ARTICLE 5

The fusogenic peptide HA2 impairs selectivity of CXCR4-targeted protein nanoparticles.

L. Sánchez-García[1], N. Serna[1], M. Mattanovich, P. Cazzanelli, A. Sánchez-Chardi, O. Conchillo-Solé, F. Cortés, X. Daura, U. Unzueta, R. Mangues, A. Villaverde and E. Vázquez.

[1]Equally contributed.

Chemical Communications. March 2017. 53:33.

Impact factor: 6.319. Quartile: Q1. Decile: D1.

ChemComm

COMMUNICATION

View Article Online
View Journal

CrossMark click for updates

Cite this: DOI: 10.1039/c6cc09900a

Received 13th December 2016,
Accepted 10th March 2017

DOI: 10.1039/c6cc09900a

rsc.li/chemcomm

The fusogenic peptide HA2 impairs selectivity of CXCR4-targeted protein nanoparticles†

L. Sánchez-García,‡[ag] N. Serna,‡[a] M. Mattanovich,[ab] P. Cazzanelli,[ab] A. Sánchez-Chardi,[c] O. Conchillo-Solé,[a] F. Cortés,[d] X. Daura,[ae] U. Unzueta,*[fg] R. Mangues,[fg] A. Villaverde*[ag] and E. Vázquez[ag]

We demonstrate here that the genetic incorporation of the fusogenic peptide HA2 into a CXCR4-targeted protein nanoparticle dramatically reduces the specificity of the interaction between nanoparticles and cell receptors, a factor to be considered when designing tumor-homing drug vehicles displaying endosomal-escape agents. The loss of specificity is concomitant with enhanced cell penetrability.

Cell-targeted intracellular delivery is a major challenge in innovative medicines, which continuously explore new and more efficient vehicles for conventional and emerging drugs.[1] Targeting can be achieved by the incorporation of ligands for cell receptors into the drug vehicle, which direct specific binding and further endosomal-mediated cell uptake. This is particularly convenient when the vehicle itself is produced in a recombinant form, which allows genetic fusion and biological production of the whole polypeptide.[2] Unfortunately, endosomal uptake drives the engulfed material to a lysosomal pathway, resulting in acidification and proteolysis. Background endosomal leakage and endosomolytic activities naturally present in the recombinant protein allow a fraction of the complex to reach the cytoplasm. Several natural or modified peptides have been identified as strongly endosomolytic, increasing the fraction of internalized material that escapes from lysosomal degradation. Among them, the N-terminal peptide HA2 from the influenza virus hemagglutinin has been widely explored in a diversity of protein constructs intended as nanoscale intracellular vehicles. In acidic environments, such as the endosome, the anionic amino acids of HA2 get protonated, an alpha helix is formed and the peptide acts as an amphiphilic anionic stretch that destabilizes the cell membrane.[3] HA2 alone,[4] or in combination with the TAT peptide from the human immunodeficiency virus-1,[5,6] promotes endosomal release of fusion proteins or nanoscale constructs, which is observed as a promising activity in vehicles for gene therapy and drug delivery.

So far, the potential use of HA2 in combination with specific cell ligands for receptor-mediated cell-targeted delivery has been neglected. However, efficiently combining the selectivity with endosomal escape would represent a step ahead towards the construction of powerful vehicles for targeted drug delivery. Here we have explored this possibility by the incorporation of peptide HA2 into a CXCR4-targeted protein nanoparticle based on a modular, single chain polypeptide (T22-GFP-H6). T22-GFP-H6 self-assembles as toroid nanoparticles of 12 nm, which penetrate CXCR4$^+$ cells with high selectivity, in cell culture and *in vivo*.[7,8] The cationic peptide T22 acts as both a promoter of protein self-assembly[9] and as a specific ligand of CXCR4,[10] a chemokine receptor whose overexpression is associated with aggressiveness in several types of human cancers.[11] In this context, an efficient HA2 version[12] was inserted at two alternative inner positions of T22-GFP-H6 (namely at the amino terminus of the core GFP, or at its carboxy terminus) (Fig. 1A). Both engineered proteins were produced well in *E. coli*, although the lower yield of soluble T22-GFP-HA2-H6 compared to T22-HA2-GFP-H6 resulted in a higher background in mass spectrometry analysis (Fig. 1B). The purity of both products and the predicted molecular mass were however fully assessed by Western blot (Fig. 1B, inset) and using the purification chromatograms (ESI,† Fig. S1). T22-HA2-GFP-H6 and T22-GFP-HA2-H6 proteins spontaneously self-assembled as stable, supramolecular structures with a toroidal shape, with a diameter of 30 nm and 45 nm, respectively, and similar surface

[a] *Institut de Biotecnologia i de Biomedicina and Departament de Genètica i de Microbiologia, Universitat Autònoma de Barcelona, Bellaterra, 08193 Barcelona, Spain. E-mail: antoni.villaverde@uab.es*
[b] *Department of Biotechnology, University of Natural Resources and Life Sciences (BOKU), Muthgasse 18, 1190 Vienna (BOKU), Austria*
[c] *Servei de Microscòpia, Universitat Autònoma de Barcelona, Bellaterra, 08193 Barcelona, Spain*
[d] *Servei de Cultius Cellulars, Producció d'Anticossos i Citometria, (SCAC), Universitat Autònoma de Barcelona, Bellaterra, 08193 Barcelona, Spain*
[e] *Catalan Institution for Research and Advanced Studies (ICREA), 08010 Barcelona, Spain*
[f] *Institut d'Investigacions Biomèdiques Sant Pau and Josep Carreras Research Institute, Hospital de la Santa Creu i Sant Pau, 08025 Barcelona, Spain. E-mail: uunzueta@santpau.cat*
[g] *CIBER de Bioingeniería, Biomateriales y Nanomedicina (CIBER-BBN), Spain*
† Electronic supplementary information (ESI) available. See DOI: 10.1039/c6cc09900a
‡ Equally contributed.

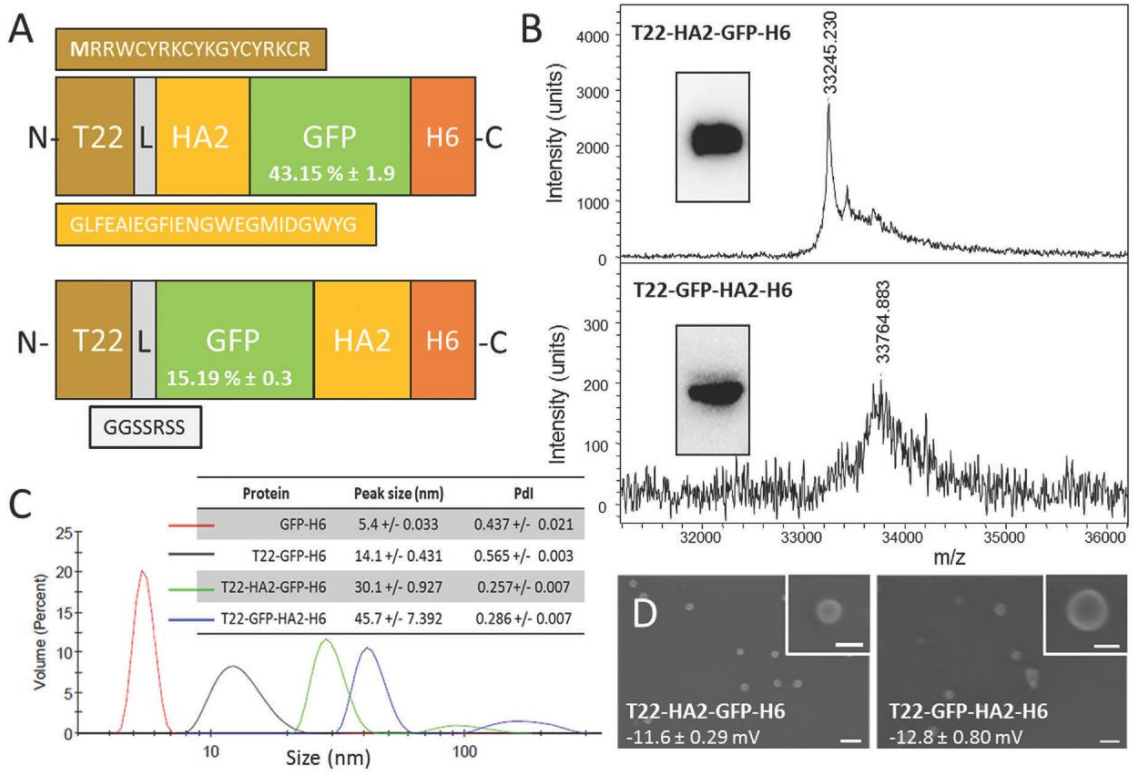

Fig. 1 Production and characterization of HA2-empowered protein nanoparticles. (A) Schematic characterization of protein constructs including a HA2 stretch.[12] The N-terminal methionine, absent in the original sequence of T22, is shown in bold. L is a ligand that offers molecular flexibility. Figures in GFP boxes represent the specific GFP fluorescence compared to the parental T22-GFP-H6. (B) Mass spectroscopy of HA2 proteins upon IMAC purification. Western blot analyses are shown in the inset. (C) DLS size analysis of the protein materials. The unassembled GFP-H6 is shown as reference. In the inset data, the peak size and the polydispersion index (PdI) are shown. (D) FESEM observations of purified material (size bars are 100 nm, 30 nm in insets). Figures indicate surface charge. Experimental procedures are shown in full in the ESI.†

charge (Fig. 1C and D). The untagged parental GFP-H6 protein version remained unassembled (Fig. 1C). Despite their good stability, T22-GFP-HA2-H6 nanoparticles showed a tendency to form aggregates, as observed from a secondary DLS peak at around 200 nm (Fig. 1C). The insertion of the HA2 peptide rendered constructs with significantly lower fluorescence than T22-GFP-H6, especially in the case of T22-GFP-HA2-H6 (Fig. 1A), indicating a conformational impact of the viral peptide on the building block. However, specific fluorescence was in both cases high enough to monitor protein internalization in cultured $CXCR4^+$ HeLa cells.

Cell penetration of both nanoparticles was monitored in the absence and in the presence of a chemical ligand of CXCR4, namely AMD3100, which inhibits binding of T22. As observed (Fig. 2A), the presence of HA2 in the particles enhanced protein penetration in comparison to T22-GFP-H6 nanoparticles, thus confirming the activity of the fusogenic peptide displayed at both accommodation sites. In T22-GFP-HA2-H6, the viral peptide was clearly superior in promoting cell penetration. Even at very low protein concentrations in which the uptake of T22-HA2-GFP-H6 was indistinguishable from that of T22-GFP-H6, its enhancing effect was perceived. Enhanced uptake was not accompanied by cell toxicity (Fig. 2A, inset), an issue that was a matter of concern because of the hemolytic activities of HA2. These effects were mainly observed in HA2 peptide versions with a free amino terminus,[12–14] which in the current construct is blocked by T22. On the other hand, the display of HA2 dramatically reduced the specificity of CXCR4-dependent penetration. While AMD3100 inhibited the uptake of T22-GFP-H6 by around 70% it only reduced the penetration of T22-GFP-HA2-H6 by 30% and no inhibition was observed in the case of T22-HA2-GFP-H6 (Fig. 2B). This last protein appears to be internalized in a completely unspecific way (Fig. 2B).

The higher penetrability of HA2-containing nanoparticles respective to the parental T22-GFP-H6 oligomers (Fig. 2A) was supposed to be linked to the enhanced endosomal escape mediated by HA2. To assess this issue, we analyzed the uptake of the HA2-empowered constructs in the presence of chloroquine that inhibits acidification and subsequent lysosomal degradation of the internalized material. This drug equally enhanced the intracellular fluorescence of cells exposed to T22-GFP-H6 and to T22-HA2-GFP-H6 by about 30 fold (Fig. 2C). This indicates that HA2 in T22-HA2-GFP-H6 does not stimulate full endosomal escape of the particles in comparison to the parental T22-GFP-H6. In contrast, chloroquine had much milder enhancing effects on T22-GFP-HA2-H6 (only five-fold increase,

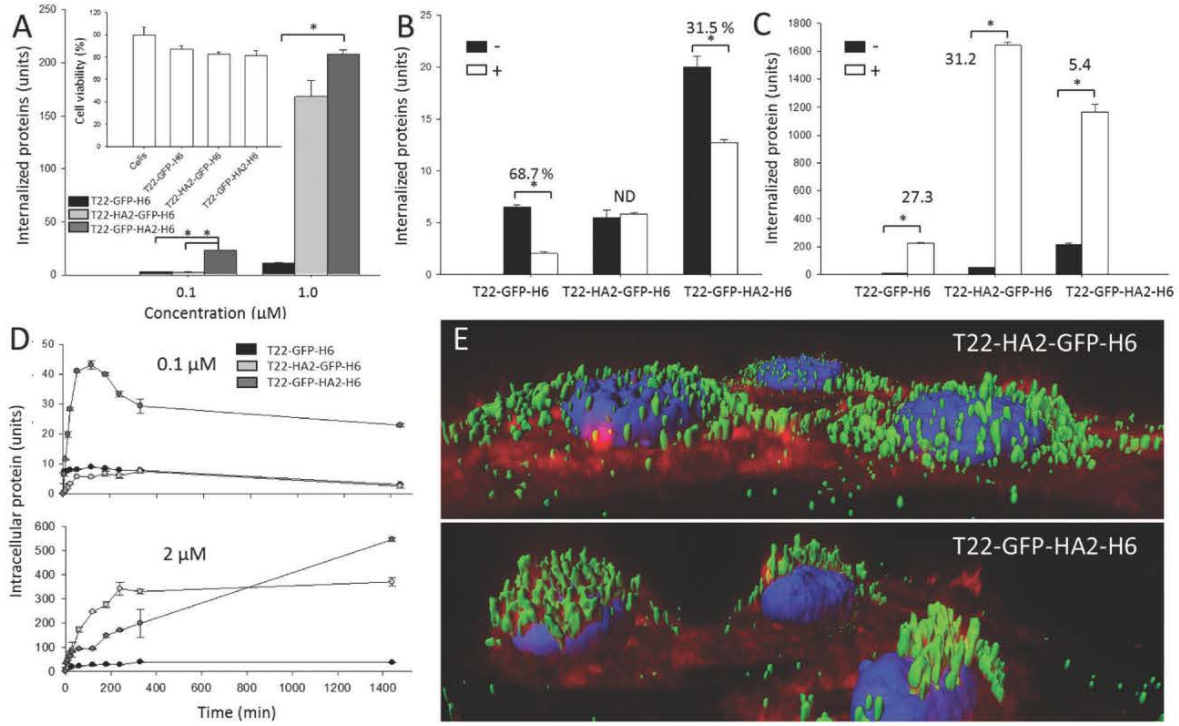

Fig. 2 Functional characterization of HA2-containing nanoparticles. (A) Internalization of T22-GFP-H6 and their HA2-containing derivatives in cultured CXCR4$^+$ HeLa cells, after 24 h exposure. Crude fluorescence values were normalized by the specific fluorescence emission of each protein (units) to allow mass-based comparison. In the inset, HeLa cell viability after exposure to 2 μM of modular proteins for 48 h. (B) Analysis of specific CXCR4-mediated internalization in the absence (–) and in the presence (+) of the CXCR4 ligand AMD3100. Data refer to 1 h after exposure. % of inhibition is indicated in each case. ND means not determinable, as the % was 0. (C) Accumulation of HA2-containing nanoparticles in cultured HeLa cells exposed to 1 μM of protein during 24 h in the absence (–) or presence (+) of chloroquine. (D) Intracellular accumulation of proteins, added to two alternative concentrations, in exposed CXCR4$^+$ HeLa cells. Data are presented as arithmetic mean ± standard deviation from two independent experiments. (E) Isosurface representation of HeLa cells within a 3D volumetric *z* axes stack after incubation for 24 h with nanoparticles (at 0.5 μM). The cell membrane was labeled with CellMask (red signal), cell DNA was labeled with Hoescht 33342 (blue signal) and proteins naturally produced a green signal.

Fig. 2C), proving that the viral peptide shows endosomolytic properties in this construct. In this regard, both HA2-displaying nanoparticles are degraded in cells (Fig. 2D) when added to cell cultures at a concentration of 0.1 μM, a dose that has been described below the threshold supporting the endosomolytic properties of HA2.[12] However, at 2 μM, over such a transition value, T22-GFP-HA2-H6 but not T22-HA2-GFP-H6 keeps accumulating in cells during prolonged exposure (Fig. 2D). This is again in the line that this protein, but not the related T22-HA2-GFP-H6 (or in a much more moderate way), is able to escape from lysosomal degradation. The enhanced perinuclear accumulation of T22-GFP-HA2-H6 (Fig. 2E) fully supports this hypothesis.

HA2 destabilizes lipid cell membranes at pH 5–5.5.[15] However, viral strains with HA2 variants show the ability to replicate in target cells at higher pH values.[16–18] Slight variations in charge distribution at the amino terminus of hemagglutinin and in the isoelectric point of the whole protein allow the fusogenic activities of HA2 at less acidic pH. In this regard, the endosomal escape of modular constructs containing histidine-rich peptides, R9, HA2 and cherry, are disrupted by a nuclear localization signal at the carboxy terminus of HA2.[12] In the constructs generated here both accommodation sites allow a dramatic enhancement of HA2-mediated cell penetration, although at the expense of a loss of specificity in the interaction with cells. This is particularly deleterious when HA2 is placed in close vicinity to the cationic T22 segment, since T22 is critical for protein–protein contacts.[19] In this case, the construct completely missed the ability to specifically interact with CXCR4$^+$ cells, and cell penetration occurs irrespective of endosomal acidification. HA2, in this position, might show enhanced membrane activities influenced by the vicinity of T22. This should produce a differential conformation in the building blocks or the whole nanoparticles already anticipated by differences in the specific fluorescence of the GFP module in both constructs (Fig. 1A). A differential conformational impact of HA2 was confirmed by temperature denaturation followed by Trp emission fluorescence and supported by the molecular modelling of both protein nanoparticles (ESI,† Fig. S2A and B), which resulted in less flexible materials in the case of T22-GFP-HA2-H6. Altogether, while HA2 generically appears as highly appealing for enhancing the integrity of protein-based nanoscale vehicles upon internalization it seems to be poorly appropriate when the efficiency of constructs is based on specific interactions with cell-surface receptors, which might be partially or totally abolished by the viral segment.

The insertion of HA2 in two alternative positions of the tumor-homing nanoparticle T22-GFP-H6 results in a dramatic enhancement of cell penetrability. In the case of T22-GFP-HA2-H6, this is executed through endosomolytic activities and linked to a mild but significant affectation of particle–cell specific interaction. However, regarding T22-HA2-GFP-H6, specificity is completely lost and cell penetration is enhanced in the absence of endosomolytic activity. Taken together, these data indicate that in T22-HA2-GFP-H6, the viral peptide HA2 acts as a cell penetrating peptide rather than as an endosomal escape agent, since it stimulates the penetration of the nanoparticle in a receptor-independent way, probably at the cell surface or at very early endosomal stages. Among the diversity of functional nanoparticles for drug delivery based on biocompatible materials,[20] protein nanoparticles offer an unusual structural versatility that allows the precise exploration of functional modular combinations by conventional genetic engineering.

We thank MINECO (BIO2013-41019-P), AGAUR (2014SGR-132) and CIBER de Bioingeniería, Biomateriales y Nanomedicina (project NANOPROTHER) to AV, Marató deTV3 foundation (TV32013-3930) and ISCIII (PI15/00272, co-founding FEDER) to EV and ISCIII (PI15/00378 and PIE15/00028, co-founding FEDER), Marató TV3 (2013-2030) and AGAUR (2014-PROD0005) to RM, for funding our research. Protein production has been partially performed by the ICTS ''NANBIOSIS'', more specifically by the Protein Production Platform of CIBER-BBN/IBB (http://www.nanbiosis.es/unit/u1-protein-production-platform-ppp/). PC and MM thank the Erasmus+ for the financial support during this project. LSG was supported by AGAUR (2016FI_B 00034), UU received a Sara Borrell postdoctoral fellowship from ISCIII and AV an ICREA ACADEMIA.

References

1 R. Duncan and R. Gaspar, *Mol. Pharmaceutics*, 2011, **8**, 2101–2141.
2 E. Vazquez, R. Mangues and A. Villaverde, *Nanomedicine*, 2016, **11**, 1333–1336.
3 M. Murata, S. Takahashi, S. Kagiwada, A. Suzuki and S. Ohnishi, *Biochemistry*, 1992, **31**, 1986–1992.
4 E. Wagner, C. Plank, K. Zatloukal, M. Cotten and M. L. Birnstiel, *Proc. Natl. Acad. Sci. U. S. A.*, 1992, **89**, 7934–7938.
5 S. F. Ye, M. M. Tian, T. X. Wang, L. Ren, D. Wang, L. H. Shen and T. Shang, *Nanomedicine*, 2012, **8**, 833–841.
6 J. S. Wadia, R. V. Stan and S. F. Dowdy, *Nat. Med.*, 2004, **10**, 310–315.
7 M. V. Cespedes, *et al.*, *ACS Nano*, 2014, **8**, 4166–4176.
8 M. V. Cespedes, *et al.*, *Nanomedicine*, 2016, **12**, 1987–1996.
9 U. Unzueta, *et al.*, *Biomaterials*, 2012, **33**, 8714–8722.
10 U. Unzueta, M. V. Cespedes, N. Ferrer-Miralles, I. Casanova, J. Cedano, J. L. Corchero, J. Domingo-Espin, A. Villaverde, R. Mangues and E. Vazquez, *Int. J. Nanomed.*, 2012, **7**, 4533–4544.
11 F. Balkwill, *Nat. Rev. Cancer*, 2004, **4**, 540–550.
12 J. S. Liou, B. R. Liu, A. L. Martin, Y. W. Huang, H. J. Chiang and H. J. Lee, *Peptides*, 2012, **37**, 273–284.
13 I. Neundorf, R. Rennert, J. Hoyer, F. Schramm, K. Lobner, I. Kitanovic and S. Wolfl, *Pharmaceuticals*, 2009, **2**, 49–65.
14 T. Sugita, T. Yoshikawa, Y. Mukai, N. Yamanada, S. Imai, K. Nagano, Y. Yoshida, H. Shibata, Y. Yoshioka, S. Nakagawa, H. Kamada, S. I. Tsunoda and Y. Tsutsumi, *Br. J. Pharmacol.*, 2008, **153**, 1143–1152.
15 J. J. Skehel, K. Cross, D. Steinhauer and D. C. Wiley, *Biochem. Soc. Trans.*, 2001, **29**, 623–626.
16 R. S. Daniels, J. C. Downie, A. J. Hay, M. Knossow, J. J. Skehel, M. L. Wang and D. C. Wiley, *Cell*, 1985, **40**, 431–439.
17 C. Scholtissek, *Vaccine*, 1985, **3**, 215–218.
18 E. E. Ooi, J. S. Chew, J. P. Loh and R. C. Chua, *Virol. J.*, 2006, **3**, 39.
19 F. Rueda, *et al.*, *Adv. Mater.*, 2015, **27**, 7816–7822.
20 N. Kamaly, B. Yameen, J. Wu and O. C. Farokhzad, *Chem. Rev.*, 2016, **116**, 2602–2663.

ANNEX 4: MANUSCRIPT 1

Tuning tumor cell targeting and penetrability of self-assembling polypeptides through funcional recruitment.

Naroa Serna, Julieta M. Sánchez, Ugutz Unzueta, Laura Sánchez-García, Ramón Mangues, Esther Vázquez and Antonio Villaverde.

Submitted to **New Biotechnology**.

Impact factor: 3.813. Quartile: Q1. Decile: D1.

Tuning tumor cell targeting and penetrability of self-assembling polypeptides through funcional recruitment.

Naroa Serna [1, 2, 3], Julieta M. Sánchez [1, 2, 4], Ugutz Unzueta [3, 5], Laura Sánchez-García[1, 2, 3], Ramón Mangues [3, 5], Esther Vázquez [1, 2, 3] *, Antonio Villaverde [1, 2, 3] *

[1] Institut de Biotecnologia i de Biomedicina, Universitat Autònoma de Barcelona, Bellaterra, 08193 Barcelona, Spain.

[2] Departament de Genètica i de Microbiologia, Universitat Autònoma de Barcelona, Bellaterra, 08193 Barcelona, Spain.

[3] CIBER de Bioingeniería, Biomateriales y Nanomedicina (CIBER-BBN), Bellaterra, 08193 Barcelona, Spain.

[4] Instituto de Investigaciones Biológicas y Tecnológicas (IIBYT) (CONICET-Universidad Nacional de Córdoba). ICTA & Cátedra de Química Biológica, Departamento de Química, FCEFyN, UNC. Av.Velez Sarsfield 1611, X 5016GCA Córdoba, Argentina.

[5] Biomedical Research Institute Sant Pau (IIB-Sant Pau) and Josep Carreras Research Institute, Hospital de la Santa Creu i Sant Pau, 08025 Barcelona, Spain.

Keywords: recombinant proteins; nanoparticles; self-assembling.

Funding: This study has been funded by the Agencia Estatal de Investigación (AEI) and Fondo Europeo de Desarrollo Regional (FEDER) (grant BIO2016-76063-R, AEI/FEDER, UE), AGAUR (2014SGR-132) and CIBER-BBN (project NANOPROTHER) granted to AV, Marató de TV3 foundation (TV32013-3930) and ISCIII (PI15/00272 co-founding FEDER) to EV and ISCIII (PI15/00378 and PIE15/00028, co-founding FEDER), Marató de TV3 foundation (2013-2030) and AGAUR 2014-PROD0005 to RM.

Abstract

The pore-forming activities of the antimicrobial peptide GWH1 have been evaluated in combination with the CXCR4-binding properties of the peptide T22, both displayed in self-assembling fusion proteins produced in recombinant bacteria. The resultin nanoparticles show a dramatically improved cell penetrability into $CXCR4^+$ cells (more than 10-fold) and endosomal escape (from 90 % to 50 % degradation), comparing with the equivalent protein nanoparticles lacking GWH1. This proves that GWH1 retains its membrane activity in form of complex fusion proteins. However, CXCR4-specificity in the cell binding is subsequently minimized by the presence of the antimicrobial peptide, as the combination T22-GWH1 results in 30 % of the nanoparticles entering cells via CXCR4, versus 98 % in the case of T22 alone. Therefore, although GWH1 results extremely valuable in promoting cell penetrability of modular polypeptides, this segment impairs, in contrast, the cell-surface receptor targeting imposed by a partner domain in the fusion protein.

1 Introduction

Cell-targeted drug delivery requires appropriate nanoscale vehicles (usually nanoparticles) for the generation of nanoconjugates [1]. These carriers have to be functionalized with appropriate ligands (usually peptides or proteins) that selectively bind to cell surface receptors overexpressed in target cells. Selective delivery is specially desired in oncology, in which conventional therapy is majorly based on the systemic administration of untargeted chemotherapeutic drugs, what is associated to severe life threatening side toxicity [2-6]. A nanoscale size of the conjugate, ranging from 10 to 100 nm, allows exploiting the enhanced permeability and retention (EPR) effect (based on the higher blood vessel permeability in tumoral tissues) while avoiding renal clearance (with a cut-of around 6-8 nm) and undesired aggregation in lung capillaries [7]. A diversity of materials is explored as nanoscale drug carriers including polymers, ceramics, metals and carbon nanotubes. The xenobiotic nature and potential toxicity of most of them pose severe concerns about their biosafety, at both individual and environmental levels [1, 8-17]. Contrarily, self-assembling proteins are promising, fully biocompatible nanostructured materials for drug delivery [18, 19], which can perform complex activities such as precise cell targeting by the incorporation of peptide ligands in modular polypeptides [20]. In this context, T22 is a cationic ligand of the cytokine receptor CXCR4, that is overexpressed in about 20 human neoplasias and that correlates with aggressiveness and metastasis [21-27]. T22 promotes the endosomal-mediated internalization of self-assembling protein nanoparticles (T22- GFP-H6) with a high level of specificity both in vitro and in vivo [28-30], showing an optimal biodistribution in tumor and metastatic foci in colorectal cancer animal models [31]. Functional recruitment by protein fusion technologies [32] might be useful to enhance the penetrability of this construct, which is now moderate, in order to improve its applicability as drug carrier. In this regard, poor endosomal escape may be a critical bottleneck for T22-GFP-H6 to efficiently deliver cytotoxic drugs into the cytoplasm. We have here studied the combined activity of T22 and that of a potent pore-forming protein, the antimicrobial peptide (AMP) GWH1, simultaneously displayed on the surface of protein nanoparticles. Although highly promising in nanomedicine, the combination of cell-targeting peptides and enhancers of cell penetrability has been so far poorly studied. The resulting data demonstrate

that GWH1 shows potent endosomolytic activity that increases transfection efficiently of functionalized protein nanoparticles into the cytoplasm. However, CXCR4 binding specificity is partially lost in these materials, being this functional divergence an issue to be considered in the design of functional drug carriers based on peptides in fusion proteins.

2 Materials and methods

2.1 Nanoparticle production and characterization

Self-assembling modular proteins T22-GFP-H6 [28], T22-GWH1-GFP-H6 [33] and GWH1 GFP-H6 [34] (Figure 1 A) have been described elsewhere. T22 is a powerful ligand of the cell surface cytokine receptor CXCR4 [28] and it mediates the endosomal internalization of fusion proteins that contain it, both in vitro and in vivo [28, 30]. These gene fusions were expressed from the plasmid pET22b in *Escherichia coli* Origami B (BL21, OmpT-, Lon-, TrxB-, Gor-, Novagen) under standard conditions [31]. Cells were disrupted in a French Press (Thermo FA-078A) at 1200 psi to obtain the soluble fraction. Protein purification was carried out through the His-tag by Immobilized Metal Affinity Chromatography (IMAC) using a HiTrap Chelating HP 1 ml column (GE Healthcare) with an AKTA purifier FPLC (GE Healthcare) [35]. Proteins were finally dialyzed against sodium bicarbonate buffer with salt (166 mM NaHCO3 pH 8 + 333 mM NaCl). Protein purity and integrity were checked by mass spectrometry (MALDI-TOF) and protein amounts by the Bradford assay. The volume size distribution of nanoparticles was determined by dynamic light scattering (DLS) at 633 nm (Zetasizer Nano ZS, Malvern Instruments Limited, Malvern) and size and shape of nanoparticles were evaluated with a Field emission scanning electron microscopy (FESEM) Zeiss Merlin (Zeiss, Oberkochen, Germany) operating at 1kV. Fluorescence of the nanoparticles was determined by a Varian Cary Eclipse fluorescence spectrophotometer (Agilent Technologies) at 523 nm using an excitation wavelength of 488 nm.

2.2 Membrane preparation and Circular dichroism (CD)

Multilamellar vesicles were prepared by evaporating, under a stream of nitrogen, chloroform:metanol (2:1 v/v) from a solution of pure egg phosphatidil choline (EPC) (Sigma Aldrich). The dry lipid was resuspended in buffer at 1 mg/mL by repeating six consecutive cycles of heating for 2 min at 21 ºC (a temperature above the phospholipid Tc) and vortexing for 1 min. In these conditions, EPC self-aggregates into multilamellar vesicles (MLVs) [36]. Small unilamellar vesicles (SUVs) were prepared using a high intensity sonicator Branson sonifier 450, with 3 mm-diameter titanium probe. 1 mL of MLVs dispersion containing 1 mg/ml of EPC maintained on ice was sonicated for six cycles of 20 s, each one with 50% pulses (0.5 s on and 0.5 s off) The last sample was centrifuged at 15000g x 15 min to discard big aggregates and titanium particles. Far-UV CD was measured at 25ºC in a Jasco J-715 spectropolarimeter to assess secondary structure information. T22-GWH1-GFP-H6 concentration was adjusted to 0.2 mg/mL in a buffer solution of 166 mM carbonate-bicarbonate at pH 8 and 333 mM NaCl. The protein spectrum was measured in the absence or the presence of small unillamellar vesicles (SUVs) (phosphatidil choline at 0.1 mg/ml). Samples were analysed with a 1mm pathlength cuvette.CD spectra were obtained over a wavelength range of 190-260 nm at a scan rate of 50 nm/min a response of 1 s and a bandwith of 1 nm. Six scans were accumulated. The magnitude of helix structures appearance was analyzed using the JASCO spectra-manager analysis software.

2.3 Cell culture and cell viability assay

The binding and uptake specificity of the recombinant proteins were studied in cultured $CXCR4^+$ HeLa cells. Cells were cultured in MEM Alpha (Minimum Essential Medium α, Gibco) supplemented with 10 % foetal calf serum (Gibco) at 37 °C and 5 % CO2 in a humidified atmosphere. The CellTiter-Glo® Luminescent Cell Viability Assay (Promega) was used to determine the cytotoxicity of protein nanoparticles. For that, cells were plated in opaque-walled 96-well plates at 3,500 cells/well in DMEM supplemented with 10 % foetal calf serum for 24 h at 37 ºC until reaching 70 % confluence. Then, cells were incubated in presence of 2, 4, 8, 12 and 24 µM nanoparticles during 48 h at 37°C. Subsequently, 100 µl of the single reagent (CellTiter-

Glo® Reagent) was added directly to cultured cells and the plates were measured in the Multilabel Plater Reader VICTOR3 (PerkinElmer).

2.4 Internalization and endosomal degradation assays

To explore internalization, culture media was exchanged for serum-free Optipro medium (Gibco) supplemented with L-glutamine prior to the addition of nanoparticles. T22-GWH1-GFP-H6 and control T22-GFP-H6 and GWH1-GFP-H6 nanoparticles were added at 0.5, 1, 2, 3 and 4 μM and left for 24h. Additionally, specific internalization through CXCR4 receptor was proved adding a specific antagonist of CXCR4, AMD3100 [37, 38], that inhibits the interaction with T22. This chemical inhibitor was added 1 h prior protein incubation (to 25 nM) at a ratio of 1:10. For the determination of endosomal escape, cells were incubated in absence and in presence of 100 μM chloroquine for 4 h before the addition of the protein at 1, 2, 3 and 4 μM.

The uptake kinetics were recorded by exposing cells to nanoparticles at 1 and 4 μM for 10 min, 20 min, 30 min, 1 h, 2 h, 5.5 h and 24 h prior to fluorescence measurement. Again, chloroquine was used for the determination of endosomal escape. Internalization was analysed by detaching the cells with 1 mg/mL trypsin-EDTA (Gibco®) for 15 min to remove externally attached protein. The samples were analysed by a FACS-Canto system (Becton Dickinson) using a 15 mW air-cooled argon ion laser at 488 nm excitation. All experiments were performed in duplicate. Fluorescence data recorded by cytometry was corrected by the specific fluorescence of the protein, previously determined by fluorescence spectrophotometry, to render comparative units in terms of protein amount.

2.5 Confocal laser scanning microscopy

For confocal microscopy HeLa cells were grown on Mat-Tek plates (MatTek Corporation). Upon exposure to nanoparticles at 4 μM for 24 h, cell nuclei were labelled with 5 μg/ml Hoechst 33342 (ThermoFischer) and the plasma membrane with 2.5 μg/ml CellMaskTM Deep Red (ThermoFischer) for 10 min at room temperature. Cells were then washed in PBS buffer (Sigma-Aldrich Chemie GmbH). Live cells were recorded with a TCS-SP5 confocal laser scanning microscope (Leica Microsystems) using 63x (1.4 NA) oil immersion objective lenses. Hoechst 33342 labelled DNA was

excited with a blue diode (405 nm) and detected in the 415-460 nm range. GFPproteins were excited with an Ar laser (488 nm) and detected in the 525-545 nm range.

CellMask was excited with a HeNe laser (633 nm) and detected in the 650-775 nm range. The confocal pinhole was set to 1 Airy unit and z-stacks acquisition intervals were selected to satisfy Nyquist sampling criteria. Three-dimensional images were processed using the Surpass Module in Imaris X64 v.7.2.1. software (Bitplane).

3 Results

T22-GWH1-GFP-H6 (Figure 1A) contains the AMP GWH1 inserted as an additional module between the N-terminal CXCR4 ligand T22, and the core GFP. We were interested in knowing if GWH1, a pore-forming peptide, might enhance the penetrability of the protein construct mediated by the specific interaction between T22 and CXCR4, upon endosomal membrane destabilization. GWH1 exerts its cytolytic activity by folding into an amphipathic helix upon selective binding and insertion into the target membrane. In order to investigate whether the addition of the T22 moiety and the nanoparticulated form itself might affect the GWH1 ability to form α-helical structures, we measured the peptide conformation by circular dichroism (CD) in the absence or the presence of small unillamellar vesicles (SUVs). The T22-GWH1-GFP-H6-spectrum in the absence of SUVs shows the typical behavior of a β-strand pattern corresponding to the expected beta-barrel structure of the GFP (Figure 1B), with a minimum around 215 nm and a positive band around 198 nm [39]. By contrast, when these nanoparticles interact with SUVs a qualitative change is observed in the DC spectrum in which the maximum moves to 195 nm (Figure 1B) corresponding to the appearance (plus 10 %) of novel helical conformation.

AMPs, as effective self-defence tools, exhibit a threshold concentration (called the lethal concentration) for their membrane activity on eukaryotic cells, below which no effect is observed [40]. This security level allows the antimicrobial activity at low concentrations, without harming own body cells. Since it had been previously described that GWH1 exhibits cytotoxic effects over cancer cells with a reported threshold ranging from 20 μM to 250 μM, we first determined the intrinsic cytotoxicity of T22- GWH1-GFP-H6 over $CXCR4^+$ HeLa cells. As observed (Figure 1C), T22-GWH1-

GFPH6 nanoparticles showed a dose-dependent cytotoxicity with a significant lethal concentration lower than the predicted for the GWH1 peptide alone. This cell killing effect, when properly targeted to tumoral tissues, has proved to be exploitable to design antitumoral drugs [33]. Under 8 µM, no cytotoxicity was observed in HeLa cells upon exposure to T22-GWH1-GFP-H6 nanoparticles, and further analysis of cell penetrability and specificity were performed in a safe margin, up to 4 µM.

Then, endosomal escape promoted by GWH1 was evaluated by comparison between T22-GWH1-GFP-H6 and its parental T22-GFP-H6. As observed (Figure 2A), over 1.5 µM, T22-GWH1-GFP-H6 is dramatically more efficient than T22-GFP-H6 in escapin the endosome, suggesting a threshold concentration for endosomal membrane destabilization. This action cannot be performed by the control nanoparticle GWH1-GFP-H6, which lacks the cell surface ligand (T22) for internalization. Such endosomal escape protects the 40 % of the internalized protein nanoparticles from lysosomal degradation (Figure 2B), that is responsible for the destruction of most T22-GFP-H6. Interestingly, the presence of GWH1 impairs, contrarily, the CXCR4-dependence in the uptake of the protein materials (Figure 2C). Less than 2 % of T22-GFP-H6 enters target cells in the presence of the CXCR4 antagonist AMD3100, while almost 70 % of T22 GWH1-GFP-H6 penetrates HeLa cells under the same conditions (Figure 2C).

In accordance to the obtained results, at a concentration (1 µM) in which GWH1 does not promote endosomal escape, the cell uptake of T22-GWH1-GFP-H6 is slightly higher than that of the parental T22-GFP-H6 (Figure 3A). The uptake slows down at about 5 h, reaching a steady constant intracellular concentration during 24 h. At a concentration above that threshold (4 µM), however, the penetration of T22-GWH1-GFP-H6 is extremely efficient. The amount of intracellular protein keeps increasing, without reaching any plateau at least during 24 h of exposure. During this experiment time, T22-GWH1-GFP-H6 is majorly degraded at 1 µM, but only 60 % of the material is destroyed at 24 h in the endosomes at 4 µM (Figure 3B). This observation confirms again, the endosomal escape of the nanoparticles promoted by GWH1. Under this situation, most of T22-GWH1-GFP-H6 is found homogenously distributed by the cell cytoplasm, while the parental T22-GFP-H6 is majorly concentrated in a perinuclear region (Figure 3C), as previously described [28].

4. Discussion

Protein-based drugs are of high interest in molecular medicines as they can be produced in microorganisms (among a limited spectrum of cell factories) by simple recombinant DNA technologies [43]. In cancer therapies, modular approaches based on fusion protein engineering [32] allow recruiting, in single chain polypeptides, diverse funcions required for efficient cell targeting, internalization and endosomal escape, that are encoded by proteins or protein domains [20, 44]. Self-assembling, that can be provided by short peptide stretches [19], allows the proteins being presented as regular oligomers within the nanoscale size, a presentation that enhances their tumoral accumulation by physical mechanisms linked to the EPR [7]. In a step further beyond the simple protein drug association principles (on which Abraxane® is based [45]), nanostructured, cell targeted proteins can be ideal vehicles for drug targeting in càncer therapy in form of drug nanoconjugates [2]. We have here tested the combination of the AMP GWH1 [46], a potent membrane pore former, with T22 [28], a potent CXCR4 ligand, in protein-only CXCR4-targeted nanoparticles, regarding efficiency and specificity of $CXCR4^+$ cell binding and penetrability. GWH1 is a synthetic AMP designed to show enhanced antimicrobial activity while reduced cell killing activity on normal eukaryotic cells, such as 3T3 fibroblasts [47] or erythrocytes (low haemolytic activity) [48]. It also shows improved selectivity for surface binding and killing of cancer cells as compared to normal cells, because of similarly to bacteria their membrane is enriched in anionic components [49]. GWH1 exerts its cytolytic activity by folding into an amphipathic helix upon selectively binding and insertion into the target membrane, leading to breakdown of the membrane structure, thus causing leakage of cell contents, resulting finally in cell death. Being used as a synthetic peptide alone, GWH1 is fully functional in form of fusion proteins [34], what opens the door to consider its inclusion in multifunctional constructs. A combination of pore-forming and cell-targeting agents, despite their obvious interest in cancer therapies, has been never explored.

In this context, we have demonstrated here that the accommodation of GWH1 in longer modular polypeptides containing the cationic CXCR4 ligand T22 (Figure 1 A) does not affect neither the functionality of GWH1 nor the ability of the T22- and H6-

empowered proteins to form regular nanoparticles (Figure 1A). Moreover, a clear membrane disrupting ability of T22-GWH1-GFP-H6 was shown over cancer cells with the expected threshold concentration (Figure 1B), showing the ability of GWH1 to create pores even in a nanoparticulated version. This fact, can be obviously exploited to construct therapeutic protein materials based on functional recruitment, through simple fusion technologies. Interestingly, at sub-lethal concentrations, the GWH1 module guarantees rapid and effective translocation of T22-GWH1-GFP-H6 nanoparticles from the endocytic vesicles into cytoplasm, when comparing with the parenteral T22-GFP-H6 (Figure 2). Notably, despite its observable endolytic activity, GWH1 does not promote release from vesicles into the cytoplasm except when administered at concentrations above 1.5 μM. This behaviour is compatible with molecular models currently proposed to explain the permeability properties of α-helical antimicrobial sequences and the need of a threshold concentration for pore formation [40, 50, 51]. In this context, a punctuate fluorescence pattern was observed for internalized T22-GFP-H6 (Figure 3), indicating endosome permanence. In contrast, a different intracellular fluorescence pattern was shown by T22-GWH1-GFP-H6, characterized by a more homogeneous distribution of the material in the cytoplasm, consistent with the release of a significant fraction of the recombinant cargo (Figure 3). Despite such appealing properties, CXCR4 specificity is dramatically lost by the presence of GWH1 in the protein constructs (Figure 2C). This indicates that enhanced cell penetrability though pore formation cannot be gained simultaneously to a high cell specificity conferred by a cell-targeting peptide; that is, a gain in anticancer activity is accompanied by a loss in targeting capacity towards specific cancer cells. Similar data has been recently obtained by combining the fusogenic peptide HA2 from the influença virus hemagglutinin with the same targeting peptide T22 [52]. Both set of data, in combination, stress the strong value of membrane active peptides used as potential enhancers of drug penetrability (by the incorporation to a nanoscale vehicle) but the incapability to maintain a high selectivity in the penetration process when cell membranes are destabilized. In the current context of innovative drug design and the generation of smart nanoscale vehicles as delivery agents, the data presented in this study offer critical clues regarding the recruitment of appropriate functional agents based on proteins.

Acknowledgments. Protein production has been partially performed by the ICTS "NANBIOSIS", more specifically by the Protein Production Platform of CIBER-BBN/ IBB (http://www.nanbiosis.es/unit/u1-protein-production-platform-ppp/). We are also indebted to SCAC (UAB) for cell culture facilities and assistance and to the Microscopy Service at the UAB NS was supported by a predoctoral fellowship from the Government of Navarra, LSG was supported by AGAUR (2017FI_B100063), UU received a Sara Borrell postdoctoral fellowship and JMS is a Career Investigators from CONICET. AV received an ICREA ACADEMIA award.

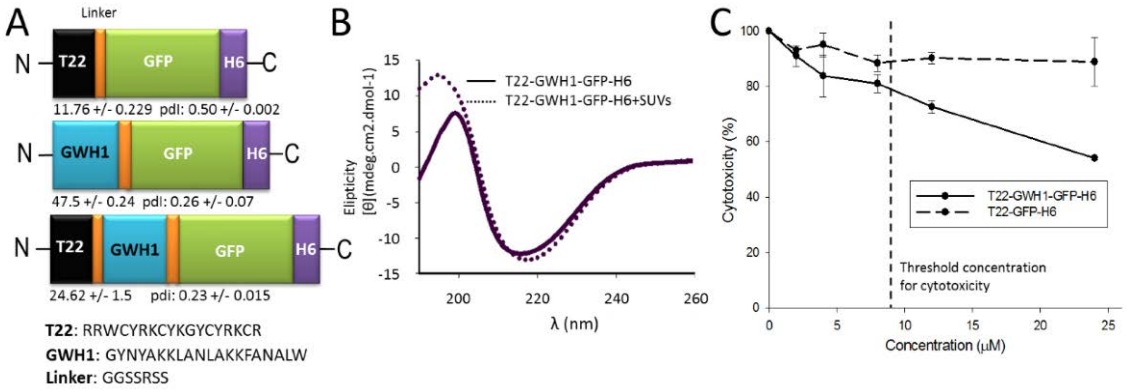

Figure 1. Features of GWH1-containing nanoparticles. A. Modular organization of the set of protein building blocks used in this study. All the shown polypeptides self-assemble as fluorescent nanoparticles, whose hydrodynamic size (in nm, measured by DLS) and polydispersion index (pdi) are shown at the bottom of each cartoon. Sizes of the modules are only indicative. B. CD spectra at wavelength range of 190–260 nm. T22-GWH1-GFP-H6 in the absence of SUVs shows a spectra of proteins containing β-sheet conformation. The CD spectra in presence of membrane shows the appearance of the helical conformation. C. Intrinsic cytotoxicity on HeLa cells imposed by the AMP GWH1. Cells were incubated in presence of 2, 4, 8, 12 and 24 μM nanoparticles during 48 h.

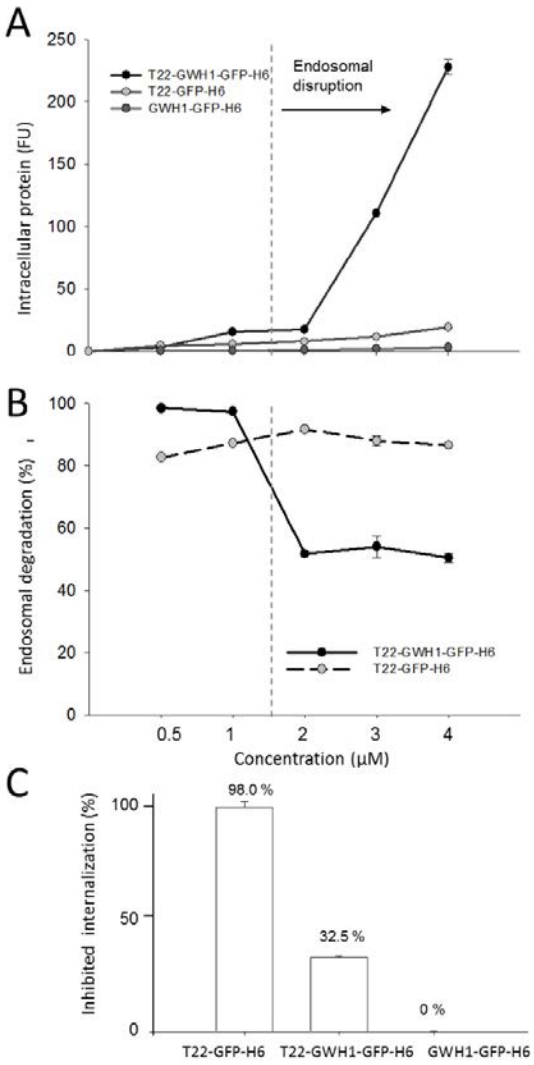

Figure 2. Internalization of GWH1-containing nanoparticles. A. Cell internalization of GWH1-carring nanoparticles measured through intracellular fluorescence, after a harsh trypsin treatment to remove external material [41]. A threshold in the endosomal escape properties is shown at 1.5 µM. FU are fluorescence units. B. Fraction of internalized protein degraded in the endosomes, as measured by chloroquine addition. Cells were incubated in the absence and in the presence of 100 µM chloroquine for 4 h before the addition of the protein at 0.5, 1, 2, 3 and 4 µM during 24 h. C. Fraction of protein internalization (25 nM) that is inhibited by the CXCR4 antagonist, AMD3100 incubated 1h prior to protein treatment [37, 38, 42].

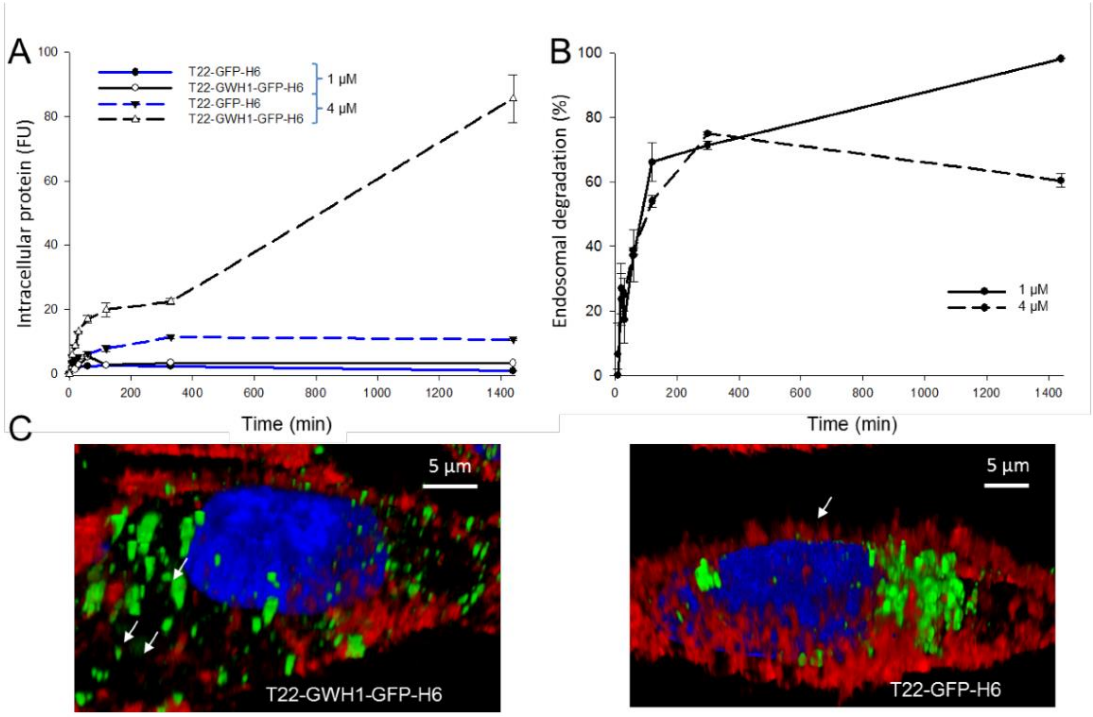

Figure 3. Kinetics of cell penetration of GWH1-empowered nanoparticles. A. Relative amounts of intracellular nanoparticles penetrating HeLa cells at different times after exposure (at 2 different concentrations). FU are fluorescence units. B. Endosomal degradation of T22-GWH1-GFP-H6 under the same conditions. C. 3D confocal reconstructions of cultured HeLa cells exposed to GWH1-empowered nanoparticles. Blue label corresponds to the nucleus, red label to membranes and green label is the natural fluorescence of the nanoparticles.

References

[1] Duncan R, Gaspar R. Nanomedicine(s) under the microscope. Molecular pharmaceutics. 2011;8:2101-41.

[2] Villaverde RMEVA. Targeting in Cancer Therapies. Medical Sciences. 2016;4:6.

[3] Moriarity A, O'Sullivan J, Kennedy J, Mehigan B, McCormick P. Current targeted therapies in the treatment of advanced colorectal cancer: a review. Therapeutic advances in medical oncology. 2016;8:276-93.

[4] Yao VJ, D'Angelo S, Butler KS, Theron C, Smith TL, Marchio S, et al. Ligandtargeted theranostic nanomedicines against cancer. Journal of controlled release : official journal of the Controlled Release Society. 2016;240:267-86.

[5] Kintzing JR, Filsinger Interrante MV, Cochran JR. Emerging Strategies for Developing Next-Generation Protein Therapeutics for Cancer Treatment. Trends in pharmacological sciences. 2016;37:993-1008.

[6] Lee MS, Dees EC, Wang AZ. Nanoparticle-Delivered Chemotherapy: Old Drugs in New Packages. Oncology. 2017;31:198-208.

[7] Shen J, Wolfram J, Ferrari M, Shen H. Taking the vehicle out of drug delivery. Materials today. 2017;20:95-7.

[8] Durnev AD. Toxicology of nanoparticles. Bulletin of experimental biology and medicine. 2008;145:72-4.

[9] Alexis F, Rhee JW, Richie JP, Radovic-Moreno AF, Langer R, Farokhzad OC. New frontiers in nanotechnology for cancer treatment. Urologic oncology. 2008;26:74-85.

[10] Yildirimer L, Thanh NT, Loizidou M, Seifalian AM. Toxicology and clinical potential of nanoparticles. Nano today. 2011;6:585-607.

[11] Sayes CM, Reed KL, Warheit DB. Nanoparticle toxicology: measurements of pulmonary hazard effects following exposures to nanoparticles. Methods in molecular biology. 2011;726:313-24.

[12] Albanese A, Tang PS, Chan WC. The effect of nanoparticle size, shape, and Surface chemistry on biological systems. Annual review of biomedical engineering. 2012;14:1-16.

[13] Elsaesser A, Howard CV. Toxicology of nanoparticles. Advanced drug delivery reviews. 2012;64:129-37.

[14] Wang AZ, Langer R, Farokhzad OC. Nanoparticle delivery of cancer drugs. Annual review of medicine. 2012;63:185-98.

[15] Shang L, Nienhaus K, Nienhaus GU. Engineered nanoparticles interacting with cells: size matters. J Nanobiotechnology. 2014;12:5.

[16] Haynes C. Editorial--analytical toxicology of nanoparticles. The Analyst. 2014;139:868-9.

[17] Stefan Wilhelm AJT, Qin Dai, Seiichi Ohta, Julie Audet, Harold F. Dvorak & Warren C. W. Chan. Analysis of nanoparticle delivery to tumours. Nature Reviews Materials 2016;1.

[18] Corchero JL, Vazquez E, Garcia-Fruitos E, Ferrer-Miralles N, Villaverde A. Recombinant protein materials for bioengineering and nanomedicine. Nanomedicine. 2014;9:2817-28.

[19] Ferrer-Miralles N, Rodriguez-Carmona E, Corchero JL, Garcia-Fruitos E, Vazquez E, Villaverde A. Engineering protein self-assembling in protein-based nanomedicines for drug delivery and gene therapy. Critical reviews in biotechnology. 2015;35:209-21.

[20] Unzueta U, Cespedes MV, Vazquez E, Ferrer-Miralles N, Mangues R, Villaverde A. Towards protein-based viral mimetics for cancer therapies. Trends in biotechnology. 2015;33:253-8.

[21] Koshiba T, Hosotani R, Miyamoto Y, Ida J, Tsuji S, Nakajima S, et al. Expression of stromal cell-derived factor 1 and CXCR4 ligand receptor system in pancreatic cancer: a possible role for tumor progression. Clinical cancer research : an oficial journal of the American Association for Cancer Research. 2000;6:3530-5.

[22] Murakami T, Cardones AR, Hwang ST. Chemokine receptors and melanoma metastasis. Journal of dermatological science. 2004;36:71-8.

[23] Balkwill F. The significance of cancer cell expression of the chemokine receptor CXCR4. Seminars in cancer biology. 2004;14:171-9.

[24] Burger JA, Kipps TJ. CXCR4: a key receptor in the crosstalk between tumor cells and their microenvironment. Blood. 2006;107:1761-7.

[25] Kim J, Mori T, Chen SL, Amersi FF, Martinez SR, Kuo C, et al. Chemokine receptor CXCR4 expression in patients with melanoma and colorectal cancer liver metastases and the association with disease outcome. Annals of surgery. 2006;244:113-20.

[26] Barbieri F, Bajetto A, Florio T. Role of chemokine network in the development and progression of ovarian cancer: a potential novel pharmacological target. Journal of oncology. 2010;2010:426956.

[27] Weiss ID, Jacobson O. Molecular imaging of chemokine receptor CXCR4. Theranostics. 2013;3:76-84.

[28] Unzueta U, Cespedes MV, Ferrer-Miralles N, Casanova I, Cedano J, Corchero JL, et al. Intracellular CXCR4(+) cell targeting with T22-empowered protein-only nanoparticles. International journal of nanomedicine. 2012;7:4533-44.

[29] Cespedes MV, Unzueta U, Tatkiewicz W, Sanchez-Chardi A, Conchillo-Sole O, Alamo P, et al. In vivo architectonic stability of fully de novo designed protein-only nanoparticles. ACS nano. 2014;8:4166-76.

[30] Cespedes MV, Unzueta U, Alamo P, Gallardo A, Sala R, Casanova I, et al. Cancer-specific uptake of a liganded protein nanocarrier targeting aggressive CXCR4+ colorectal cancer models. Nanomedicine : nanotechnology, biology, and medicine. 2016;12:1987-96.

[31] Rueda F, Cespedes MV, Conchillo-Sole O, Sanchez-Chardi A, Seras-Franzoso J, Cubarsi R, et al. Bottom-Up Instructive Quality Control in the Biofabrication of Smart Protein Materials. Advanced materials. 2015;27:7816-22.

[32] Vazquez E, Mangues R, Villaverde A. Functional recruitment for drug delivery through protein-based nanotechnologies. Nanomedicine. 2016;11:1333-6.

[33] Naroa Serna MVC, Laura Sánchez-García, Ugutz Unzueta, Rita Sala, Alejandro Sánchez-Chardi, Francisco Cortés, Neus Ferrer-Miralles, Ramón Mangues, Esther Vázquez and Antonio Villaverde. Peptide-Based Nanostructured Materials with Intrinsic Proapoptotic Activities in CXCR4+ Solid Tumors. Advanced Functional Materials. 2017.

[34] Serna N, Sanchez-Garcia L, Sanchez-Chardi A, Unzueta U, Roldan M, Mangues R, et al. Protein-only, antimicrobial peptide-containing recombinant nanoparticles with inherent built-in antibacterial activity. Acta biomaterialia. 2017;60:256-63.

[35] Pesarrodona M, Crosas E, Cubarsi R, Sanchez-Chardi A, Saccardo P, Unzueta U, et al. Intrinsic functional and architectonic heterogeneity of tumor-targeted protein nanoparticles. Nanoscale. 2017;9:6427-35.

[36] Sanchez JM, Nolan V, Perillo MA. beta-galactosidase at the membrane-water interface: a case of an active enzyme with non-native conformation. Colloids and surfaces B, Biointerfaces. 2013;108:1-7.

[37] Kawaguchi A, Orba Y, Kimura T, Iha H, Ogata M, Tsuji T, et al. Inhibition of the SDF-1alpha-CXCR4 axis by the CXCR4 antagonist AMD3100 suppresses the migration of cultured cells from ATL patients and murine lymphoblastoid cells from HTLV-I Tax transgenic mice. Blood. 2009;114:2961-8.

[38] Kim HY, Hwang JY, Kim SW, Lee HJ, Yun HJ, Kim S, et al. The CXCR4 Antagonist AMD3100 Has Dual Effects on Survival and Proliferation of Myeloma Cells In Vitro. Cancer research and treatment : official journal of Korean Cancer Association. 2010;42:225-34.

[39] Fasman G. Circular Dichroism and the Conformational Analysis of Biomolecules. . New York Plenum Press. ; 1996.

[40] Huang HW. Free energies of molecular bound states in lipid bilayers: lethal concentrations of antimicrobial peptides. Biophys J. 2009;96:3263-72.

[41] Richard JP, Melikov K, Vives E, Ramos C, Verbeure B, Gait MJ, et al. Cellpenetrating peptides. A reevaluation of the mechanism of cellular uptake. The Journal of biological chemistry. 2003;278:585-90.

[42] Song JS, Kang CM, Kang HH, Yoon HK, Kim YK, Kim KH, et al. Inhibitory effect of CXC chemokine receptor 4 antagonist AMD3100 on bleomycin induced murine pulmonary fibrosis. Experimental & molecular medicine. 2010;42:465-72.

[43] Sanchez-Garcia L, Martin L, Mangues R, Ferrer-Miralles N, Vazquez E, Villaverde A. Recombinant pharmaceuticals from microbial cells: a 2015 update. Microbial cell factories. 2016;15:33.

[44] Vazquez E, Ferrer-Miralles N, Mangues R, Corchero JL, Schwartz S, Jr., Villaverde A. Modular protein engineering in emerging cancer therapies. Current pharmaceutical design. 2009;15:893-916.

[45] Gradishar WJ. Albumin-bound paclitaxel: a next-generation taxane. Expert opinion on pharmacotherapy. 2006;7:1041-53.

[46] Felicio MR, Silva ON, Goncalves S, Santos NC, Franco OL. Peptides with Dual Antimicrobial and Anticancer Activities. Frontiers in chemistry. 2017;5:5.

[47] Chen YL, Li JH, Yu CY, Lin CJ, Chiu PH, Chen PW, et al. Novel cationic antimicrobial peptide GW-H1 induced caspase-dependent apoptosis of hepatocellular carcinoma cell lines. Peptides. 2012;36:257-65.

[48] Chou HT, Kuo TY, Chiang JC, Pei MJ, Yang WT, Yu HC, et al. Design and synthesis of cationic antimicrobial peptides with improved activity and selectivity against Vibrio spp. International journal of antimicrobial agents. 2008;32:130-8.

[49] Hoskin DW, Ramamoorthy A. Studies on anticancer activities of antimicrobial peptides. Biochimica et biophysica acta. 2008;1778:357-75.

[50] Lee MT, Hung WC, Chen FY, Huang HW. Many-body effect of antimicrobial peptides: on the correlation between lipid's spontaneous curvature and pore formation. Biophys J. 2005;89:4006-16.

[51] Hall K, Lee TH, Mechler AI, Swann MJ, Aguilar MI. Real-time measurement of membrane conformational states induced by antimicrobial peptides: balance between recovery and lysis. Scientific reports. 2014;4:5479.

[52] Sanchez-Garcia L, Serna N, Mattanovich M, Cazzanelli P, Sanchez-Chardi A, Conchillo-Sole O, et al. The fusogenic peptide HA2 impairs selectivity of CXCR4-targeted protein nanoparticles. Chemical communications. 2017;53:4565-8.

ANNEX 5: MANUSCRIPT 2

Switching cell penetrating and CXCR4-binding activities of nanoscale-organized arginine-rich peptides.

Marianna Teixeira de Pinho Favaro[1], Naroa Serna[1], Laura Sánchez-García, Rafael Cubarsi, Mónica Roldán, Alejandro Sánchez-Chardi, Ugutz Unzueta, Ramón Mangues, Neus Ferrer-Miralles, Adriano Rodrigues Azzoni, Esther Vázquez and Antonio Villaverde.

[1]Equally contributed.

Submitted to **Nanomedicine: Nanotechnology, Biology and Medicine.**

Impact factor: 5.720. Quartile: Q1. Decile: D1.

Switching cell penetrating and CXCR4-binding activities of nanoscale-organized arginine-rich peptides

Marianna Teixeira de Pinho Favaro [1, 2 π], Naroa Serna [2, 3, 4 π], Laura Sánchez-García [2, 3, 4], Rafael Cubarsi [5], Mónica Roldán [6¥], Alejandro Sánchez-Chardi [6], Ugutz Unzueta [4, 7], Ramón Mangues [4, 7], Neus Ferrer-Miralles [2, 3, 4], Adriano Rodrigues Azzoni [8], Esther Vázquez [2, 3, 4 *], Antonio Villaverde [2, 3, 4 *]

[1] Centro de Biologia Molecular e Engenharia Genética, Universidade Estadual de Campinas, Av Candido Rondon, 400, 13083-875 Campinas, SP, Brazil.

[2] Institut de Biotecnologia i de Biomedicina (IBB), Universitat Autònoma de Barcelona, 08193 Cerdanyola del Vallès, Spain.

[3] Departament de Genètica i de Microbiologia, Universitat Autònoma de Barcelona, 08193 Cerdanyola del Vallès, Spain.

[4] CIBER de Bioingeniería, Biomateriales y Nanomedicina (CIBER-BBN), 08193 Cerdanyola del Vallès, Spain.

[5] Departament de Matemàtiques, Campus Nord C3-212, Universitat Politècnica de Catalunya, 08034 Barcelona, Spain.

[6] Servei de Microscòpia, Universitat Autònoma de Barcelona, 08193 Cerdanyola del Vallès, Spain.

[7] Institut d'Investigacions Biomèdiques Sant Pau and Josep Carreras Research Institute, Hospital de la Santa Creu i Sant Pau, 08025 Barcelona, Spain.

[8] Departamento de Engenharia Química, Escola Politécnica, Universidade de São Paulo, Av. Prof. Luciano Gualberto, Trav. 3, Nº 380, 05508-900, São Paulo, SP, Brazil.

π Equally contributed

¥ Present address: Hospital Sant Joan de Déu, Passeig de Sant Joan de Déu, 2, 08950 Esplugues de Llobregat, Barcelona

* Corresponding authors

ABSTRACT

Arginine-rich protein motifs have been described as potent cell-penetrating peptides (CPPs) but also as rather specific ligands of the cell surface chemokine receptor CXCR4, involved in the infection by the human immunodeficiency virus (HIV). Polyarginines are commonly used to functionalize nanoscale vehicles for gene therapy and drug delivery, aimed to enhance cell penetrability of the therapeutic cargo. However, under which conditions these peptides do act as either unspecific or specific ligands is unknown. We have here explored the cell penetrability of differently charged polyarginines in two alternative presentations, namely as unassembled fusion proteins or assembled in multimeric protein nanoparticles. By this, we have observed that arginine-rich peptides switch between receptor-mediated and receptor-independent mechanisms of cell penetration. The relative weight of these activities is determined by the electrostatic charge of the construct and the oligomerization status of the nanoscale material, both regulatable by conventional protein engineering approaches.

Keywords: Protein materials; protein engineering; self-assembling; CXCR4; tumour-homing peptides

INTRODUCTION

The cell surface chemokine receptor CXCR4 is of high clinical relevance, as it acts as a co-receptor during the cell infection by the human immunodeficiency virus (HIV) [1]. In addition, CXCR4 is a pivotal cancer marker over-expressed in the stem cells of more than 20 human neoplasias, including frequent ones such as colorectal and pancreatic cancers and lymphoma [2]. In colorectal cancer, over-expression of CXCR4 is correlated with aggressiveness and metastatic potential. This fact has attracted interest over this membrane protein as a potential target for drug delivery [3-5]. Polyarginines (like R9 and others) are cell penetrating peptides (CPPs) that being cationic, efficiently condensate nucleic acids and promote nuclear localization of attached molecules [6]. Such pleiotropic profiling has empowered some members of the Rn series as valuable functionalizing agents in gene therapy and non-targeted drug delivery. However, under some experimental conditions, polyarginines such as R12 (but not R8), presented as free synthetic peptides, are endocyted by cultured cells in a CXCR4-dependent fashion [7]. In addition, it has been recently reported that a fraction of R9-displaying bacterial amyloids internalize cultured cells by direct binding to CXCR4 [8], while a part of the material penetrates by rather unspecific mechanisms. The possibility to specifically mediate the internalization of macromolecular complexes via CXCR4 is highly appealing in the context of drug delivery. Then, appropriate polyarginine candidates might represent novel and valuable peptidic ligands for CXCR4 that might offer innovative pharmacological opportunities over the currently explored peptide ligands of CXCR4, whose performance is highly variable [9]. In this context, it would be very convenient to define the optimal form and presentation of a given polyarginine domain to unbalance the alternative routes of cell penetration to favour the specific, CXCR4-dependent cell penetrability. This is of special interest when polyarginines are linked to high molecular weight cargos such as full-length recombinant proteins or different types of nanoparticles or other nanostructured entities. Then, we have explored here the dependence on CXCR4 in the internalization of four members of the Rn family when fused to a soluble functional GFP. The fluorescent protein acts as a convenient reporter for image-based monitoring and analysis and as an efficient building block for the generation of protein-based nanoparticles [10]. We have

specially focused our study on the length of the cationic segment (the n value) and on the multivalent versus monovalent display of the ligand on the surface of the protein material. By taking this approach, we have identified both parameters as determinants of the CXCR4 specificity in the cellular penetrability of Rn-empowered constructs.

METHODS

Proteins and protein production

Four GFP-derived fusion proteins, namely R3-GFP-H6, R6-GFP-H6, R7-GFP-H6 and R9-GFP-H6 [11] were used in the present study upon recombinant production in bacteria. As previously described, R9-GFP-H6 was modified by directed mutagenesis to generate the other constructions, replacing arginines by glycines and alanines, in order to maintain the same length of peptide tag with different charges [11]. All of the fusion proteins are based on the same modular scheme (Figure 1A), in which the cationic peptide is placed at the N-terminal end of a His-tagged GFP. For highly cationic peptide segments such arrangement promotes the self-assembling of GFP as highly stable protein nanoparticles, which act as multivalent materials usable as vehicles for cell-targeted drug delivery [12-14]. *Escherichia coli* Rosetta (Novagen, Madison, WI, USA) was grown in shaker flask in Lysogenic broth (LB) medium containing 34 mg/ml chloramphenicol, 12.5 mg/ml tetracycline (strain resistance) and 100 mg/ml ampicillin (vector resistance) at 37 ºC 250 rpm, to reach an OD_{550} of ~0.6 units. Then, induction of gene expression was triggered by 0.1 mM isopropyl-b-D-thiogalactopyronaside (IPTG, Merck, Kenilworth, NJ, USA), and it was prolonged overnight at 20 ºC. Bacterial cells were collected by centrifugation and resuspended in Wash buffer (20 mM Tris , 500 mM NaCl, 10 mM Imidazole; pH 8.0) in the presence of EDTA-Free protease inhibitor (Complete EDTA-Free; Roche, Manheim, Germany), to be disrupted at 1200 psi using a French Press (Thermo FA-078A, Thermo Electron Corporation, Needham Heights, MA, USA). The soluble fraction of lysed cells was loaded on a HiTrap Chelating HP 1 ml column (GE Healthcare, Chicago, IL, USA) to be purified by 6x His-tag affinity chromatography on an ÄKTA purifier (GE Healthcare, Chicago, IL, USA). Bound proteins were eluted with Elution Buffer (20 mM Tris , 500 mM NaCl, 500 mM Imidazole; pH 8.0) in a linear gradient, and fractions containing the protein were then dialysed overnight at 4 ºC against Tris Dextrose buffer (20 mM Tris 5 % dextrose; pH 7.4, referred as *Dextrose* in the Figures) or Tris NaCl buffer (20 mM Tris, 500 mM NaCl; pH 7.4, referred as *NaCl* in the Figures), depending on the solubility of each protein. The purity of the protein was determined by denaturing SDS-polyacrylamide gel electrophoresis (12 % polyacrylamide) and anti-6x-His-tag Western Blot.

Concentrations were determined by Bradford's assay. R9-GFP-H6 had been extensively characterized regarding several of its physicochemical properties, including self-assembling [15].

Fluorescence determination and dynamic light scattering (DLS)

The specific fluorescence of protein variants was determined in a Varian Cary Eclipse Fluorescence Spectrophotometer (Agilent Technologies, Santa Clara, CA, USA) with all proteins being diluted to the same concentration (0.1 mg/ml). For measurements, samples were excited at a wavelength of 488 nm and the emission collected in the range 500-548 nm, with maximum emission detected at 510 nm. Volume size distribution of nanoparticles and monomeric proteins were determined by dynamic light scattering at 633 nm (Zetasizer Nano ZS, Malvern Instruments Limited, Malvern, Worcestershire, UK). Measurements were performed in triplicate. For disassembling assays, SDS (to 0.1 % or 0.05 %, final) was added to proteins previously diluted at 1 mg/ml, and the samples were incubated for 10 min and finally submitted to light scattering analysis.

Ultrastructural characterization

Morphometry (size and shape) of representative nanoparticles was evaluated quantitatively and qualitatively both with field emission scanning electron microscopy (FESEM) and transmission electron microscopy (TEM). Drops of 3 µl of R7-GFP-H6 in both Tris Dextrose and Tris NaCl buffers and R9-GFP-H6 in Tris Dextrose buffer were directly deposited on silicon wafers (Ted Pella Inc., Redding, CA, USA) for 1 min, excess blotted with Whatman filter paper number 1 (GE Healthcare, Little Chalfont, UK), air dried, and immediately observed without coating at a nearly native state in a FESEM Zeiss Merlin (Zeiss, Oberkochen, Germany) operating at 1 kV with a high resolution in-lens secondary electron detector. Drops of 3 µl of the same three samples were directly deposited on 200 mesh carbon-coated copper grids (Electron Microscopy Sciences, Hatfield, PA, USA) for 1 min, excess blotted with Whatman filter paper number 1 (GE Healthcare), contrasted with 3 µl of 1 % uranyl acetate (Polysciences

Inc., Warrington, PA, USA) for 1 min, blotted again and observed in a TEM Jeol 1400 (Jeol Ltd., Tokyo, Japan) operating at 80 kV with a Gatan Orius SC200 CCD camera (Gatan Inc. Abingdon, UK), For each sample and EM technique, the size of 50 randomly distributed particles was measured from TIFF and DM3 files with ImageJ software (NIH, Bethesda, MA,USA).

Cell culture and internalization

HeLa (ATCC-CCL-2, ATCC, Manassas, VA, USA) cells were cultured in MEM-alpha (GIBCO) supplemented with 10 % Foetal Calf Serum (GIBCO BRL, Grand Island, NY, USA) and incubated at 37ºC and 5 % CO_2. For internalization assays, cells were grown in 24-well plates on complete medium, which was replaced by OptiPro supplemented with L-Glutamine before the addition of the proteins. After 2 or 24 h of incubation, cells were detached from the plate with Trypsin (GIBCO) 1 mg/ml for 15 min before being analysed by flow cytometry on a FACS Canto (Becton Dickinson, Franklin Lakes, NJ, USA). Protein fluorescence was excited using a 15 mW air-cooled argon ion laser at 488 nm and detected by a 530/30 nm band pass filter D detector. In all internalization experiments the same concentration of protein was used (1 or 2 µM, as specified). The results were corrected with the fluorescence values obtained from fluorimeter to render data comparable in terms of protein mass. For competition assays, the specific CXCR4 antagonist AMD3100 [16] (octahydrochloride hydrate, Sigma-Aldrich) was added to fresh OptiPRO medium to a 1:10 (protein: AMD3100) molar ratio. Nanoparticles were added after a 1 h incubation with AMD3100.

Confocal microscopy

For confocal microscopy HeLa cells were grown on Mat-Tek plates (MatTek Corporation, Ashland, MA, USA). The nuclei were labelled with 10 µg/ml Hoechst 33342 (Invitrogen, Waltham, MA, USA) and the plasma membrane with 2.5 µg/ml CellMask™ Deep Red (Molecular Probes, Eugene, OR, USA) for 10 min at room temperature and then washed in PBS buffer (Sigma-Aldrich Chemie GmbH, Taufkirchen, Germany). Live cells were recorded by TCS-SP5 confocal laser microscopy

(Leica Microsystems, Wetzlar, Germany) using a Plan Apo 63x/1.4 (oil HC x PL APO lambda blue) objective. Hoechst 33342 DNA label was excited with a blue diode (405 nm) and detected in the 415–460 nm range. GFP-proteins were excited with an Ar laser (488 nm) and detected in the 525–545 nm range. CellMask™ Deep Red was excited with a HeNe laser (633 nm) and detected in the 650–775 nm range. To determine the protein localization inside the cell, stacks of 20–30 sections were collected with 0.5 µm of thickness, and 3D models were generated using the Leica LAS X software (Leica Microsystems, Wetzlar, Germany).

Statistical analysis

Values are expressed as mean data and standard error ($\bar{x}$ ± SD). Data were tested for normal distribution and for homogeneity of variance prior the use of parametric tests with Kolmogorov-Smirnov and Levene tests, respectively. Multiple comparisons were performed by one-way ANOVAs followed by Fisher's least significant difference (LSD, two tailed) and pairwise comparisons by two-tailed Student t-tests using Microsoft Excel 2011 and SPSS 15.0 softwares.

Numerical modelling

To model the penetration of protein nanoparticles in a kinetic way we selected the simplest model by assuming a constant rate of nanoparticle uptake $m(t)$ as a function of time t,

$$\frac{dm}{dt} = -k, 0 \leq k < 1 \Rightarrow m(t) = Me^{-kt} \quad (1)$$

The intracellular fluorescence emission $f(t)$ is proportional to the amount of internalized protein,

$$f(t) = L\,(1 - e^{-kt}) \quad (2)$$

and the initial entry rate of fluorescent materials is

$$\left(\frac{df(t)}{dt}\right)_{t=0} = Lk \equiv v \quad (3)$$

The value of *k* refers to the time $\tau = ln2/k$ needed to reach one half of the maximum fluorescence *L* accumulated in target cells. The model depends on the parameter *k* and the integration constant *L*. To determine *k* and *L,* two couples of measurements (2 h and 24 h) were employed, namely t_1, $f_1 = f(t_1)$, and t_2, $f_2 = f(t_2)$. We assume $t_1 < t_2$; $f_1 < f_2$. Therefore, according to Eq. (2),

$$k = -\frac{1}{t1}\ln\left(1-\frac{f1}{L}\right) = -\frac{1}{t2}\ln\left(1-\frac{f2}{L}\right) \quad (4)$$

By defining $x = f_1/L < 1$, $\mu = t_2/t_1 > 1$, and $\alpha = f_2/f_1 > 1$, the second equality in the above equation leads to the following non-linear equation

$$(1 - x)^{\mu} + \alpha x - 1 = 0 \quad (5)$$

If μ is an integer, the above equation is a polynomial. In a general case, a fixed point Newton-Raphson method will be applied to obtain the single root x_0 satisfying $0 < x_0 < 1$. Finally, we get $k = -\frac{1}{t1} ln(1 - x_0)$, $L = \frac{f1}{x0}$.

RESULTS

R3-GFP-H6, R6-GFP-H6, R7-GFP-H6 and R9-GFP-H6 (Figure 1, A) were successfully bio-produced in *E. coli* (Figure 1B) and stored in either Tris Dextrose buffer (named as *Dextrose* in the Figures) or Tris NaCl buffer (named as *NaCl* in the Figures), depending on their solubility. R3 and R6 derivatives were preferentially soluble in Tris NaCl buffer, R9 in Tris Dextrose buffer and R7 was found to be soluble in both (data not shown). All produced proteins were fluorescent, although with important variability between the checked species (Figure 1, C). This observation, strongly suggested a differential impact (direct or indirect) of the differently charged amino terminal Rn tails on the folding status of the GFP variants. Since the buffer is not expected to affect fluorescence by itself, oligomerization and associated conformational changes might affect the emission capacity of the fluorophore or quench it. When analysing by DLS the potential of these constructs to form nanoparticles, linked to the nature of the cationic terminal domain, we confirmed the inability of R3 and R6 to promote self-assembling (Figure 2), in agreement with a previous preliminary screening [11]. Interestingly, R7-GFP-H6 showed self-assembling properties in Tris Dextrose resulting in nanoparticles of about 30 nm, but not in Tris NaCl in which the protein remained unassembled (Figure 2, and Figure 3, A and B). The higher salt content in the latest buffer might interfere with the electrostatic interactions needed between building blocks to start the oligomerization process [11], thus preventing nanoparticle formation. As previously described [15], R9-GFP-H6 efficiently assembled as regular, toroid-shaped materials of about 30 nm (Figure 2). The size measurements of nanoparticles obtained from FESEM and TEM images were in deep agreement with the values obtained by DLS (Figures 2, 3). In Dextrose-containing buffer, the R9-GFP-H6 nanomaterial appeared larger than in conventional buffers [15], as the sugar probably stabilizes protein-protein cross-interactions. Interestingly, the protein versions that self-organize as oligomers rendered lower fluorescence emission levels than those that remained as building blocks (Figure 1, C). This fact indicated that the architectonic organization of the whole material has an impact on the fluorescent emission of the core GFP, either by a perturbation on the individual building block conformation, as suggested by previous analyses of related self-assembling fluorescent proteins [10, 17], or by fluorophore

quenching due to specific protein-protein cross interactions [18]. Irrespective of these differences, the fluorescence emission was, in all cases, high enough to monitor fast and accurately the cell internalization process upon exposure, and for the evaluation of the potential mediation of CXCR4 in the uptake process.

Cell penetrability of all these constructs was explored by the accumulation of intracellular fluorescence in cultured HeLa cells exposed to them, after a harsh trypsin treatment to remove externally associated protein. As observed (Figure 4A), all proteins penetrate cells since early contact times in a dose-dependent manner, with efficacies that clearly depend on the number of arginines composing the tag at the protein amino terminus. Previous studies showed that 6-12 arginine residues are necessary to promote unspecific entry, with guanidino groups forming hydrogen bonds and ion-pairs with lipid head groups and hydrophobic tails to assist in membrane binding [19]. Here we observed that differences between proteins were largely amplified at long exposure times (24 h), especially in the case of R9-GFP-H6, that was clearly superior than the related polypeptides in the uptake.

Although the number of arginine residues had been implicated in membrane permeability [20], there was a lack of systematic comparisons to clearly understand the role of oligomerization in promoting internalization and how the entry mechanism is affected by these factors. At 24 h, a penetrability of the assembled R7-GFP-H6 (in Tris Dextrose) higher than the unassembled version (in Tris NaCl) was evidenced, pointing out the assembled form and the multivalent display of R7 as favouring agents of cell uptake. Although the number of arginine residues was a parameter that positively affected internalization, multimerization appeared to have an additive and more potent weight. Confocal imaging of the penetration process (Figure 4 B and C) revealed clustering of fluorescent materials in the perinuclear region essentially in the case of the R9-based construct, with an intracellular distribution that might be compatible with both endosomal uptake and transmembrane penetration. In this regard, it must be stressed that endocytic vesicles engulfing fluorescent material were

hardly identified during the penetration of R9-GFP-H6, while they were more apparent in the penetration of the assembled R7-GFP-H6. In this regard, it must be noted the merging yellow signal (co-localization between red membrane and green protein, arrows) revealed in confocal images of cells exposed to R7-GFP-H6 nanoparticles (Figure 4 B).

It has been reported that CXCR4 is involved in internalization of R12 through macropinocytosis, while R8 and TAT seemed to follow a CXCR4-independent route [7]. To determine the involvement of CXCR4 as mediator of internalization of R7 and R9, we monitored this event in presence of AMD3100, a chemical ligand of CXCR4 that inhibits the binding of CXCR4-reactive proteins [16, 21]. As observed (Figure 5, A), at early times after exposure the CXCR4 specificity of the uptake of monomeric versions increases with the number or arginine residues in a linear way. However, the multivalent presentation of polyarginines seemed to promote receptor-independent penetrability, probably linked to the CPP nature of Rn, since the intracellular accumulation of fluorescence is poorly prevented by AMD3100 in the case of the oligomers. However, after 24 h of exposure, the inhibitory effect of AMD3100 was clearly more evident in the case of R9-GFP-H6 (and also R7-GFP-H6) than in the rest of the materials. In this context, it must be noted that the assembled R7 and R9 versions of GFP are indistinguishable regarding stability, as both are equally dissociated by different concentrations of SDS (Figure 5, B). Therefore, dissociation for R7 and R9 constructs (and differential dissociation) was not expected under these experimental conditions. Since both the number of N-terminal arginine residues and the oligomerization process might influence efficiency and specificity of protein penetration is highly relevant for the design of cell-targeted nanoparticle, we presented the obtained data (from Figure 5, A) in a more visual way for further analysis.

As observed (Figure 6, A), the number of arginine residues positively influenced the amount of internalized fluorescence both 2 h and 24 h upon exposure.

Oligomerization, affecting only R7- and R9-based materials, showed a moderate impact on the global uptake process that was dissimilar when comparing short and long times. On the other hand, the % of uptake inhibition mediated by AMD3100 also increased along the number of arginine residues, at 24 h but not from the determinations done 2 h upon exposure. While the specificity for CXCR4 appears as being globally gained by the accumulation of cationic residues, that progressively convert Rn-based CPPs into CXCR4 ligands, data also suggested a differential uptake mechanisms acting at short and long incubation times. To better analyze this possibility, we modelled the penetration of protein nanoparticles in a kinetic way. For that, we explored the factors *L, k,* τ and *v* as defined in the materials and methods section. When these parameters were determined versus the number of arginine residues at the N terminus of the proteins (Rn) for exposures in absence and in presence of the inhibitor AMD3100, we obtained graphical determinations of their behaviour (Figure 6, B). Importantly, the global amount of internalized protein *L* increased with the Rn value, confirming the positive impact that the number of arginines has in the global penetrability of proteins, that appears as being further (but slightly) enhanced by the oligomerization of the building blocks.

Irrespective of the precise mechanism of entrance, this can be accounted by the increase in the positive charge, but also by the multivalent exposure of Rn versus a monovalent display in unassembled proteins [3]. On the other hand, the initial penetration velocity of proteins (*v*) increased with Rn values for unassembled proteins but it was inversely proportional to the number of arginines in the nanoparticles. In presence of AMD3100, that blocks CXCR4-specific penetration and only unspecific CPP-based uptake is allowed, *v* tends to be constant. This is indicative that the number or arginines impacts only (or majorly) on the receptor-dependent penetration of the proteins, which starts very fast upon protein-cell contact. In addition, the comparative behaviour of *v* in absence and in presence of AMD3100 also indicates that oligomerization globally enhances the CPP properties of proteins, a fact that promotes a fast and early entrance into the cells upon exposure. Inversely, oligomerization, and the increase of the number of arginine residues in the oligomers minimized specificity

in early penetration stages. By analyzing *k*, which can be also interpreted in terms of the half time (τ) to reach the maximal intracellular accumulation of protein, we determined that the jump from R7 to R9 (but not oligomerization itself) expands the time period in which the penetration process does occur. However, when AMD3100 is present, the duration of the penetration process is also expanded depending on the Rn value. Therefore, the unspecific penetrability of Rn-based nanoconstructs sustained by their CPP properties is a time-prolonged process that is favoured when the CXCR4-dependent endosomal penetration is not available.

DISCUSSION

The delivery of therapeutic molecules into cells requires the smart engineering of fusogenic agents, mainly lipids [22, 23] and proteins [24, 25], that act as unspecific but highly efficient cell penetrating agents. Alternatively, cell-targeting tools, such as antibodies or peptidic ligands, provide selectivity in the cell binding of drug vehicles [26, 27], although they are generically less competent than unspecific CPP tools in promoting internalization [28, 29]. The still poorly explored combination of both agents in the same vehicle, namely the incorporation of a CPP and a peptidic ligand of a target cell surface receptor has so far resulted in very high cell penetration levels but at expenses of specificity [30].

Among the CPPs recognized as useful and with potential for realistic development and applicability in biomedicine, arginine-rich peptides are indeed being translated from bench to bedside in several pre-clinical and clinical trials [31]. Even though the internalization mechanisms of polyarginines are not completely understood, they are being combined to different formulations due to their penetration enhancing properties, being applied even in highly challenging conditions such as oral administration [32]. Interestingly, it has been separately suggested that polyarginines exhibit either unspecific (CPP) or specific (receptor-dependent) cell penetration activities [7, 8]. Receptor-dependent internalization of polyarginines can be seen as an entangled scenario affected by multiple factors. For instance, the contribution of Syndecan-4, a receptor known to be involved in R8 internalization, was also reported to depend on parameters such as the extracellular concentration of the peptide but not affected by the presence of a protein fused to R8 [33].

This unusual pleiotropic profile might be highly relevant when designing new generation protein-based vehicles for cell-targeted drug delivery, especially regarding efficiency and when looking for selectivity in a drug delivery process. Therefore, the highly versatile mechanism of entry of polyarginines has been dissected here through the use of several Rn constructs, showing or not self-assembling properties that affect

the multivalent display of the peptide to exposed cells. In this context, the obtained data indicate the coexistence of two different mechanism of penetrability of Rn-empowered proteins, namely CXCR4-dependent uptake and unspecific CPP-based internalization, which act differentially during the time of contact between cells and materials. In presence of free CXCR4 on the cell surface, proteins probably remain attached to the receptor and initiate a fast process of penetration. When CXCR4 is blocked by AMD3100, or CXCR4 paratopes are saturated by earlier contacts, cell penetrability is unspecific and takes place much slower (Figure 5). The relative prevalence of both mechanisms is also largely influenced by the value of Rn and by the oligomerization status of the protein. The specificity in the cell penetration is reduced by oligomerization and by the Rn value of the oligomers at short times upon exposure (Figure 6). However, globally, the increase of Rn length and the formation of multivalent structures increase the total amount of intracellular material and its receptor-depended uptake.

In summary, despite polyarginines have been generically observed as highly potent CPPs useful as an internalization tag in cell therapy and drug delivery [6], their known residual specificity for the cell surface cytokine receptor CXCR4 can be enhanced by a proper presentation of the cationic stretch. As shown here, this can be achieved by extending the number of arginine residues and, with a milder impact, of the multimeric presentation on the surface of targeting vehicles. Since polyarginines are highly cationic and they act also as oligomerization domains [9], R9 and related species can confer to fusion proteins both self-assembling and cell-targeting properties. Being CXCR4 an appealing target in innovative cancer therapies and in antiretroviral treatments [2, 4, 5, 7, 16, 21, 34-37], R9 and related peptides might represent an additional instrument for the design of improved vehicles for intracellular drug delivery. Albeit the CXCR4 specificity of polyarginines might not be absolute, even in their optimal presentation (Figure 5, A), their use in combination with other CXCR4 ligands might allow the generation of new-generation bi-paratopic vehicles, that are extremely appealing for enhanced specificities and cell surface avidity in receptor-mediated drug delivery [38-42]. In vehicles with such combined functional agents, the

residual CPP activities of polyarginines might enhance penetrability and endosomal escape more efficiently than completely unspecific fusogenic peptides that such as HA2, tend to impair selectivity of the accompanying cell ligands [30].

Acknowledgments: Protein production has been partially performed by the ICTS "NANBIOSIS", more specifically by the Protein Production Platform of CIBER-BBN/ IBB, at the UAB SepBioES scientific-technical service (http://www.nanbiosis.es/unit/u1-protein-production-platform-ppp/). Nanoparticle size determination was performed at the NANBIOSIS Biomaterial Processing and Nanostructuring Unit of CIBER-BBN (http://www.nanbiosis.es/portfolio/u6-biomaterial-processing-and-nanostructuring-unit).

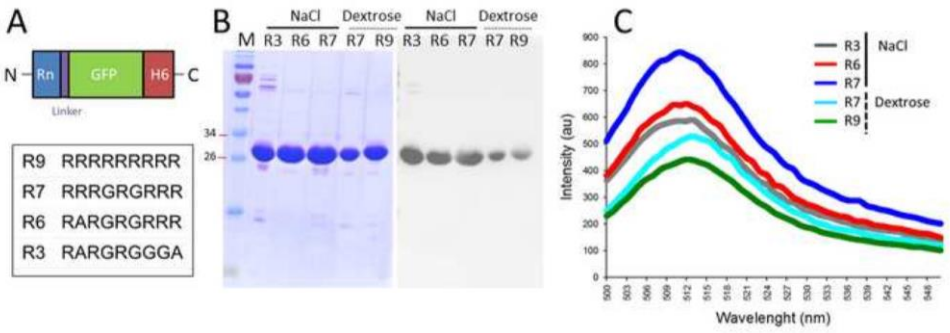

Figure 1

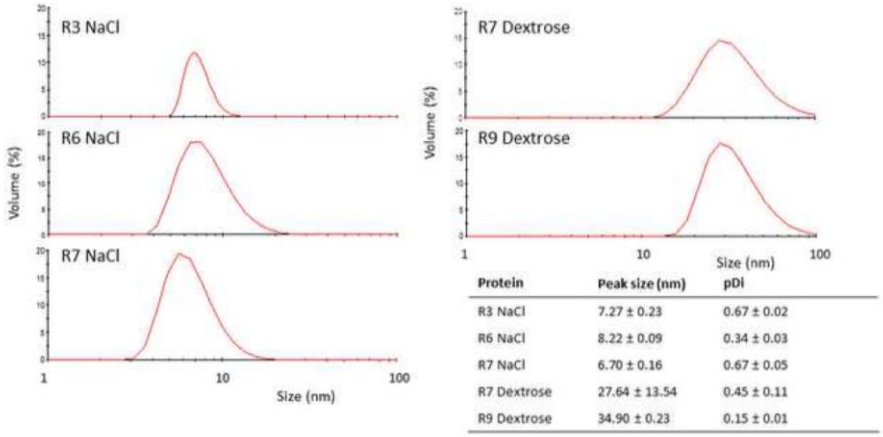

Protein	Peak size (nm)	pDi
R3 NaCl	7.27 ± 0.23	0.67 ± 0.02
R6 NaCl	8.22 ± 0.09	0.34 ± 0.03
R7 NaCl	6.70 ± 0.16	0.67 ± 0.05
R7 Dextrose	27.64 ± 13.54	0.45 ± 0.11
R9 Dextrose	34.90 ± 0.23	0.15 ± 0.01

Figure 2

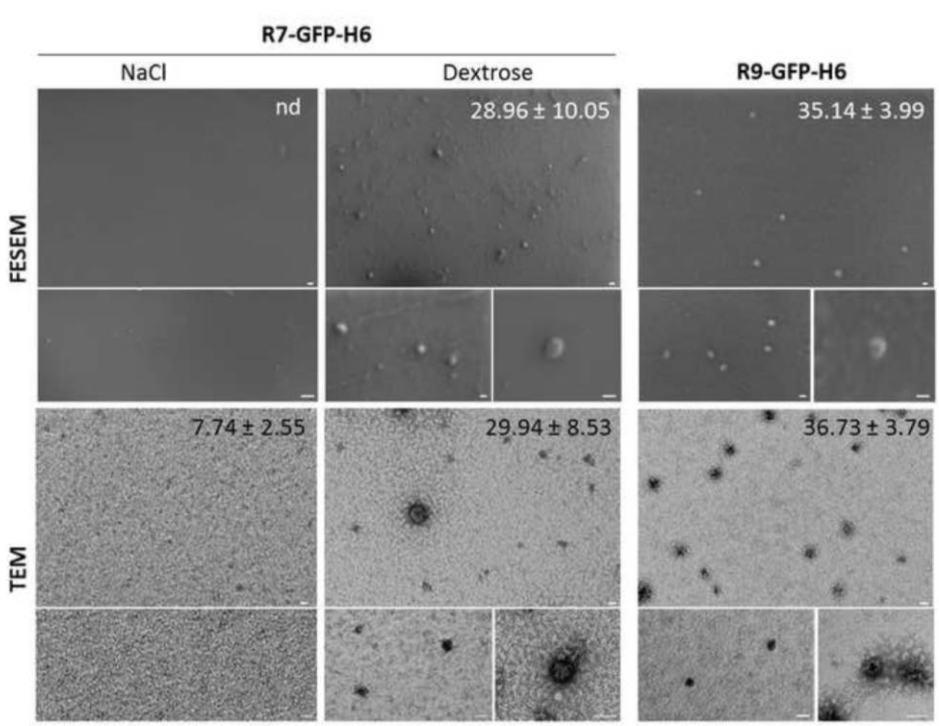

Figure 3

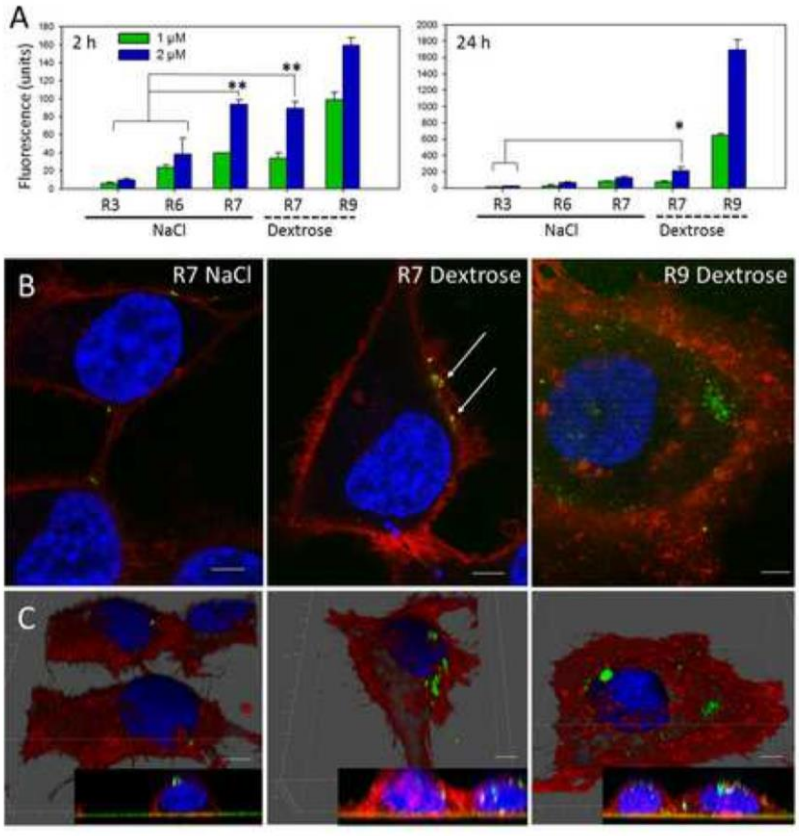

Figure 4

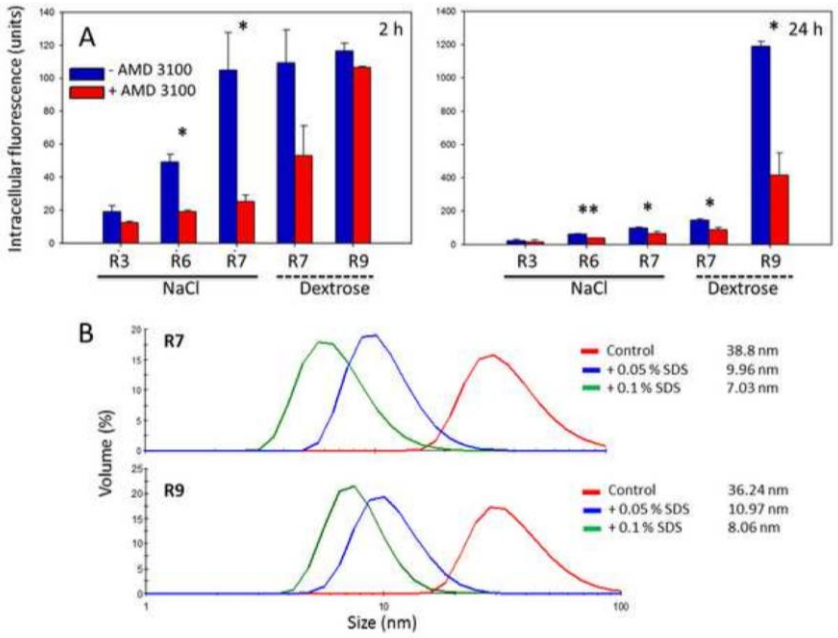

Figure 5

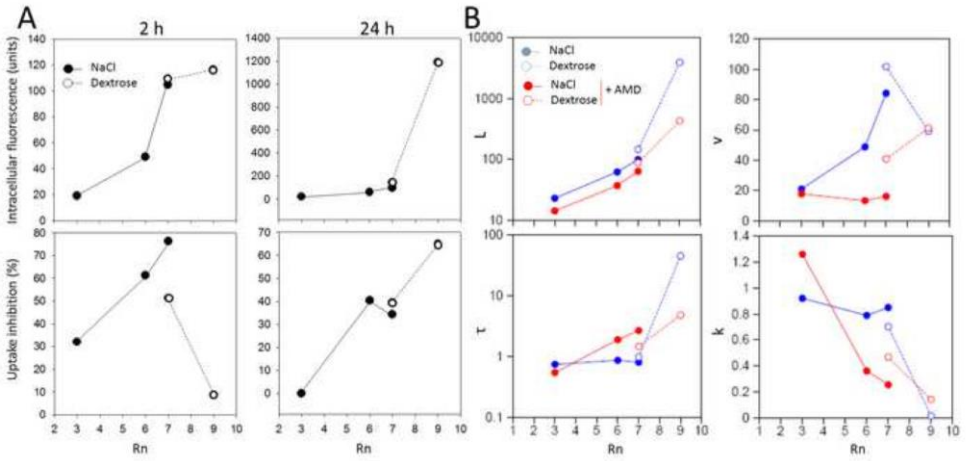

Figure 6

Legends

Figure 1. Production and preliminary characterization of Rn-containing GFP protein versions. A. Generic scheme of the modular protein construction. The linker sequence is GGGNS, and the precise amino acid sequence of the Rn peptides is indicated in the box. B Coomassie blue-stained PAGE-SDS gel showing the integrity and purity of Rn-GFP-H6 recombinant proteins upon affinity chromatography (left). Proteolytic stability was confirmed by Western blot (right). The type of buffer used is indicated at the top, as well as the number of amino-terminal arginine residues in each protein. The molecular mass of relevant markers (M) is indicated in kDa. C. Fluorescence emission spectra of equal amounts of each protein.

Figure 2. Assembling of Rn-containing GFP proteins. DLS size determination of protein self-assembling. The size of unassembled proteins (6-8 nm) might correspond to GFP dimers acting as building blocks. In the inset, peak (expressed in nm) and PDI as mean values and standard deviation ($\bar{x}$ ± SD) for each protein sample obtained by DLS.

Figure 3. Ultrastructural analysis of Rn-containing GFP proteins. FESEM and TEM imaging of protein nanoparticles formed in *Dextrose* buffer. Representative fields of R7-GFP-H6 samples in *NaCl* buffer are also shown as negative controls. Bars size is 20 nm. The size of the nanomaterials (in nm) determined from images is indicated as mean values and standard deviation ($\bar{x}$ ± SD) for each protein sample and EM technique (nd indicates that the material has not been detected).

Figure 4. Cell penetrability of Rn-containing GFP proteins. A. Intracellular fluorescence accumulated in $CXCR4^+$ HeLa cells upon exposure to unassembled and assembled Rn-based proteins, for different times and protein doses. Symbols are ** $p< 0.01$; * $p <$

0.05. B. Conventional confocal images of target HeLa cells exposed for 24 h to 2 µM of either R7 or R9-based proteins. The green signal results from the protein fluorescence, while red signals label membranes and blue signals the cell nuclei. Arrows indicate yellow merging signals. C. 3D reconstructions based on stacks of 20–30 sections of protein-exposed HeLa cells. In the insets, orthogonal sections of 3D confocal images Bars indicate 5 µm.

Figure 5. CXCR4-dependence in the internalization of Rn-based protein materials. A. Accumulation of intracellular fluorescence into $CXCR4^+$ HeLa cells associated to different Rn-based materials, and AMD3100-mediated inhibition of the process. The signals were recorded at two different times after exposure. Symbols are ** $p< 0.01$; * $p < 0.05$. B. DLS size measurements of R7 and R9-based proteins upon incubation with SDS for 10 min.

Figure 6. Internalization of Rn-based protein materials. A. Intracellular florescence in HeLa cells and percentage of AMD3100-mediated uptake inhibition upon 2 h and 24 h of exposure to Rn-based nanoparticles. B. Plotting of main kinetic parameters of protein uptake, namely L, τ, , k and v (see Eq 1-3) versus the number of arginine residues at the N-terminus of proteins (Rn). Uptake experiments in presence of AMD3100 are indicated (+AMD).

References

[1] Chan DC, Kim PS. HIV entry and its inhibition. Cell. 1998;93:681-4.

[2] Burger JA, Kipps TJ. CXCR4: a key receptor in the crosstalk between tumor cells and their microenvironment. Blood. 2006;107:1761-7.

[3] Unzueta U, Cespedes MV, Vazquez E, Ferrer-Miralles N, Mangues R, Villaverde A. Towards protein-based viral mimetics for cancer therapies. Trends in biotechnology. 2015;33:253-8.

[4] Barbieri F, Bajetto A, Florio T. Role of chemokine network in the development and progression of ovarian cancer: a potential novel pharmacological target. Journal of oncology. 2010;2010:426956.

[5] Choi WT, Yang Y, Xu Y, An J. Targeting chemokine receptor CXCR4 for treatment of HIV-1 infection, tumor progression, and metastasis. Current topics in medicinal chemistry. 2014;14:1574-89.

[6] Saccardo P, Villaverde A, Gonzalez-Montalban N. Peptide-mediated DNA condensation for non-viral gene therapy. Biotechnology advances. 2009;27:432-8.

[7] Tanaka G, Nakase I, Fukuda Y, Masuda R, Oishi S, Shimura K, et al. CXCR4 stimulates macropinocytosis: implications for cellular uptake of arginine-rich cell-penetrating peptides and HIV. Chemistry & biology. 2012;19:1437-46.

[8] Unzueta U, Seras-Franzoso J, Cespedes MV, Saccardo P, Cortes F, Rueda F, et al. Engineering tumor cell targeting in nanoscale amyloidal materials. Nanotechnology. 2017;28:015102.

[9] Unzueta U, Cespedes MV, Ferrer-Miralles N, Casanova I, Cedano J, Corchero JL, et al. Intracellular CXCR4(+) cell targeting with T22-empowered protein-only nanoparticles. International journal of nanomedicine. 2012;7:4533-44.

[10] Rueda F, Cespedes MV, Conchillo-Sole O, Sanchez-Chardi A, Seras-Franzoso J, Cubarsi R, et al. Bottom-Up Instructive Quality Control in the Biofabrication of Smart Protein Materials. Advanced materials. 2015;27:7816-22.

[11] Unzueta U, Ferrer-Miralles N, Cedano J, Zikung X, Pesarrodona M, Saccardo P, et al. Non-amyloidogenic peptide tags for the regulatable self-assembling of protein-only nanoparticles. Biomaterials. 2012;33:8714-22.

[12] Serna N, Cespedes MV, Saccardo P, Xu Z, Unzueta U, Alamo P, et al. Rational engineering of single-chain polypeptides into protein-only, BBB-targeted nanoparticles. Nanomedicine : nanotechnology, biology, and medicine. 2016;12:1241-51.

[13] Serna NC, M; Sánchez-García, L; Unzueta, U; Sala, R; Sánchez-Chardi, A; Cortés, F; Ferrer-Miralles, N; Mangues, R; Vázquez, E; Villaverde, A. Peptide-Based Nanostructured Materials with Intrinsic Proapoptotic Activities in CXCR4+ Solid Tumors. Advanced Functional Materials. 2017;27:1700919.

[14] Serna N, Sanchez-Garcia L, Sanchez-Chardi A, Unzueta U, Roldan M, Mangues R, et al. Protein-only, antimicrobial peptide-containing recombinant nanoparticles with inherent built-in antibacterial activity. Acta biomaterialia. 2017. 60:256-63.

[15] Vazquez E, Roldan M, Diez-Gil C, Unzueta U, Domingo-Espin J, Cedano J, et al. Protein nanodisk assembling and intracellular trafficking powered by an arginine-rich (R9) peptide. Nanomedicine. 2010;5:259-68.

[16] Kim HY, Hwang JY, Kim SW, Lee HJ, Yun HJ, Kim S, et al. The CXCR4 Antagonist AMD3100 Has Dual Effects on Survival and Proliferation of Myeloma Cells In Vitro. Cancer research and treatment : official journal of Korean Cancer Association. 2010;42:225-34.

[17] Pesarrodona M, Crosas E, Cubarsi R, Sanchez-Chardi A, Saccardo P, Unzueta U, et al. Intrinsic functional and architectonic heterogeneity of tumor-targeted protein nanoparticles. Nanoscale. 2017;9:6427-35.

[18] Pesarrodona M, Fernandez Y, Foradada L, Sanchez-Chardi A, Conchillo-Sole O, Unzueta U, et al. Conformational and functional variants of CD44-targeted protein nanoparticles bio-produced in bacteria. Biofabrication. 2016;8:025001.

[19] Futaki S, Nakase I. Cell-Surface Interactions on Arginine-Rich Cell-Penetrating Peptides Allow for Multiplex Modes of Internalization. Accounts of chemical research. 2017;50:2449-56.

[20] Nakase I, Niwa M, Takeuchi T, Sonomura K, Kawabata N, Koike Y, et al. Cellular uptake of arginine-rich peptides: roles for macropinocytosis and actin rearrangement. Molecular therapy : the journal of the American Society of Gene Therapy. 2004;10:1011-22.

[21] Jung YH, Lee DY, Cha W, Kim BH, Sung MW, Kim KH, et al. Antitumor effect of CXCR4 antagonist AMD3100 on the tumorigenic cell line of BHP10-3 papillary thyroid cancer cells. Head & neck. 2016;38:1479-86.

[22] Atif SM, Hasan I, Ahmad N, Khan U, Owais M. Fusogenic potential of sperm membrane lipids: nature's wisdom to accomplish targeted gene delivery. FEBS letters. 2006;580:2183-90.

[23] Ahmad N, Masood AK, Owais M. Fusogenic potential of prokaryotic membrane lipids. Implication in vaccine development. European journal of biochemistry. 2001;268:5667-75.

[24] Ye J, Liu E, Yu Z, Pei X, Chen S, Zhang P, et al. CPP-Assisted Intracellular Drug Delivery, What Is Next? International journal of molecular sciences. 2016;17.

[25] Ye J, Shin MC, Liang Q, He H, Yang VC. 15 years of ATTEMPTS: a macromolecular drug delivery system based on the CPP-mediated intracellular drug delivery and antibody targeting. Journal of controlled release : official journal of the Controlled Release Society. 2015;205:58-69.

[26] Dai Q, Bertleff-Zieschang N, Braunger JA, Bjornmalm M, Cortez-Jugo C, Caruso F. Particle Targeting in Complex Biological Media. Advanced healthcare materials. 20118; 7..

[27] Mangues RV, E; Villaverde, A. Targeting in Cancer Therapies. Medical Sciences. 2016;4:6.

[28] Vazquez E, Ferrer-Miralles N, Villaverde A. Peptide-assisted traffic engineering for nonviral gene therapy. Drug discovery today. 2008;13:1067-74.

[29] Ferrer-Miralles N, Vazquez E, Villaverde A. Membrane-active peptides for non-viral gene therapy: making the safest easier. Trends in biotechnology. 2008;26:267-75.

[30] Sanchez-Garcia L, Serna N, Mattanovich M, Cazzanelli P, Sanchez-Chardi A, Conchillo-Sole O, et al. The fusogenic peptide HA2 impairs selectivity of CXCR4-targeted protein nanoparticles. Chemical communications. 2017;53:4565-8.

[31] Guidotti G, Brambilla L, Rossi D. Cell-Penetrating Peptides: From Basic Research to Clinics. Trends in pharmacological sciences. 2017;38:406-24.

[32] Niu Z, Tedesco E, Benetti F, Mabondzo A, Montagner IM, Marigo I, et al. Rational design of polyarginine nanocapsules intended to help peptides overcoming intestinal barriers. Journal of controlled release : official journal of the Controlled Release Society. 2017;263:4-17.

[33] Kawaguchi Y, Takeuchi T, Kuwata K, Chiba J, Hatanaka Y, Nakase I, et al. Syndecan-4 Is a Receptor for Clathrin-Mediated Endocytosis of Arginine-Rich Cell-Penetrating Peptides. Bioconjugate chemistry. 2016;27:1119-30.

[34] Cespedes MV, Unzueta U, Alamo P, Gallardo A, Sala R, Casanova I, et al. Cancer-specific uptake of a liganded protein nanocarrier targeting aggressive CXCR4+ colorectal cancer models. Nanomedicine : nanotechnology, biology, and medicine. 2016;12:1987-96.

[35] de Nigris F, Crudele V, Giovane A, Casamassimi A, Giordano A, Garban HJ, et al. CXCR4/YY1 inhibition impairs VEGF network and angiogenesis during malignancy. Proceedings of the National Academy of Sciences of the United States of America. 2010;107:14484-9.

[36] Murakami T, Cardones AR, Hwang ST. Chemokine receptors and melanoma metastasis. Journal of dermatological science. 2004;36:71-8.

[37] Song JS, Kang CM, Kang HH, Yoon HK, Kim YK, Kim KH, et al. Inhibitory effect of CXC chemokine receptor 4 antagonist AMD3100 on bleomycin induced murine pulmonary fibrosis. Experimental & molecular medicine. 2010;42:465-72.

[38] Kontermann RE. Dual targeting strategies with bispecific antibodies. mAbs. 2012;4:182-97.

[39] Kontermann RE, Brinkmann U. Bispecific antibodies. Drug discovery today. 2015;20:838-47.

[40] Muller D, Kontermann RE. Recombinant bispecific antibodies for cellular cancer immunotherapy. Current opinion in molecular therapeutics. 2007;9:319-26.

[41] Weidle UH, Kontermann RE, Brinkmann U. Tumor-antigen-binding bispecific antibodies for cancer treatment. Seminars in oncology. 2014;41:653-60.

[42] Unzueta U, Serna N, Sanchez-Garcia L, Roldan M, Sanchez-Chardi A, Mangues R, et al. Engineering multifunctional protein nanoparticles by in vitro disassembling and reassembling of heterologous building blocks. Nanotechnology. 2017;28:505102.

ANNEX 6: REFERENCE 295

Engineering multifunctional protein nanoparticles by in vitro disassembling and reassembling of heterologous building blocks.

Ugutz Unzueta, Naroa Serna, Laura Sánchez-García, Mónica Roldán, Alejandro Sánchez-Chardi, Ramón Mangues, Antonio Villaverde and Esther Vázquez.

Nanotechnology. October 2017. 28: 505102**.**

Impact factor: 3.44. Quartile: Q1. Decile: D1.

IOP Publishing Nanotechnology
Nanotechnology 28 (2017) 505102 (9pp) https://doi.org/10.1088/1361-6528/aa963e

Engineering multifunctional protein nanoparticles by *in vitro* disassembling and reassembling of heterologous building blocks

Ugutz Unzueta[1,2], Naroa Serna[2,3,4], Laura Sánchez-García[2,3,4], Mónica Roldán[5], Alejandro Sánchez-Chardi[6], Ramón Mangues[1,2], Antonio Villaverde[2,3,4,7] and Esther Vázquez[2,3,4,7]

[1] Institut d'Investigacions Biomèdiques Sant Pau and Josep Carreras Research Institute, Hospital de la Santa Creu i Sant Pau, E-08025 Barcelona, Spain
[2] CIBER de Bioingeniería, Biomateriales y Nanomedicina (CIBER-BBN), Spain
[3] Institut de Biotecnologia i de Biomedicina, Universitat Autònoma de Barcelona, Bellaterra, E-08193 Barcelona, Spain
[4] Departament de Genètica i de Microbiologia, Universitat Autònoma de Barcelona, Bellaterra, E-08193 Barcelona, Spain
[5] Unitat de Microscòpia Confocal. Servei d'Anatomia Patològica, Institut Pediàtric de Malalties Rares (IPER). Hospital Sant Joan de Déu, Universitat de Barcelona, Esplugues de Llobregat, E-08950 Barcelona, Spain
[6] Servei de Microscòpia, Universitat Autònoma de Barcelona, Bellaterra, E-08193 Barcelona, Spain

E-mail: Antoni.Villaverde@uab.es and Esther.Vazquez@uab.es

Received 15 September 2017, revised 18 October 2017
Accepted for publication 26 October 2017
Published 22 November 2017

Abstract

The engineering of protein self-assembling at the nanoscale allows the generation of functional and biocompatible materials, which can be produced by easy biological fabrication. The combination of cationic and histidine-rich stretches in fusion proteins promotes oligomerization as stable protein-only regular nanoparticles that are composed by a moderate number of building blocks. Among other applications, these materials are highly appealing as tools in targeted drug delivery once empowered with peptidic ligands of cell surface receptors. In this context, we have dissected here this simple technological platform regarding the controlled disassembling and reassembling of the composing building blocks. By applying high salt and imidazole in combination, nanoparticles are disassembled in a process that is fully reversible upon removal of the disrupting agents. By taking this approach, we accomplish here the *in vitro* generation of hybrid nanoparticles formed by heterologous building blocks. This fact demonstrates the capability to generate multifunctional and/or multiparatopic or multispecific materials usable in nanomedical applications.

Supplementary material for this article is available online

Keywords: recombinant proteins, self-assembling, viral mimetics, cell targeting, multifunctional nanoparticles

(Some figures may appear in colour only in the online journal)

[7] Authors to whom any correspondence should be addressed.

Introduction

Among the diversity of materials used in nanomedicine, proteins offer full biocompatibility, structural and functional versatility and the possibility to control their oligomerization status to reach defined supramolecular architectures [1–5]. For use as biomaterials, self-assembling can be promoted either by adapting natural oligomerization domains [6] or by the *de novo* design of interacting stretches [5, 7, 8]. Virus-like particles are the paradigm of self-organizing oligomeric structures that directly derive from nature. Produced in recombinant cell factories, selected structural viral proteins spontaneously assemble as nanoscale entities, usually homomeric, that mimic viral capsids and that have applicability as immunogens for vaccination [9] and as drug delivery systems [10]. Cellular elements such as bacterial flagella [11] or mammalian cell vaults [12] are equally produced by recombinant DNA technologies upon convenient tailoring.

Regarding *de novo* designed nanoscale multimers, a diversity of rational and semi-rational approaches are available [3]. In this context, we have previously described an oligomerization platform based on the fusion of an N-terminal cationic peptide plus a C-terminal histidine-rich peptide, to diverse central polypeptides that act as a core of the whole fusion [13, 14]. Both end-terminal tails promote protein–protein contacts between the building blocks that render a category of non-toxic planar nanoparticles [15], whose formation and final architecture is modulated by the number of cationic residues at the N-terminus and by the electrostatic charge distribution in the building block [16, 17]. Mimicking viral properties, these materials are highly convenient as drug carriers [18]. When the N-terminal cationic peptide is a specific ligand of a cell surface tumoral marker (such as binders of cell surface proteins CD44 or CXCR4), this protein segment contributes to the self-assembling but it also endorses the penetration of the whole construct in a receptor-specific way, as demonstrated *in vivo* in breast and colorectal cancer models [17, 19–21]. In particular, T22-GFP-H6 is a paradigmatic construct that self-assembles as 12 nm nanoparticles, and in which the cationic peptide T22 acts as a specific ligand of CXCR4, both *in vitro* and *in vivo* [13, 20]. Envisaging the clinically appealing possibility to generate hybrid nanoparticles made of different building blocks or displaying different cell-targeting agents in multiparatopic or multi-specific constructs [22], we have explored here the generation of multifunctional hybrid materials based on this oligomerization platform. This has been successfully achieved through novel but simple procedures that allow the reversible disassembling of protein homomeric oligomers and their controlled re-association, upon convenient ratiometric mixing, to form regular but heteromeric multifunctional nanoparticles.

Methods

Protein design, production and purification

The gene encoding T22-BFP-H6 was designed in house, provided by Geneart (Invitrogen) and cloned in pET22b (Novagen). The construction of the related gene fusions encoding T22-GFP-H6 and R9-GFP-H6 had been described previously [16, 23]. Proteins were produced in *Escherichia coli* Origami B overnight at 20 °C upon addition of 0.1 mM IPTG for T22-GFP-H6 and T22-BFP-H6 and in *Escherichia coli* Rosetta, overnight at 25 °C, upon addition of 1 mM of IPTG for R9-GFP-H6. These strains were selected because of their less reducing cytoplasm that ensure the formation of the two disulphide bridges of T22, necessary for T22-CXCR4 interaction. Cells were then centrifuged for 10 min (5000 g) and resuspended in Tris buffer (20 mM Tris, 500 mM NaCl, 10 mM Imidazole) in presence of the protease inhibitor Complete EDTA-Free (Roche). Cells were then disrupted by three rounds at 1200 psi in a French Press (Thermo) and subsequently purified by IMAC affinity chromatography using HiTrap Chelating HP 1 ml column in an ÄKTA pure (GE Healthcare). Proteins were eluted by a linear gradient of elution buffer (20 mM Tris, 500 mM NaCl, 500 mM Imidazole) and once collected, they were dialysed against sodium carbonate buffer (166 mM $NaCO_3H$ pH = 8) for T22-GFP-H6 and T22-BFP-H6 and against Tris Dextrose buffer (20 mMTris + 5% Dextrose pH = 8) for R9-GFP-H6. Protein purity was determined by polyacrylamide gel electrophoresis (SDS-PAGE) and Western blot immunodetection with anti-His monoclonal antibody (Santa Cruz Biotechnology). Finally, protein integrity was determined by MALDI-TOF mass spectrometry.

Production of hybrid nanoparticles

T22-GFP-H6, T22-BFP-H6 and R9-GFP-H6 protein nanoparticles (at 1.5 mg ml^{-1}) were disassembled by adding NaCl (500 mM Na^+ final concentration) and Imidazole (300 mM final concentration) into their respective buffers. T22-GFP-H6/T22-BFP-H6 and R9-GFP-H6/T22-BFP-H6 hybrid nanoparticles were generated by mixing T22-GFP-H6 and T22-BFP-H6 monomers and R9-GFP-H6 and T22-BFP-H6 monomers respectively in a 1:1 molar ratio and subsequently dialyzing them against a low Na^+ and Imidazole buffer (166 mM $NaCO_3H$ pH = 8 and 20 mM Tris + 5% Dextrose pH = 8 respectively).

Dynamic light scattering (DLS)

Volume size distribution of parental and hybrid protein nanoparticles at 1.5 mg ml^{-1} and under different buffer conditions was determined by DLS at 633 nm in a Zetasizer Nano ZS (Malvern).

Field emission scanning electron microscopy (FESEM)

Native ultrastructure of the nanoparticles was evaluated with a microscope Zeiss Merlin (Zeiss) operating at 2 kV. Drops of 3 μl of each sample (T22-GFP-H6, R9-GFP-H6, T22-BFP-H6, T22-GFP-H6/T22-BFP-H6 and R9-GFP-H6/T22-BFP-H6) were directly deposited on silicon wafers (Ted Pella Inc.) for 1 min, excess blotted with Whatman filter paper number 1 (GE Healthcare), air dried, and observed without coating with a high resolution in-lens secondary electron detector.

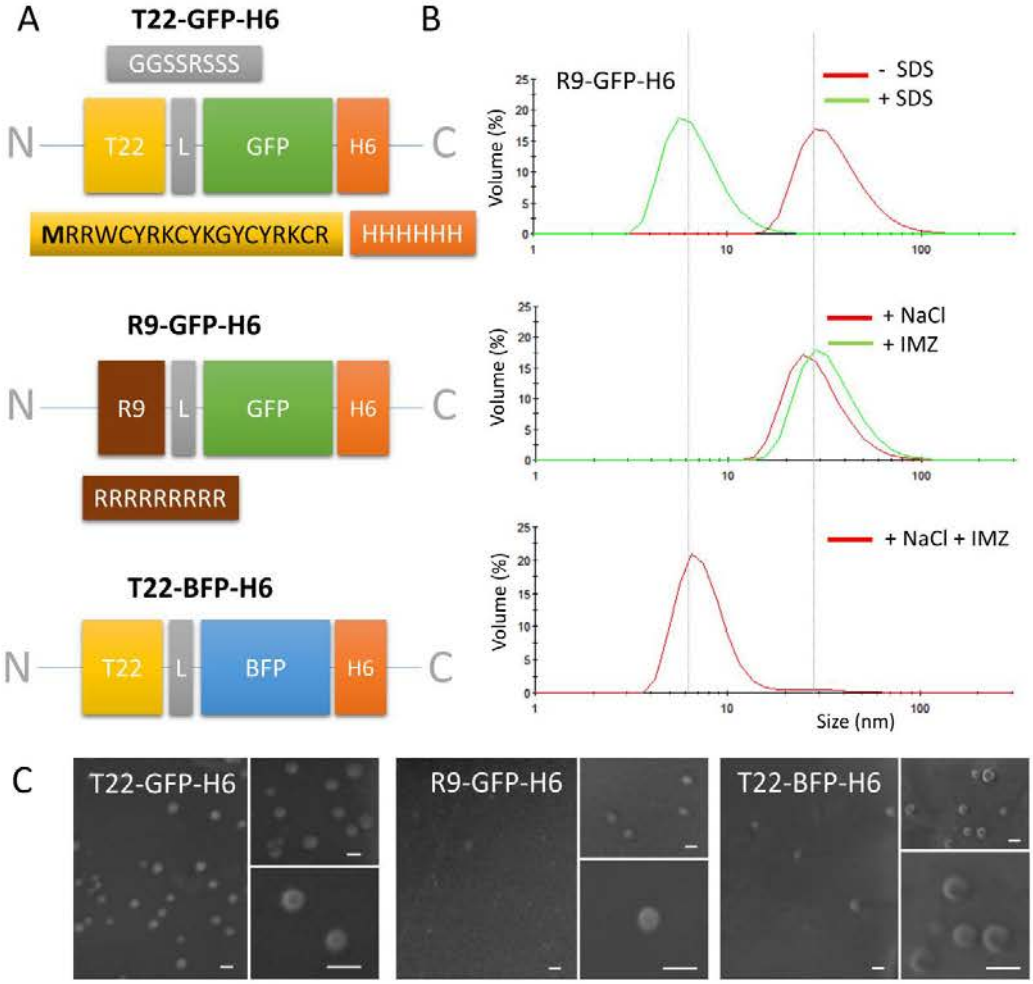

Figure 1. Architecture of protein nanoparticles. (A) Modular organization of the protein building blocks, indicating the relevant amino acid stretches. Box sizes and proportions are only indicative. (B) DLS analysis of R9-GFP-H6 nanoparticles, in the native assembled state or disassembled upon incubation with SDS 0.1%. The sizes of the material treated with imidazole (300 mM, IMZ) and incubated in high salt (500 mM, Na^+) buffer are also indicated. Raw data for R9-GFP-H6 and for T22-GFP-H6 and T22-BFP-H6 are shown in table 1. The vertical lines indicate the expected location of assembled and unassembled materials. (C) FESEM imaging of the resulting nanoparticles at different magnifications. Bars represent 20 nm.

Table 1. Size of protein nanoparticles under different buffer conditions.

			T22-GFP-H6		R9-GFP-H6		T22-BFP-H6	
Buffer[a,b]	Na^+ (mM)[c]	Imidazole (mM)	Size (nm)	Pdi	Size (nm)	Pdi	Size (nm)	Pdi
Buffer[a,b,d]	166[a]/0[b]	0	11.01/9.1[e]	0.454	36.02/19.7[e]	0.150	8.6/9.0[e]	0.500
+NaCl	500	0	10.17	0.798	29.7	0.486	8.8	0.495
+IMZ	166[a]/0[b]	300	10.79	0.411	34.3	0.129	8.5	0.395
+NaCl +IMZ	500	300	6.5	0.561	7.50	0.734	6.8	0.451
+SDS (0.1%)	166[a]/0[b]	0	7.9	0.332	6.9	0.225	6.91	0.198

[a] $NaCO_3H$ buffer has been used to dissolve T22-GFP-H6 and T22-BFP-H6.
[b] Tris Dextrose has been used for R9-GFP-H6.
[c] Total Na^+ concentration reached in buffer.
[d] The parental GFP-H6 sizes 7.0 nm[a] and 7.2 nm[b] in the same buffers.
[e] Size peak of particles reassembled in the original buffer after Na^+ +IMZ-mediated disassembling. IMZ, Imidazole.

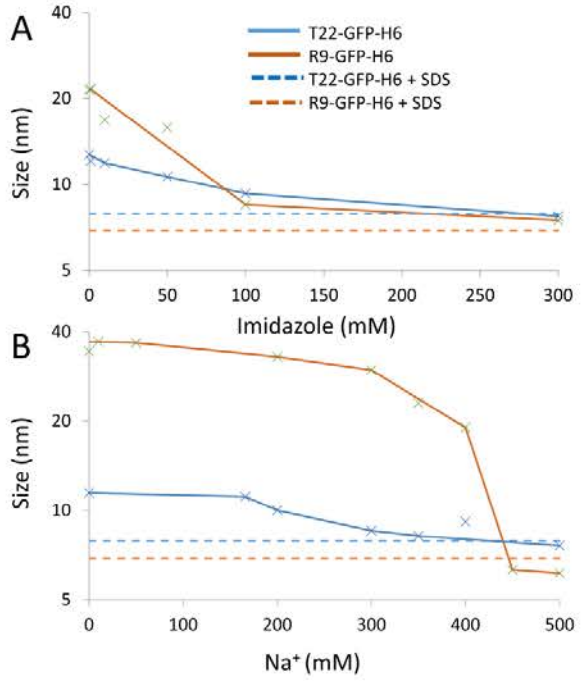

Figure 2. Controlled disassembling of T22-GFP-H6 and R9-GFP-H6 nanoparticles. Disassembling is mediated by increasing concentrations of either imidazole ((A), in 500 mM Na^+) or salt ((B), in 300 mM imidazole), keeping the rest of conditions constant. The monomer size upon SDS-mediated disassembly is indicated in each case by horizontal dashed lines.

FRET determination

Fluorescence emission spectrum (400–600 nm) of hybrid protein nanoparticles in different buffers was measured in a Cary Eclipse fluorescence spectrophotometer (Agilent Technologies) upon excitation at 387 nm. Acceptor photobleaching experiments were performed on a TCS SP5 Leica Spectral confocal microscope (Leica Microsystems) equipped with a HCX PL Apo CS lambda blue 63×/1.4NA oil objective. We used BFP as the donor fluorochrome paired with GFP as the acceptor fluorochrome. BFP was excited with the 405 nm line (diode laser) and the emission was collected at 420–475 nm. GFP was excited with the 488 nm line of the argon laser and the emission was collected at 500–550 nm. In the presence of FRET, bleaching of the acceptor (GFP) resulted in a significant increase in fluorescence of the donor (BFP). Selective photobleaching of GFP was performed by repeatedly scanning a region of the sample (10 × 10 μm) with the 488 nm argon laser set at 100% intensity to photobleach at least 85% of the original acceptor fluorescence. Pre-bleach and post-bleach images were collected sequentially. To minimize the effect of photobleaching caused by imaging, images were collected at low laser intensity. The amount of proteins used in all these experiments was equivalent to prevent potential influences of protein concentration on FRET efficiency.

The FRET efficiency using the acceptor photobleaching paradigm is calculated as the percentage of increased BFP emission after GFP photobleaching:

$$\%\ \text{FRET efficiency} = \frac{\text{BFP post} - \text{BFP pre}}{\text{BFP post}} \times 100,$$

where BFPpre and BFPpost are the BFP emission before and after GFP photobleaching, respectively. Positive and negative controls were used as measure of the highest and lowest percentage of FRET possible, respectively. Mean FRET efficiencies ± standard error were reported ($n \geqslant 6$). FRET image is presented in pseudocolor for better visualization.

Cell culture and nanoparticle internalization

HeLa cells were obtained from the American Type Culture Collection (reference CCL-2) and cultured in 24 well plates in MEM ALPHA medium (Gibco) supplemented with 10% foetal bovine serum (Gibco), and incubated at 37 °C in a 5% CO_2 humidified atmosphere. For internalization assays 1 μM of hybrid nanoparticles were added in presence of serum free Optipro medium (Gibco) 24 h before flow cytometer analysis. Cells were then analysed after 15 min treatment with 1 mg ml^{-1} trypsin (Gibco) on a FACS-Canto system (Becton Dichkinson) at 488 nm excitation with a 15 mW air-cooled argon ion laser and a D detector (530/30 nm band pass filter). For competition assays, 5 μM of the CXCR4 receptor-specific antagonist AMD3100 (octohydrochloride hydrate, Sigma) was added to the cells 1 h before nanoparticle addition.

For confocal analysis, cells were grown on MatTek culture dishes (MatTek Corporation) and protein nanoparticles added in presence of serum free Optipro medium (Gibco) 24 h before analysis. Cell membranes were then labelled with 2.5 μg ml^{-1} CellMasK™ deep red (Molecular Probes) and nuclei with 0.2 μg ml^{-1} Hoechst 33342 (molecular probes) for 10 min. Cells were finally washed in PBS (Sigma) and analysed by TCS-SP5 confocal laser scanning microscopy (Leica Microsystems) using a HCX PL Apo CS lambda blue 63×/1.4NA oil objective. A blue diode (405 nm) was used for Hoechst and BFP excitation, an Ar laser (488 nm) for GFP excitation and a HeNe laser (633 nm) for CellMask™ excitation. To localize the protein materials inside the cells, Z stacks of different sections were acquired along the cell thickness following Nyquist criterion. Final images were processed using LAS AF™ software (Leica Microsystems, Heidelberg, Germany) and 3D models were generated using Imaris x64 v7.2.1 software (Bitplane, Zurich Switzerland) with Surpass Mode.

Statistical analyses

Quantitative data of competition assays and FRET analyses are expressed as mean ± standard error. Data of competition assays were log transformed and checked for normal distribution and homogeneity of variances with Kolmogorov–Smirnov and Levene tests, respectively. Then, pairwise comparisons were performed using Student *t* tests. FRET data were compared using Mann–Whitney U tests. Statistical differences were assumed at $p < 0.05$. All statistical analyses were performed with SPSS 15.0 software (SPSS Inc.).

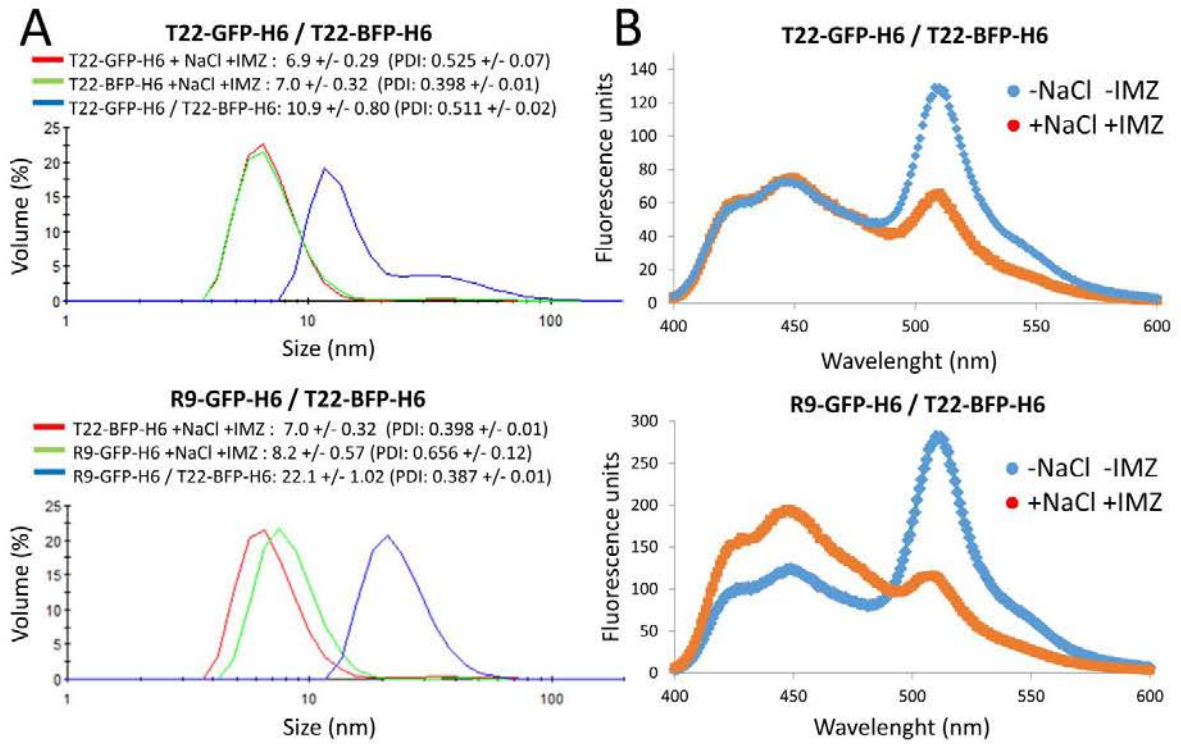

Figure 3. Controlled formation of hybrid materials. Reconstitution of hybrid T22-GFP-H6/T22-BFP-H6 and R9-GFP-H6/ T22-BFP-H6 nanoparticles monitored by DLS (A) and FRET (B) determinations. DLS size of starting building blocks (A) and NaCl and Imidazole-mediated loss of FRET (B) are shown as references. Peak sizes and pdi values are shown for all DLS plots and expressed as mean +/− standard error.

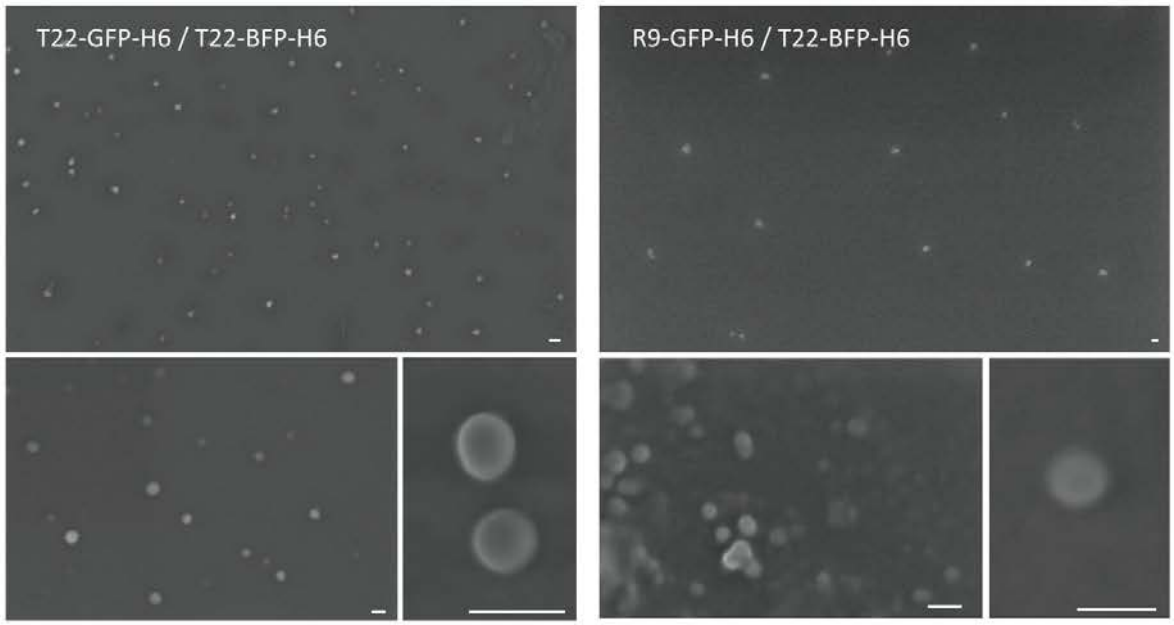

Figure 4. Morphometric analysis of hybrid nanoparticles. FESEM determinations of T22-BFP-H6/T22-GFP-H6 and R9-GFP-H6/T22-BFP-H6 materials, at increasing levels of magnification. White bars indicate 20 nm.

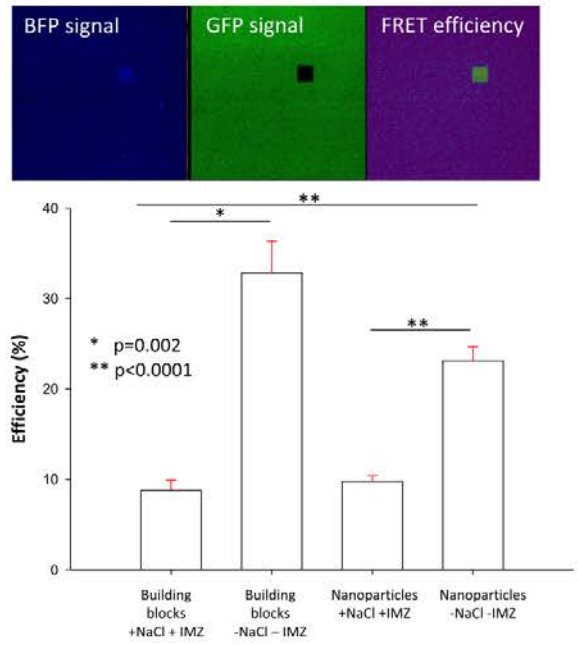

Figure 5. FRET analyses of T22-GFP-H6/T22-BFP-H6 particles and building blocks. Confocal images of T22-GFP-H6/T22-BFP-H6 after photobleaching of GFP molecules showing an increase in fluorescence intensity of donor BFP in the rectangle area, also evident by pseudocolor FRET image (top). Average FRET efficiency of different conditions of building blocks and nanoparticles. Both mixed T22-GFP-H6 and T22-BFP-H6 building blocks and assembled T22-GFP-H6/T22-BFP-H6 nanoparticles were incubated either under low salt conditions in absence of imidazole, or in a high salt buffer in presence of imidazole (bottom).

Results

T22-GFP-H6, T22-BFP-H6 and R9-GFP-H6 fusion proteins were easily produced as full-length polypeptides in bacteria without signs of proteolysis (supplementary figure 1 is available online at stacks.iop.org/NANO/28/505102/mmedia). R9 and in particular T22, are potent ligands of the cell surface protein CXCR4 [21, 24, 25], both acting in the fusion proteins as oligomerization agents but also as cell surface cell ligands. Each of these polypeptides assemble as regular homomeric nanoparticles (figures 1(A)–(C)) because of the combination of cationic peptides and polyhistidines. Upon systemic injection, they show high structural stability, reaching target organs in absence of evident disassembling [17]. Such architectonic robustness was challenged *in vitro* under high salt content conditions (what promotes charge neutralization) or in presence of imidazole (competing for ligands of reactive histidine residues). None of these conditions alone, within the tested ranges, disassembled the oligomers (table 1). However, the combination of both high salt and imidazole disrupted all the materials into smaller building blocks, as realized by denaturing concentrations of SDS (table 1, figure 1(B)).

These data indicated that both architectonic tags (the cationic peptide and the H6 tail) probably have a combined role in nanoparticle formation. The contribution of each end-terminal segment in the material stability was further dissected by keeping constant one disassembling condition while increasing the strength of the secondary parameter. At 500 mM Na^+, between 100 and 300 mM imidazole (the whole buffer composition slightly influencing the threshold) translated both T22-GFP-H6 and R9-GFP-H6 nanoparticles into single building blocks (table 1, figure 2(A)). On the other hand, at 300 mM imidazole, T22-GFP-H6 was disassembled by 350 mM Na^+ while R9-GFP-H6 required up to 450 mM (figure 2(B)). Once the disassembling conditions were set, we wondered if hybrid nanoparticles formed by heterologous building blocks might be generated by mixing distinct disassembled materials and dialysing then against a physiological buffer to allow the formation of hybrid oligomers. In this context, we tested the combinations involving T22-GFP-H6 with T22-BFP-H6 (same targeting agent but different building block) and R9-GFP-H6 with T22-BFP-H6 (different targeting agent and building block), that should both allow observing FRET between green and blue fluorescence as an assessment of the hybrid materials being formed.

Reconstitution of nanoparticles was indeed successful, resulting in materials with defined DLS profiles and relatively low polydispersion (figure 3(A)). The intrinsic hybrid nature of the materials was demonstrated by the occurrence of FRET, which was immediately disrupted upon incubation in high salt buffer with imidazole (figure 3(B)). R9-GFP-H6/T22-BFP-H6 materials peaked at 22 nm as a monodisperse population of nanoparticles (figures 3, 4), while T22-GFP-H6/T22-BFP-H6 materials peaked at 10 nm, with a secondary peak at around 30 nm. The prevalence of the 10 nm oligomers was confirmed by FESEM (figure 4), that offered images similar to the parental materials. FRET appearance and disappearance upon disassembling was fully assessed for T22-GFP-H6/T22-BFP-H6, by acceptor photo-bleaching under confocal microscopy (figure 5).

The successful generation of hybrid nanoparticles prompted us to explore their ability to internalize target cells in a stable and specific way. For that, cultured $CXCR4^+$ HeLa cells were exposed to T22-GFP-H6/T22-BFP-H6 and R9-GFP-H6/T22-BFP-H6 nanoparticles and investigated for internalization. As observed (figure 6(A)), both materials penetrated HeLa cells after 24 h of exposure. In addition, their uptake was inhibited by the specific chemical ligand of CXCR4, AMD3100 (figure 6(B)). AMD3100-mediated inhibitory effect was observed to be milder in the case of particles containing R9, that acts as both CXCR4 ligand [24] but also as a potent cell penetrating peptide [26,27, 28]. Probably, both internalization mechanisms (CXCR4-dependent and CXCR4-independent) were active in the case of R9-GFP-H6/T22-BFP-H6, while penetration appeared as exclusively CXCR4-dependent in the case of T22-GFP-H6/T22-BFP-H6. The intracellular localization of T22-GFP-H6/T22-BFP-H6 hybrid materials (revealed by the co-localization of blue and green signals in confocal reconstructions) was revealed to be perinuclear (figures 6(C), (D)). This is the same

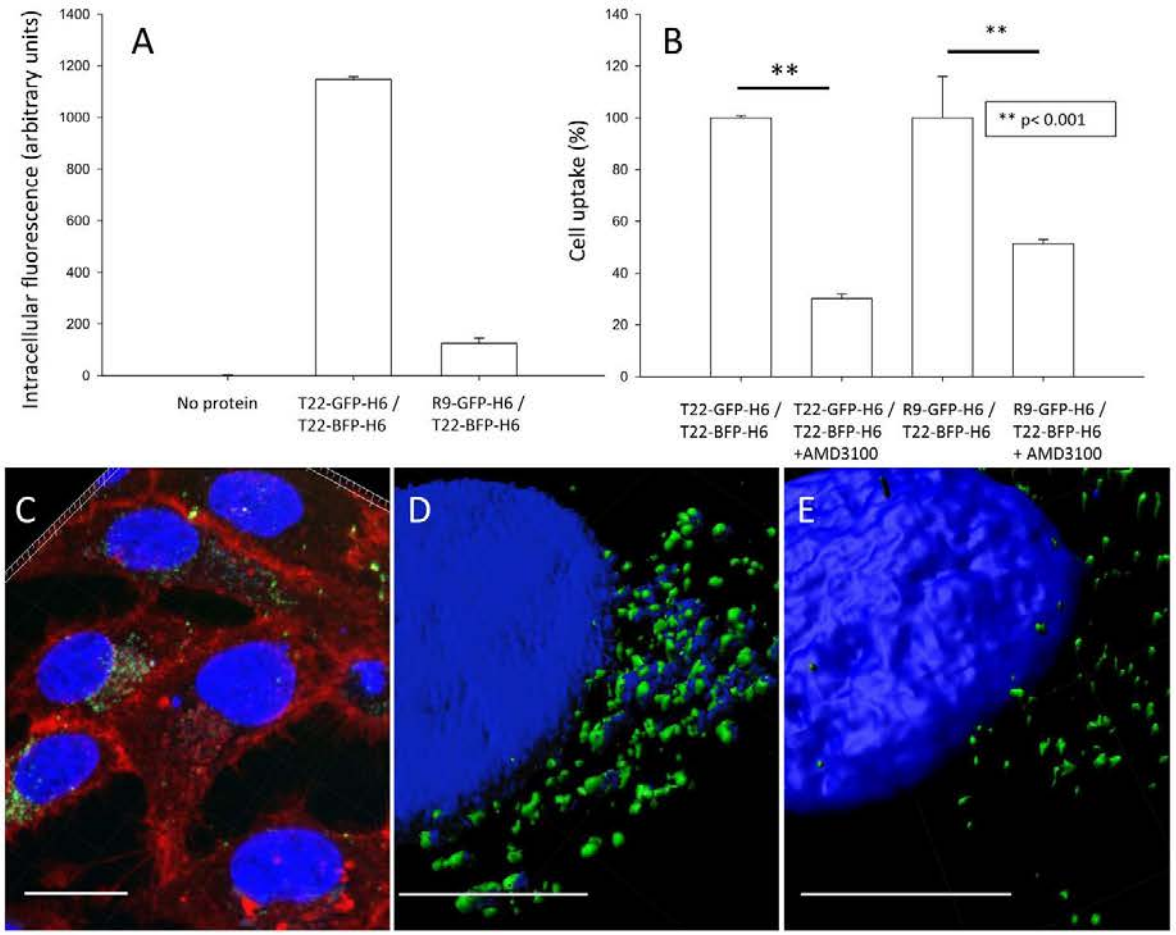

Figure 6. Cell internalization of hybrid nanoparticles. (A) Uptake of hybrid nanoparticles (1 μM) in CXCR4$^+$ HeLa cells upon exposure for 24 h. (B). AMD3100-mediated inhibition of cell internalization. (C) Confocal imaging of cultured CXCR4$^+$ HeLa cells exposed to T22-GFP-H6/T22-BFP-H6 nanoparticles during 24 h. Blue and green fluorescence of the materials are apparent. Membranes are stained in red and nuclear DNA in blue. The bar indicates 20 μm (D) *Z* axis stack and 3D reconstruction of internalized T22-GFP-H6/T22-BFP-H6 nanoparticles, probably clustered in endosomes, showing mutual embedment of blue and green fluorescence. The bar indicates 10 μm. (E) *Z* axis stack and 3D reconstruction of control, internalized T22-GFP-H6 nanoparticles, showing only green fluorescent signal. The bar indicates 10 μm.

location reached by homogeneous, green fluorescent T22-GFP-H6 constructs [16] (figure 6(E)).

Discussion

We have demonstrated here the possibility to disassemble toroid protein nanoparticles formed by modular proteins that cross-interact through cationic and histidine-rich end terminal peptides (figure 1). These materials fall within the category of cyclic assemblies, that allow the multivalent display of peptide motives in highly symmetric lattices [15]. Importantly, this configuration is highly convenient for cell-targeted vehicles for drug delivery [18], since it empowers the constructs to act as viral mimetics regarding their interaction with target cells. The disruption of the homomeric materials was fully reversible upon dialysis against physiological buffers, proving that the disassembling buffer breaks specific cross-protein interactions without affecting the global conformation of the building block. The exclusive impact of high salt combined with imidazole proves that nanoparticles based on cationic peptides and polyhistidines might result from synergies between both type of tags, accounting for the high *in vivo* stability of these materials [17]. Controlling the disassembling and reassembling in this platform has allowed the *in vitro* generation of heteromeric nanoparticles (figures 3, 4) that keep the cell targeting properties mediated by the end terminal cationic ligand of CXCR4 (T22, figure 6), a cell-surface receptor linked to several aggressive human cancers [29, 30]. However, these targeting activities might result combined with the cell penetration properties of an additional cell ligand (R9) incorporated in the heteromeric particles. The robustness of the materials formed by heterogeneous building blocks proves the possibility to incorporate diverse biological

activities into multifunctional vehicles, illustrated here by the blue and green fluorescence emission. In addition, it also proves the possibility to integrate different cell ligands with targeted or non-targeted cell penetrating peptides (supplementary figure 2, illustrated here by the simultaneous display of T22 and R9), what represents a promising strategy in the development of smart and biocompatible materials in nanomedicine. Among other applications, the potential for a controlled combination of distinct cell-ligands fits with the increasing interest in the design of bispecific or biparatopic vehicles for drug delivery [31–34]. This dual target strategy, still in early conceptual stages, might dramatically improve the specificity and efficacy of drug delivery in therapeutic fields such as cancer and inflammation. In a related context, cell-targeted protein-only building blocks with intrinsic therapeutic activities have been recently developed, formed by antimicrobial peptides [35] or by pro-apoptotic peptides [36] in addition to fluorescent proteins. These self-assembling protein drugs, reaching a nanoscale organization, exploit the emerging concept of vehicle-free nanoscale drugs [37]. The combination of different building blocks might allow the ratiometric administration of synergistically acting protein drugs or fluorescent probes, in a new approach to combined therapies or theragnosis (supplementary figure 2). Finally, the possibility to generate protein-only self-assembling nanoparticles in endotoxin-free microorganisms such as *Lactococcus lactis* [38] or endotoxin-free strains of *Escherichia coli* [39] prompts to envisage protein-based hybrid nanoparticles as flexible and promising tools for the generation of multifunctional agents for *in vivo* biomedical applications, such as drug delivery, imaging or theragnosis, fields that had been in the past dominated by the use of non-biological materials such as ceramics, metals and polymers [2].

Conclusions

We have here described a methodological approach to generate protein nanoparticles in the viral size range and formed by heterologous building blocks. The structural robustness of these materials proves the feasibility to recruit diverse biological activities into multifunctional vehicles, which would serve as an appealing approach to simultaneously deliver synergistically acting drugs, in a defined ratio, at the cell level. In addition, it also demonstrates the possibility to incorporate, in single nanoscale vehicles, different cell ligands to easily approach the emerging challenge in targeted drug delivery regarding the design of multiparatopic or multispecific drugs.

Acknowledgments

We are indebted to AGAUR (2014SGR-132) and CIBER-BBN (project NANOPROTHER) granted to AV, Marató de TV3 foundation (TV32013-3930) and ISCIII (PI15/00272 co-founding FEDER) to EV and ISCIII (PI15/00378 and PIE15/00028, co-founding FEDER), Marató de TV3 foundation (TV32013-2030) and AGAUR 2014-PROD0005 to RM. Protein production has been partially performed by the ICTS 'NANBIOSIS', more specifically by the Protein Production Platform of CIBER-BBN/ IBB (http://nanbiosis.es/unit/u1-protein-production-platform-ppp/). LSG was supported by AGAUR (2017FI_B100063), NS by a predoctoral fellowship from the Government of Navarra, UU received a Sara Borrell postdoctoral fellowship from ISCIII and AV an ICREA ACADEMIA award.

ORCID iDs

Antonio Villaverde https://orcid.org/0000-0002-2615-4521

References

[1] Kumar V A, Wang B K and Kanahara S M 2016 Rational design of fiber forming supramolecular structures *Exp. Biol. Med.* **241** 899–908
[2] Webber M J, Appel E A, Meijer E W and Langer R 2016 Supramolecular biomaterials *Nat. Mater.* **15** 13–26
[3] Corchero J L, Vazquez E, Garcia-Fruitos E, Ferrer-Miralles N and Villaverde A 2014 Recombinant protein materials for bioengineering and nanomedicine *Nanomedicine* **9** 2817–28
[4] Ferrer-Miralles N, Rodriguez-Carmona E, Corchero J L, Garcia-Fruitos E, Vazquez E and Villaverde A 2015 Engineering protein self-assembling in protein-based nanomedicines for drug delivery and gene therapy *Crit. Rev. Biotechnol.* **35** 209–21
[5] Yeates T O, Liu Y and Laniado J 2016 The design of symmetric protein nanomaterials comes of age in theory and practice *Curr. Opin. Struct. Biol.* **39** 134–43
[6] Engel J and Kammerer R A 2000 What are oligomerization domains good for? *Matrix Biol.* **19** 283–8
[7] Doll T A P F, Dey R and Burkhard P 2015 Design and optimization of peptide nanoparticles *J Nanobiotechnol.* **13** 73
[8] Li D *et al* 2014 Structure-based design of functional amyloid materials *J. Am. Chem. Soc.* **136** 18044–51
[9] Lua L H, Connors N K, Sainsbury F, Chuan Y P, Wibowo N and Middelberg A P 2014 Bioengineering virus-like particles as vaccines *Biotechnol. Bioeng.* **111** 425–40
[10] Molino N M and Wang S W 2014 Caged protein nanoparticles for drug delivery *Curr. Opin. Biotechnol.* **28** 75–82
[11] Deng L *et al* 2017 Protein nanoparticle vaccine based on flagellin carrier fused to influenza conserved epitopes confers full protection against influenza A virus challenge *Virology* **509** 82–9
[12] Benner N L *et al* 2017 Vault nanoparticles: chemical modifications for imaging and enhanced delivery *ACS Nano* **11** 872–81
[13] Rueda F *et al* 2015 Bottom-up instructive quality control in the biofabrication of smart protein materials *Adv. Mater.* **27** 7816–22
[14] Pesarrodona M *et al* 2017 Intrinsic functional and architectonic heterogeneity of tumor-targeted protein nanoparticles *Nanoscale* **9** 6427–35
[15] Goodsell D S and Olson A J 2000 Structural symmetry and protein function *Annu. Rev. Biophys. Biomol. Struct.* **29** 105–53

[16] Unzueta U *et al* 2012 Non-amyloidogenic peptide tags for the regulatable self-assembling of protein-only nanoparticles *Biomaterials* **33** 8714–22

[17] Cespedes M V *et al* 2014 *In vivo* architectonic stability of fully *de novo* designed protein-only nanoparticles *ACS Nano* **8** 4166–76

[18] Unzueta U, Cespedes M V, Vazquez E, Ferrer-Miralles N, Mangues R and Villaverde A 2015 Towards protein-based viral mimetics for cancer therapies *Trends Biotechnol.* **33** 253–8

[19] Pesarrodona M *et al* 2014 Intracellular targeting of $CD44^{+}$ cells with self-assembling, protein only nanoparticles *Int. J. Pharm.* **473** 286–95

[20] Cespedes M V *et al* 2016 Cancer-specific uptake of a liganded protein nanocarrier targeting aggressive $CXCR4^{+}$ colorectal cancer models *Nanomed.: Nanotechnol., Biol., Med.* **12** 1987–96

[21] Unzueta U *et al* 2012 Intracellular CXCR4(+) cell targeting with T22-empowered protein-only nanoparticles *Int. J. Nanomed.* **7** 4533–44

[22] Chari R V 2016 Expanding the reach of antibody-drug conjugates *ACS Med. Chem. Lett.* **7** 974–6

[23] Vazquez E *et al* 2010 Protein nanodisk assembling and intracellular trafficking powered by an arginine-rich (R9) peptide *Nanomedicine* **5** 259–68

[24] Tanaka G *et al* 2012 CXCR4 stimulates macropinocytosis: implications for cellular uptake of arginine-rich cell-penetrating peptides and HIV *Chem. Biol.* **19** 1437–46

[25] Unzueta U *et al* 2017 Engineering tumor cell targeting in nanoscale amyloidal materials *Nanotechnology* **28** 015102

[26] Alhakamy NA and Berckland CJ 2013 Polyarginine molecular weight determines transfection efficiency of calcium condensed complexes *Mol. Pharmaceutics* **10** 1940–8

[27] Bilichak A, Luu J and Eudes F 2015 Intracellular delivery of fluorescent protein into viable wheat microspores using cationic peptides *Frontiers Plant Sci.* **6** 666

[28] Liu B R, Lin M D, Chiang H J and Lee H J 2012 Arginine-rich cell-penetrating peptides deliver gene into living human cells *Gene* **505** 37–45

[29] Balkwill F 2004 The significance of cancer cell expression of the chemokine receptor CXCR4 *Seminars Cancer Biol.* **14** 171–9

[30] Kim J *et al* 2006 Chemokine receptor CXCR4 expression in patients with melanoma and colorectal cancer liver metastases and the association with disease outcome *Ann. Surg.* **244** 113–20

[31] Vazquez-Lombardi R, Phan T G, Zimmermann C, Lowe D, Jermutus L and Christ D 2015 Challenges and opportunities for non-antibody scaffold drugs *Drug Discovery Today* **20** 1271–83

[32] Kontermann R E 2012 Dual targeting strategies with bispecific antibodies *mAbs* **4** 182–97

[33] Weidle U H, Kontermann R E and Brinkmann U 2014 Tumor-antigen-binding bispecific antibodies for cancer treatment *Seminars Oncol.* **41** 653–60

[34] Kontermann R E and Brinkmann U 2015 Bispecific antibodies *Drug Discovery Today* **20** 838–47

[35] Serna N *et al* 2017 Protein-only, antimicrobial peptide-containing recombinant nanoparticles with inherent built-in antibacterial activity *Acta Biomater.* **60** 256–63

[36] Serna N *et al* 2017 Peptide-based nanostructured materials with intrinsic proapoptotic activities in CXCR4+ solid tumors *Adv. Funct. Mater.* **27** 1700919

[37] Shen J, Wolfram J, Ferrari M and Shen H 2017 Taking the vehicle out of drug delivery *Mater. Today* **20** 95–7

[38] Cano-Garrido O *et al* 2016 CXCR4(+)-targeted protein nanoparticles produced in the food-grade bacterium *Lactococcus lactis Nanomedicine* **11** 2387–98

[39] Rueda F *et al* 2016 Structural and functional features of self-assembling protein nanoparticles produced in endotoxin-free *Escherichia coli Microbial Cell Factories* **15** 59

ANNEX 7: EUROPEAN PATENT

Nanostructured proteins and uses thereof.

Europäisches Patentamt
European Patent Office
Office européen des brevets

Acknowledgement of receipt

We hereby acknowledge receipt of your request for grant of a European patent as follows:

Submission number	5255596
Application number	EP17169722.0
File No. to be used for priority declarations	EP17169722
Date of receipt	05 May 2017
Your reference	T-2017-018EP2
Applicant	UNIVERSITAT AUTONOMA DE BARCELONA
Country	ES
Title	NANOSTRUCTURED PROTEINS AND USES THEREOF
Documents submitted	package-data.xml application-body.xml OLF-ARCHIVE.zip\Functionalized cellulose fabrics_UAB_Final version.zip SPECEPO-2.pdf\T-2017-018EP Claims.pdf (5 p.) SPECEPO-4.pdf\T-2017-018EP Figs.pdf (17 p.) f1002-1.pdf (2 p.) ep-request.xml ep-request.pdf (5 p.) SPECEPO-1.pdf\T-2017-018EP Description.pdf (65 p.) SPECEPO-3.pdf\T-2017-018EP Abstract.pdf (1 p.) SEQLTXT.txt\Sequence Listing - T-2017-018.txt
Submitted by	CN=Xavier Vallvé Sanchez 24825
Method of submission	Online

Acknowledgement of receipt - application number EP17169722.0 **Page 1 of 2**

Date and time receipt generated	05 May 2017, 13:58 (CEST)
Message Digest	B7:88:E5:60:51:F6:E3:7C:B3:60:DB:11:1B:D1:1D:08:AB:BB:BC:95

Correction by the EPO of errors in debit instructions filed by eOLF
Errors in debit instructions filed by eOLF that are caused by the editing of Form 1038E entries or the continued use of outdated software (all forms) may be corrected automatically by the EPO, leaving the payment date unchanged (see decision T 152/82, OJ EPO 1984, 301 and point 6.3 ff ADA, Supplement to OJ EPO 10/2007).

/European Patent Office/

Form 1002 - 1: Public inventor(s)

Designation of inventor

User reference: T-2017-018EP2
Application No:

Public

	Inventor	
	Name:	VILLAVERDE CORRALES, Mr. ANTONIO
	Company:	UAB
	Department:	IBB
	Address:	IBB Campus de la UAB s/n 08193 Cerdanyola del Vallès Spain
	The applicant has acquired the right to the European patent:	As employer
	Inventor	
	Name:	VÁZQUEZ GÓMEZ, Ms. ESTHER
	Company:	UAB
	Department:	IBB
	Address:	Campus de la UAB s/n 08193 Cerdanyola del Vallès Spain
	The applicant has acquired the right to the European patent:	As employer
	Inventor	
	Name:	Serna Romero, Ms. Naroa
	Company:	Universitat Autònoma de Barcelona
	Department:	IBB
	Address:	IBB Campus de la UAB s/n 08193 Cerdanyola del Vallès Spain
	The applicant has acquired the right to the European patent:	As employer
	Inventor	
	Name:	Sánchez García, Ms. Laura
	Company:	Universitat Autònoma de Barcelona
	Department:	IBB
	Address:	IBB Campus de la UAB s/n 08193 Cerdanyola del Vallès Spain
	The applicant has acquired the right to the European patent:	As employer

User reference: T-2017-018EP2
Application No:

	Inventor	
	Name:	UNZUETA ELORZA, Mr. UGUTZ
	Company:	Hospital de la Santa Creu i Sant Pau
	Address:	Antoni Mª Claret, 167 08025 Barcelona Spain
	The applicant has acquired the right to the European patent:	As employer
	Inventor	
	Name:	MANGUES BAFALLUY, Mr. RAMON
	Company:	Hospital de la Santa Creu i Sant Pau
	Address:	Antoni Mª Claret, 167 08025 Barcelona Spain
	The applicant has acquired the right to the European patent:	As employer
	Inventor	
	Name:	CÉSPEDES NAVARRO, Ms. MARÍA VIRTUDES
	Company:	Hospital de la Santa Creu i Sant Pau
	Address:	Antoni Mª Claret, 167 08025 Barcelona Spain
	The applicant has acquired the right to the European patent:	As employer
	Inventor	
	Name:	CASANOVA RIGAT, Ms. ISOLDA
	Company:	Centro de Investigación Biomédica en Red
	Address:	c/ Monforte de Lemos, 5 08025 Barcelona Spain
	The applicant has acquired the right to the European patent:	As employer

Signature(s)

Place:	Bellaterra
Date:	05 May 2017
Signed by:	/Armando Sanchez Bonastre/
Capacity:	(Applicant: UNIVERSITAT AUTONOMA DE BARCELONA)
Function of person signing:	Vicerector for Research and Technology Transfer

FIELD OF THE INVENTION

The present invention relates to the field of nanostructured protein materials, more specifically to fusion proteins which can be used for therapy.

BACKGROUND OF THE INVENTION

The systemic administration of drugs in form of nanoconjugates benefits from enhanced drug stability when compared to free molecules. Valuable additional properties such as cell targeting might be also merged into a given hybrid composite through the chemical incorporation of functional groups in nanoscale vehicles, taking profit from the high surface/volume ratio of nanomaterials. When administered systemically, the resulting drug loaded conjugates sizing between ~8 and 100 nm escape from renal filtration in absence of aggregation in lung or other highly vascularized organs. This fact, combined with appropriate physicochemical properties of the material might result in extended circulation time and prolonged drug exposure to target organs, thus enhancing the therapeutic impact and benefits for the patient.

Among the diversity of materials under investigation as drug carriers, that includes metals, ceramics, polymers and carbon nanotubes, proteins offer unique properties regarding biocompatibility and degradability that, in the context of rising nanotoxicological concerns, make them especially appealing.

However, many protein species are themselves, efficient drugs usable in human therapy, as attested by more than 400 protein-based products approved by main medicines agencies. Therefore, the engineering of protein drugs as self-organizing building blocks, that exhibit intrinsic therapeutic activities upon self-assembling as nanoparticles, constitutes an advantageous concept. Thus, this methodology excludes the need of further activation and drug conjugation, as the nanomaterial itself acts as a nanoscale drug (desirably between 8 and 100 nm). In that way, chemically homogenous protein nanoparticles, showing intrinsic therapeutic activities (like the current plain protein species used in human medicine -e.g, hormones, growth factors, vaccines etc.) can be biologically produced in a single step (as nanoscale assembled entities). Since the material itself acts as a drug, the possibility of drug leakage during circulation, an

undesired possibility especially worrying in the case of cytotoxic agents, can be completely abolished, which becomes a significant advantage with respect to the state of the art.

The inventors previously probed into the field by applying a nanoarchitectonic principle based on the addition, to a core protein, of a cationic N-terminal domain plus a C-terminal poly-histidine. [Serna, N. *et al.* 2016. Nanomedicine, 12:1241-51]. It has been described in the art that these end-terminal tags and the resulting charge balance in the whole fusion promote self-assembling and oligomerization of monomeric proteins as robust toroid nanoparticles, stable in plasma [Cespedes, M. V. *et al.* 2014. ACS Nano., 8:4166-4176] and with high cellular penetrability if empowered with cell-targeting peptides. [Xu, Z. K. *et al.* 2015. Materials Letters, 154:140-3] Nonetheless, the building blocks of these protein protein structures might also contain functional peptides such as cell-targeting agents, endosomolytic agents or nuclear localization signals, in form of fused stretches with modular organization.

Therefore, to take advantage of such easy protein engineering will be highly beneficial, since a need persists in the art for drug delivery systems with enhanced selectivity and biodisponibility.

SUMMARY OF THE INVENTION

In a first aspect, the invention relates to a fusion protein comprising

(i) a polycationic peptide,

(ii) an intervening polypeptide region and

(iii) a positively charged amino acid-rich region,

wherein wherein the intervening polypeptide region is not a fluorescent protein alone or human p53.

In a second aspect, the invention relates to a method to prepare nanoparticles comprising multiple copies of the fusion protein according to the first aspect of the invention comprising placing a preparation of said fusion protein in a low salt buffer.

In further aspects, the invention relates to a polynucleotide encoding a fusion protein according to the first aspect of the invention, a vector comprising said polynucleotide, and a host cell comprising either said polynucleotide or said vector.

In an additional aspect, the invention relates to a nanoparticle comprising multiple copies of the fusion protein of the invention or a nanoparticle which has been obtained by the method of the invention to prepare nanoparticles.

In yet another additional aspect, the invention relates to a fusion protein, a polynucleotide, a vector, a host cell or a nanoparticle according to the invention for use in medicine.

ACKNOWLEDGEMENTS

No one can whistle a symphony. It takes a whole orchestra to play it.

Halford Luccock

Esta tesis es el resumen de casi 4 años de trabajo intenso y constante, pero gratificante.

Paso a paso va haciendo uno el camino, cumpliendo pequeños objetivos que, finalmente, le llevan a cerrar una etapa tan importante como ésta. De ella me quedo con la ilusión puesta en este proyecto, con todas las veces que he pensado lo mucho que me apasiona y me gusta mi trabajo y con todas las personas que me han acompañado a lo largo de este camino. Por ello, me gustaría agradecer a todas estas personas que han hecho mi tesis doctoral posible:

Al grupo de Nanobiotecnología por el buen ambiente, por estar siempre dispuesto a ayudar y ser personas trabajadoras, competentes y efectivas. Un placer trabajar con vosotros.

Toni, gracias por confiar en mí desde el primer día y darme la oportunidad de empezar esta aventura. Ha sido un placer trabajar junto a tí y aprender de una mente tan privilegiada como la tuya.

Esther, muchísimas gracias por estar a mi lado cada día y por tus sabios consejos. Por dirigir esta tesis y por tu apoyo cada jueves. Por confiar en mi trabajo, impulsarlo y potenciarlo.

Neus, ha sido enriquecedor trabajar a tu lado. De ti he aprendido el esfuerzo, tu gran capacidad de trabajo y constancia.

Pepe, gracias también por los momentos compartidos y por tu trabajo.

Ugutz, todo lo que ponga aquí no es suficiente para agradecerte todo lo que me has apoyado durante la tesis. Gracias por todo lo que he aprendido de ti, tus consejos y por confiar en mí y dejar desarrollarme de forma independiente aprendiendo de mis errores. Has sido más que un director de tesis, has estado a mi lado cada día dándome tu cariño y apoyo.

Paolo ¡qué voy a decir de ti…..! Fue un placer empezar a trabajar el primer año contigo y aprender de ti en cada paso del camino, pero de ti me quedo con nuestra amistad. Simplemente me has aportado felicidad, cariño y alegría cada día de esta tesis. Muchísimas gracias por estar ahí SIEMPRE. Has sido el compañero y el amigo perfecto,

en los buenos y en los malos momentos, y eso, es impagable. Nunca dejarás de formar parte de mi vida.

Laura…..mi compañera, mi confidente. Gracias por ayudarme en todo, has sido una pieza clave en esta tesis tanto por el trabajo puesto en ella como por la amistad que hemos construido. Hemos trabajado de forma intensa y conjunta y sólo tu y yo conocemos esos momentos de auténtica locura pero que siempre hemos estado una para la otra. No podría haber imaginado una compañera mejor.

Quim, nos hemos conocido más fuera del laboratorio que dentro de él. Gracias por tu humor, por escucharme, por estar ahí cuando lo he necesitado y por acompañarme en mis locuras y potenciarlas. Gracias por ser mi amigo y compartir conmigo momentos que nunca se olvidan.

Josevi, es increíble lo mucho que nos hemos demostrado en tan poco tiempo. Me alegro muchísimo de tenerte de compi de mesa, de gym y de salidas. Gracias por todas las risas compartidas y charlas interminables.

Olivia, me ha encantado haber tenido la oportunidad de conocerte más en los últimos meses. Gracias por darme la motivación para salir a correr, por las risas en Italia y otros momentos divertidos. Tienes mucha fuerza y eres una crack trabajando.

Raquel, gracias por tu trabajo y esfuerzo en el laboratorio. Espero que podamos compartir más momentos juntas en él.

Hector, eres un gran fichaje para el grupo de nano. Tu pasión y actitud en el trabajo es envidiable. Espero seguir conociéndote y compartir momentos juntos.

Marianna, la alegría del laboratorio. Se te ha echado de menos desde el minuto uno que te fuiste y me alegro muchísimo de haberte conocido. He aprendido de ti y de tus consejos. Gracias por ser tan positiva y contagiárnoslo a todos.

Fabián, me encantó conocerte y gracias por apoyarme tanto en mi primer año de doctorado. Por las charlas en carrer blai y tus sabios consejos.

Mireia, gracias por todo lo aprendido trabajando contigo y los momentos fuera del labo.

Rosa y Mercedes…el laboratorio sería un desastre sin vosotras. Gracias por la organización, por salvarnos cuando necesitamos algo. Ha sido muy agradable trabajar con vosotras.

Julieta, te conozco desde hace poco, pero ha sido un placer conocerte y trabajar contigo. . Aprecio muchísimo tu actitud y amabilidad durante estos meses.

Ana, también ha sido un placer trabajar contigo.

Eric, Amanda, Aida, Andrés….gracias a todos por los momentos compartidos. Espero que sigamos viéndonos y que consigáis hacer lo que os gusta y queréis cuando terminéis el Máster.

Agradecer a Ramón, Virtudes y Patricia por toda la ayuda, por su gran esfuerzo y colaboración en este trabajo. Virtudes, gracias por confiar tanto en mí, ha sido un absoluto placer trabajar contigo.

Olga, gracias por todos los momentos juntas en el trabajo y fuera de él. Gracias por ayudarme con las celulitas y ser muchas veces mi confidente.

Fran, muchas gracias por tu profesionalidad y por estar siempre dispuesto a ayudarme en todo.

Alex, gracias por tu trabajo, por poner todo tu esfuerzo en él. Gracias también por tu sentido del humor y cuidarnos tanto.

Mónica, un placer trabajar contigo. Espero que sigamos colaborando.

Thank you J.P. Medema for receiving me in you laboratory. It has been a great experience to spend this period time in Amsterdam. Thanks also to Dasha, Prashanthi and all the people from the lab for helping me and make my internship unforgettable.

Por último me gustaría agradecer a toda mi familia por todo el apoyo recibido. Para mí ha sido imprescindible sentir que siempre habéis estado a mi lado y sobre todo por ser los primeros en confiar en mí, en impulsarme a empezar esta aventura y acompañarme en ella. Gracias por darme la oportunidad de hacer lo que amo.

Eskerrik asko, Aita eta Ama, por escucharme durante horas sobre proteínas y nanoparticulas sin entender de lo que hablaba, pero no interrumpirme ni una vez y mirarme con admiración. Gracias por hacerme ver que lo importante es poner todo el esfuerzo en lo que hago y que me sienta orgullosa de mi trabajo.

Sister, no tengo palabras. Eres de las personas más importantes en mi vida y has estado a mi lado cada día. Me haces sentir invencible.

Celia, Jose, primitas….gracias por estar ahí cada día. Sois muy importantes en mi vida. Amona Teo, Amona Mila eta Ibon. Eskerrik asko denagatik, Ibon.

Raquel, gracias por compartir conmigo la pasión por la ciencia, por estar a mi lado siempre que lo he necesitado y porque sé que estaremos una para la otra siempre. A Markel, gracias por haberme acompañado en este largo camino, apoyarme y enseñarme tantas cosas. A Bella, por todo lo compartido juntas y apoyarme siempre. A Ana, Alexia y Tori por todo el amor que me habéis demostrado durante estos años en Barcelona. A mi kuadrilla, muchas gracias por los momentos compartidos y apoyarme cuando lo he necesitado. Especialmente a Napi por ser una pieza clave a comienzos de esta tesis y por nuestra experiencia! A Gerard, por darme la energía extra que he necesitado para escribir esta tesis. A mis amigos de la uni, gracias por sentir que tengo una minifamilia cuando nos volvemos a reunir. A Aitziber, Sandra y Maialen, porque RQC nunca muere y seguimos estando unidas como el primer día.

En resumen, MUCHAS GRACIAS A TODOS por hacer esto posible. El 100% de esta tesis es vuestra.

Naroa Serna Romero

PhD Thesis 2018

Departament de Genètica i de Microbiologia
Facultat de Biociències

Universitat Autònoma de Barcelona

Institut de Biotecnologia i de Biomedicina

NanoBioTechnology